

**International Journal of  
Biometrics and Bioinformatics (IJBB)**

ISSN : 1985-2347



VOLUME 4, ISSUE 2

PUBLICATION FREQUENCY: 6 ISSUES PER YEAR

Copyrights © 2010 Computer Science Journals. All rights reserved.

**International Journal of  
Biometrics and Bioinformatics  
(IJBB)**

**Volume 4, Issue 2, 2010**

**Edited By**  
**Computer Science Journals**  
[www.cscjournals.org](http://www.cscjournals.org)

**Editor in Chief Professor João Manuel R. S. Tavares**

## **International Journal of Biometrics and Bioinformatics (IJBB)**

Book: 2010 Volume 4, Issue 2

Publishing Date: 31-05-2010

Proceedings

ISSN (Online): 1985-2347

This work is subjected to copyright. All rights are reserved whether the whole or part of the material is concerned, specifically the rights of translation, reprinting, re-use of illusions, recitation, broadcasting, reproduction on microfilms or in any other way, and storage in data banks. Duplication of this publication of parts thereof is permitted only under the provision of the copyright law 1965, in its current version, and permission of use must always be obtained from CSC Publishers. Violations are liable to prosecution under the copyright law.

IJBB Journal is a part of CSC Publishers

<http://www.cscjournals.org>

©IJBB Journal

Published in Malaysia

Typesetting: Camera-ready by author, data conversation by CSC Publishing Services – CSC Journals, Malaysia

**CSC Publishers**

## **Editorial Preface**

This is the Second issue of volume fourth of International Journal of Biometric and Bioinformatics (IJBB). The Journal is published bi-monthly, with papers being peer reviewed to high international standards. The International Journal of Biometric and Bioinformatics is not limited to a specific aspect of Biology but it is devoted to the publication of high quality papers on all division of Bio in general. IJBB intends to disseminate knowledge in the various disciplines of the Biometric field from theoretical, practical and analytical research to physical implications and theoretical or quantitative discussion intended for academic and industrial progress. In order to position IJBB as one of the good journal on Bio-sciences, a group of highly valuable scholars are serving on the editorial board. The International Editorial Board ensures that significant developments in Biometrics from around the world are reflected in the Journal. Some important topics covers by journal are Bio-grid, biomedical image processing (fusion), Computational structural biology, Molecular sequence analysis, Genetic algorithms etc.

The coverage of the journal includes all new theoretical and experimental findings in the fields of Biometrics which enhance the knowledge of scientist, industrials, researchers and all those persons who are coupled with Bioscience field. IJBB objective is to publish articles that are not only technically proficient but also contains information and ideas of fresh interest for International readership. IJBB aims to handle submissions courteously and promptly. IJBB objectives are to promote and extend the use of all methods in the principal disciplines of Bioscience.

IJBB editors understand that how much it is important for authors and researchers to have their work published with a minimum delay after submission of their papers. They also strongly believe that the direct communication between the editors and authors are important for the welfare, quality and wellbeing of the Journal and its readers. Therefore, all activities from paper submission to paper publication are controlled through electronic systems that include electronic submission, editorial panel and review system that ensures rapid decision with least delays in the publication processes.

To build its international reputation, we are disseminating the publication information through Google Books, Google Scholar, Directory of Open Access Journals (DOAJ), Open J Gate, ScientificCommons, Docstoc and many more. Our International Editors are working on establishing ISI listing and a good impact factor for IJBB. We would like to remind you that the success of our journal depends directly on the number of quality articles submitted for review. Accordingly, we would like to request your participation by submitting quality manuscripts for review and encouraging your colleagues to submit quality manuscripts for review. One of the great benefits we can

provide to our prospective authors is the mentoring nature of our review process. IJBB provides authors with high quality, helpful reviews that are shaped to assist authors in improving their manuscripts.

**Editorial Board Members**

International Journal of Biometrics and Bioinformatics (IJBB)

## **Editorial Board**

### **Editor-in-Chief (EiC)**

**Professor. João Manuel R. S. Tavares**  
*University of Porto (Portugal)*

### **Associate Editors (AEiCs)**

**Assistant Professor. Yongjie Jessica Zhang**  
*Mellon University (United States of America)*

**Professor. Jimmy Thomas Efird**  
*University of North Carolina (United States of America)*

**Professor. H. Fai Poon**  
*Sigma-Aldrich Inc (United States of America)*

**Professor. Fadiel Ahmed**  
*Tennessee State University (United States of America)*

**Mr. Somnath Tagore (AEiC - Marketing)**  
*Dr. D.Y. Patil University (India)*

**Professor. Yu Xue**  
*Huazhong University of Science and Technology (China )*

**Professor. Calvin Yu-Chian Chen**  
*China Medical university (Taiwan)*

### **Editorial Board Members (EBMs)**

**Assistant Professor. M. Emre Celebi**  
*Louisiana State University in Shreveport (United States of America)*

**Dr. Wichian Sittiprapaporn**  
*(Thailand)*

# Table of Contents

Volume 4, Issue 2, May 2010.

## Pages

- |         |  |
|---------|--|
| 13 - 21 | Detection of Quantitative Trait Loci in Presence of Phenotypic Contamination.<br><br><b>Md. Nurul Haque Mollah</b>   |
| 22 - 33 | Identification of Obstructive Sleep Apnea from Normal Subjects: FFT Approaches Wavelets<br><br><b>Abdulnasir Hossen</b>  |
| 34 - 41 | Experimental Design and Predictive Computational Modeling for the Toxicity of Nanomaterials on the Human Epidermal Cells<br><br><b>Natarajan Meghanathan, Raphael Isokpehi, Hari Har Parshad Cohly</b> |
| 42 – 51 | Eigenvectors of Covariance Matrix using Row Mean and Column Mean Sequences for Face Recognition<br><br><b>H. B. Kekre, Sudeep D. Thepede, Akshay Maloo</b>   |
| 52 - 62 | Gouraud Shading to Improve Appearance of Neuronal Morphology Visualization<br><br><b>Norhasana Razzali, Mohd Shafry Mohd Rahim, Rosely Kumoi, Daut Daman</b>   |

- 63- 70      Detection of Some Major Heart Diseases Using Fractal Analysis  
**Nahina Islam, Nafiz Imtiaz Bin Hamid, Adnan Mahmud, Sk.M. Rahman, Arafat H. Khan**
- 71 – 85     Effective Morphological Extraction of True Fingerprint Minutiae based on the Hit or Miss Transform  
**Roli Bansal, Priti Sehgal, Punam Bedi**
- 86 - 99     Incremental PCA-LDA Algorithm  
**Issam Dagher**

## Detection of Quantitative Trait Loci in Presence of Phenotypic Contamination

**Md. Nurul Haque Mollah**

*Department of Statistics,*

*Faculty of Science,*

*University of Rajshahi,*

*Rajshahi-6205, Bangladesh*

[mnhmollah@yahoo.co.in](mailto:mnhmollah@yahoo.co.in)

### Abstract

Genes controlling a certain trait of organism is known as quantitative trait loci (QTL). The standard Interval mapping [8] is a popular way to scan the whole genome for the evidence of QTLs. It searches a QTL within each interval between two adjacent markers by performing likelihood ratio test (LRT). However, the standard Interval mapping (SIM) approach is not robust against outliers. An attempt is made to robustify SIM for QTL analysis by maximizing  $\beta$ -likelihood function using the EM like algorithm. We investigate the robustness performance of the proposed method in a comparison of SIM algorithm using synthetic datasets. Experimental results show that the proposed method significantly improves the performance over the SIM approach for QTL mapping in presence of outliers; otherwise, it keeps equal performance.

**Keywords:** Quantitative trait loci (QTL), Gaussian mixture distribution, Likelihood ratio test (LRT), Method of maximum likelihood, Method of maximum  $\beta$  -likelihood and Robustness.

## 1. INTRODUCTION

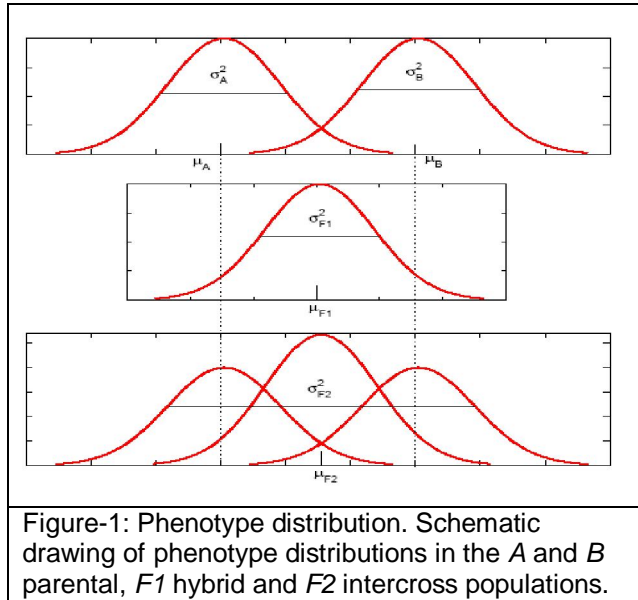
The basic methodology for mapping QTLs involves arranging a cross between two inbred strains differing substantially in a quantitative trait: segregating progeny are scored both for the trait and for a number of genetic markers. A cross between two parental inbred lines *A* and *B* is performed to produce an *F*1 population. The *F*1 progeny are all heterozygote's with the same genotype [4]. Typically, the segregating progeny are produced by a backcross *B*1 = *F*1 × parent or an intercross *F*2 = *F*1 × *F*1.

Let  $(\mu_A, \sigma_A^2)$ ,  $(\mu_B, \sigma_B^2)$ ,  $(\mu_{F1}, \sigma_{F1}^2)$  and  $(\mu_{F2}, \sigma_{F2}^2)$

denote the set of mean and variance of a phenotype in the *A*, *B*, *F*1 and *F*2 population, respectively. Let  $\mu_B - \mu_A > 0$  denote the phenotypic difference between the strains. The cross will be analyzed under the classical assumption that the phenotypic variations are influenced by the effects of both genetic and non-genetic (environmental) factors. In particular, we assume complete codominance and no epistasis. These implies that

$$\mu_{F1_1} = \frac{1}{2}(\mu_A + \mu_B), \quad \mu_{F1} = \frac{1}{3}(\mu_A + \mu_{F1} + \mu_B) \quad \text{and} \quad \sigma_A^2 = \sigma_B^2 = \sigma_{F1}^2 < \sigma_{F2}^2.$$

The variance within the *A*, *B* and *F*1 populations equal the environmental variance,  $\sigma_E^2$  among genetically identical individuals, while the variance within the *F*2 progeny also includes genetic variance,  $\sigma_G^2 = \sigma_{F2}^2 - \sigma_E^2$ . Frequently, phenotypic measurements must be mathematically transformed so that parental phenotypes are approximately normally distributed.



With the rapid advances in molecular biology, it has become possible to gain fine-scale genetic maps for various organisms by determining the genomic positions of a number of genetic markers (RFLP, isozymes, RAPDs, AFLP, VNTRs, etc.) and to obtain a complete classification of marker genotypes by using codominant markers. These advances greatly facilitate the mapping and analysis of quantitative trait loci(QTLs). Thoday [12] first proposed the idea of using two markers to bracket a region for testing QTLs. Lander and Botstein [8] implemented a similar, but much improved, method to use two adjacent markers to test the existence of a QTL in the interval by performing a likelihood ratio test (LRT) at every position in the interval. This is known as standard interval mapping (SIM) approach. It is a comparatively popular way to detect a QTL position in a chromosome [11]. However, It is not robust against outliers [5, 8, 9]. In this project, an attempt is made to robustify the SIM approach [8] by maximizing  $\beta$ -likelihood function [10] using EM like algorithm [3].

In section 2, we discuss the genetic model and its extension to statistical SIM model. Section 3 introduce the robustification of SIM approach for QTL analysis. We demonstrate the performance of the proposed method using simulated datasets in section 4 and make a conclusion of our study in section 5.

## 2. GENETIC MODEL FOR SIM APPROACH

Let us consider a putative QTL locus *Q* of two alleles *Q* and *q* with allelic frequencies *p* and  $(1-p)$ , respectively. Define an indicator variable for alleles by

$$u = \begin{cases} 1 & \text{for } Q \\ 0 & \text{for } q \end{cases}$$

and

$$v = u - E(u) = u - p = \begin{cases} 1-p & \text{for } Q \\ -p & \text{for } q, \end{cases}$$

where  $v$  is a standardized indicator variable with mean zero. Then the genetic-effect design variables for two alleles are defined as

$$x = v_1 + v_2 = \begin{cases} 2(1-p) & \text{for } QQ \\ 1-2p & \text{for } Qq \\ -2p & \text{for } qq \end{cases}$$

and

$$x = -2v_1v_2 = \begin{cases} -2(1-p)^2 & \text{for } QQ \\ 2p(1-p) & \text{for } Qq \\ -2p^2 & \text{for } qq, \end{cases}$$

where  $v_1$  and  $v_2$  are for the two alleles in an individual. Then the genetic model for a QTL in the  $F_2$  population is defined as

$$G = \mu + ax^* + dz^*, \quad (1)$$

where  $a$  and  $d$  are additive and dominance effects of QTL, and  $x^*=x$  and  $z^*=z$  are the genetic-effect design variables with  $p=1/2$ . Therefore, in matrix notation, the genetic model for a QTL in the  $F_2$  population can be written as

$$G = \begin{bmatrix} G_2 \\ G_1 \\ G_0 \end{bmatrix} = \begin{bmatrix} 1 \\ 1 \\ 1 \end{bmatrix} \mu + \begin{bmatrix} 1 & \frac{-1}{2} \\ 0 & \frac{1}{2} \\ -1 & \frac{-1}{2} \end{bmatrix} \begin{bmatrix} a \\ d \end{bmatrix} = \mathbf{1}_{3 \times 1} \mu + D\mathbf{E}.$$

It was proposed to model the relation between a genotypic value  $G$  and the genetic parameters  $\mu$ ,  $a$  and  $d$ . Here  $G_2$ ,  $G_1$  and  $G_0$  are the genotypic values of genotypes  $QQ$ ,  $Qq$  and  $qq$ . We call  $D$  the genetic design matrix. The first and second columns of  $D$ , denoted by  $D_1$  and  $D_2$ , represent the status of the additive and dominance parameters of the three different genotypes.

Let loci M, with alleles  $M$  and  $m$ , and N with alleles  $N$  and  $n$ , denote two flanking markers for an interval where a putative QTL is being tested. Let the unobserved QTL locus Q with alleles Q and q be located in the interval flanked by markers M and N. The distribution of unobserved QTL genotypes can be inferred from the observed flanking marker genotypes according to the recombination frequencies between them. To infer the distribution of QTL genotype, we assume

Table 1: Conditional Probabilities of a putative QTL genotype given the flanking marker genotypes for an  $F_2$  population.

Marker genotypes	Expected frequency	QTL genotypes		
		$QQ(p_{j1})$	$Qq(p_{j2})$	$qq(p_{j3})$
$MN/MN$	$(1-r)^2/4$	1	0	0
$MN/Mn$	$r(1-r)/2$	$1-p$	$p$	0
$Mn/Mn$	$r^2/4$	$(1-p)^2$	$2p(1-p)$	$p^2$
$MN/mN$	$r(1-r)/2$	$p$	$1-p$	0
$MN/mn$ (or $mN/Mn$ )	$(1-r)^2/2 + r^2/2$	$cp(1-p)$	$1-2cp(1-p)$	$cp(1-p)$
$Mn/mn$	$r(1-r)/2$	0	$1-p$	$p$
$mN/mN$	$r^2/4$	$p^2$	$2p(1-p)$	$(1-p)^2$
$mN/mn$	$r(1-r)/2$	0	$p$	$1-p$
$mn/mn$	$(1-r)^2/4$	0	0	1

$p=r_{MQ}/r_{MN}$ , where  $r_{MQ}$  is the recombination fraction between the left marker M and the putative QTL and  $r_{MN}$  is the recombination fraction between two flanking markers M and N.  $c=r_{MN}^2/[r_{MN}^2+(1-r_{MN})^2]$ . The possibility of a double recombination event in the interval is ignored.

that there is no crossover interference and also that double recombination events within the interval are very rare and can be ignored to simplify the analysis. The conditional probabilities of the QTL genotypes given marker genotypes are given in Table 1 for the  $F2$  population. We extract the conditional probabilities from this table to form a matrix  $\mathbf{Q}$  for  $F2$  population.

## 2.1 Statistical Model for SIM Approach

Let us assume no epistasis between QTLs, no interference in crossing over, and only one QTL in the testing interval. A statistical model for SIM approach based on the genetic model (1) for testing a QTL in a marker interval is defined as

$$y_j = \mu + ax_j^* + dz_j^* + e_j^*, \quad (2)$$

where

$$(x_j^*, z_j^*) = \begin{cases} (1, -1/2) & \text{for } QQ \\ (0, 1/2) & \text{for } Qq \\ (-1, -1/2) & \text{for } qq \end{cases}$$

$y_j$  is the phenotypic value of the  $j$ th individual,  $\mu$  is the general mean effect; and  $e_j$  is a random error. We assume  $e_j \sim N(0, \sigma^2)$ . To investigate the existence of a QTL at a given position in a marker interval, we want to test the following statistical hypothesis.

Null Hypothesis,  $H_0$ :  $a=0$  and  $d=0$  (i.e. there is no QTL at a given position).

Alternative Hypothesis,  $H_1$ :  $H_0$  is not true (i.e. there is a QTL at a given position).

## 2.2 SIM Approach by Maximizing Likelihood Function

In the SIM model (2), each phenotypic observation ( $y_j$ ) is assumed to follow a mixture of three possible Gaussian densities with different means and mixing proportion, since observation  $y_j$ 's are influenced by three QTL genotypes  $QQ$ ,  $Qq$  and  $qq$ . Therefore, the density of each phenotypic observation ( $y_j$ ) is defined as

$$f(y_j | \theta) = \sum_{i=1}^3 p_{ji} \phi\left(\frac{y_j - \mu_{ji}}{\sigma}\right), \quad (3)$$

where  $\theta=(\mu, p, a, d, \sigma^2)$ ,  $\phi$  is a standard normal probability density function,  $\mu_{j1}=\mu+a-d/2$ ,  $\mu_{j2}=\mu + d/2$  and  $\mu_{j3} = \mu - a - d/2$ . The mixing proportions  $p_{ji}$ 's which are functions of the QTL position parameter  $p$ , are conditional probabilities of QTL genotypes given marker genotypes. For  $n$  individuals, the likelihood function for  $\theta=(\mu, p, a, d, \sigma^2)$  is given by

$$L(\theta | \mathbf{Y}) = \prod_{j=1}^n f(y_j | \theta). \quad (4)$$

To test  $H_0$  against  $H_1$ , the likelihood ratio test (LRT) statistic is defined as

$$\begin{aligned} \text{LRT} &= -2 \log \left[ \frac{\sup_{\theta_0} L(\theta | \mathbf{Y})}{\sup_{\theta} L(\theta | \mathbf{Y})} \right] \\ &= 2[\log \sup_{\theta} L(\theta | \mathbf{Y}) - \log \sup_{\theta_0} L(\theta | \mathbf{Y})], \end{aligned} \quad (5)$$

where  $\theta_0$  and  $\theta$  are the restricted and unrestricted parameter spaces. The threshold value to reject the null hypothesis can't be simply chosen from a chi-square distribution because of the violation of regularity conditions of asymptotic theory under  $H_0$ . The number and size of intervals should be considered in determining the threshold value since multiple tests are performed in mapping. The hypothesis are usually tested at every position of an interval and for all intervals of the genome to produce a continuous LRT statistic profile. At every position, the position parameter  $p$  is predetermined and only  $a, d, \mu$  and  $\sigma^2$  are involved in estimation and testing. If the tests are significant in a chromosome region, the position with the largest LRT statistic is inferred as the estimate of the QTL position  $p$ , and the MLEs at this position are the estimates of  $a, d, \mu$  and  $\sigma^2$  obtained by EM algorithm treating the normal mixture model as an incomplete-data problem [8]. Note that EM algorithm has been also used to obtain MLEs in several studies of QTL mapping analysis [6, 7].

### 3. ROBUSTIFICATION OF SIM APPROACH BY MAXIMIZING $\beta$ -LIKELIHOOD FUNCTION

The  $\beta$ -likelihood function for  $\theta = (\mu, p, a, d, \sigma^2)$  as defined in equation (3) is given by

$$L_\beta(\theta | \mathbf{Y}) = \frac{1}{\beta} \left[ \frac{1}{n l_\beta(\theta)} \sum_{j=1}^n \{f(y_j | \theta)\}^\beta - 1 \right], \quad (6)$$

where

$$l_\beta(\theta) = \left[ \int \{f(y | \theta)\}^\beta dy \right]^{\beta/(1+\beta)}.$$

Note that maximization of  $\beta$ -likelihood function is equivalent to the minimization of  $\beta$ -divergence for estimating  $\theta$  [10]. The  $\beta$ -likelihood function reduces to the log-likelihood function for  $\beta \rightarrow 0$ . In this paper, our proposal is to use the  $\beta$ -LOD score for the evidence of a QTL in a marker interval from the robustness point of view. It is defined by

$$\text{LOD}_\beta = 2n[\sup_\theta L_\beta(\theta | \mathbf{Y}) - \sup_{\theta_0} L_\beta(\theta | \mathbf{Y})], \quad (7)$$

where  $\theta_0$  and  $\theta$  are the restricted and unrestricted parameter spaces as before. For  $\beta \rightarrow 0$ , the  $\text{LOD}_\beta$  reduces to the likelihood ratio test (LRT) criterion as defined in equation. The threshold value to reject the null hypothesis  $H_0$  can be computed by permutation test following the work of Churchill and Doerge [2]. At every position, the position parameter  $p$  is predetermined and only  $a, d, \mu$  and  $\sigma^2$  are involved in estimation and testing as before. If the tests are significant in a chromosome region, the position with the largest  $\text{LOD}_\beta$  is inferred as the estimate of the QTL position  $p$ , and the  $\beta$ -estimators at this position are the estimates of  $a, d, \mu$  and  $\sigma^2$  obtained by EM algorithm treating the normal mixture model as an incomplete-data problem.

#### 3.1 Maximization of $\beta$ -Likelihood Function Using EM Algorithm

The EM algorithm can be used for obtaining the maximum  $\beta$ -likelihood estimators of  $a, d, \mu$  and  $\sigma^2$  treating the normal mixture model as an incomplete-data density. Let

$$(x_j^*, z_j^*) = \begin{cases} p_{j1} & \text{if } x_j^* = 1, z_j^* = -\frac{1}{2} \\ p_{j2} & \text{if } x_j^* = 0, z_j^* = \frac{1}{2} \\ p_{j3} & \text{if } x_j^* = -1, z_j^* = -\frac{1}{2} \end{cases}$$

be the distribution of QTL genotype specified by  $x_j^*$  and  $z_j^*$ . Let us treat the unobserved QTL genotypes ( $x_j^*$  and  $z_j^*$ ) as missing data, denoted by  $y_{j(\text{mis})}$ , and the trait  $y_j$  as observed data, denoted by  $y_{j(\text{obs})}$ . Then, the combination of  $y_{j(\text{mis})}$  and  $y_{j(\text{obs})}$  is the complete data, denoted by  $y_{j(\text{com})}$ . The conditional distribution of observed data, given missing data, is considered as an independent sample from a population such that  $y_j | (\theta, x_j^*, z_j^*) \sim N(\mu + ax_j^* + dz_j^*, \sigma^2)$

The complete-data density model in this problem is regarded as a two-stage hierarchical model. First the values of random variables ( $x_j^*, z_j^*$ ) are sampled by a trinomial experiment to decide QTL genotype, and then a normal variate for that genotype is generated. The values of random variables ( $x_j^*, z_j^*$ ) of individual  $j$  are (1, -1/2), (0, 1/2) or (-1, -1/2) for QTL genotype QQ, Qq, or qq with probability  $p_{j1}$ ,  $p_{j2}$  or  $p_{j3}$ , respectively. Thus the complete-data density function is given by

$$\varphi(y_{j(\text{com})} | \theta) = \left\{ p_{j1} \phi\left(\frac{y_j - \mu_{j1}}{\sigma}\right) \right\}^{-\frac{1}{2}(x_j^*+1)(z_j^*-\frac{1}{2})} \times \left\{ p_{j2} \phi\left(\frac{y_j - \mu_{j2}}{\sigma}\right) \right\}^{(x_j^*+1)(z_j^*+\frac{1}{2})} \\ \times \left\{ p_{j3} \phi\left(\frac{y_j - \mu_{j3}}{\sigma}\right) \right\}^{\frac{1}{2}(x_j^*-1)(z_j^*-\frac{1}{2})}. \quad (8)$$

At a given position,  $p$  is determined. The EM algorithm is used for obtaining the maximum  $\beta$ -likelihood estimators of  $a$ ,  $d$ ,  $\mu$  and  $\sigma^2$  for the complete-data density. The iteration of the  $(t+1)$  EM-step is as follows:

**E-step:** The conditional expected complete-data  $\beta$ -likelihood with respect to the conditional distribution of  $Y_{\text{mis}}$  given  $Y_{\text{obs}}$  and the current estimated parameter value  $\theta^{(t)}$  is given by

$$Q_\beta(\theta | \theta^{(t)}) = \int L_\beta(\theta | Y_{\text{com}}) h(Y_{\text{mis}} | Y_{\text{obs}}, \theta = \theta^{(t)}) dY_{\text{mis}} \\ = \frac{1}{n \beta b_\beta(\theta)} \sum_{j=1}^n \sum_{i=1}^3 \left\{ p_{ji} \phi\left(\frac{y_j - \mu_{ji}}{\sigma}\right) \right\}^\beta \times \pi_{ji}^{(t)} - \frac{1}{\beta}, \quad (9)$$

where

$$b_\beta(\theta) = (1 + \beta)^{-\beta/2(1+\beta)} (2\pi\sigma^2)^{-\beta^2/2(1+\beta)}$$

and

$$\pi_{ji} = \frac{p_{ji} \phi\left(\frac{y_j - \mu_{ji}}{\sigma}\right)}{\sum_{i=1}^3 p_{ji} \phi\left(\frac{y_j - \mu_{ji}}{\sigma}\right)}$$

which is the posterior probability of  $j$ -th individual given the  $i$ -th QTL genotype,  $i=1, 2$  and  $3$  for QTL genotypes QQ, Qq and qq, respectively.

**M-step:** Find  $\theta^{(t+1)}$  to maximize the conditional expected  $\beta$ -likelihood by taking the derivatives of  $Q_\beta(\theta | \theta^{(t)})$  with respect to each parameter. The solutions of parameters in closed form are as follows.

$$\mu^{(t+1)} = \left[ \mathbf{1}_n^T \left\{ \mathbf{Y} \# (\Pi_\beta^{(t)} \mathbf{1}_3) - \Pi_\beta^{(t)} \mathbf{D} \mathbf{E}^{(t)} \right\} \mathbf{1}_n^T \Pi_\beta^{(t)} \mathbf{1}_3 \right]^{-1}, \quad (10)$$

$$a^{(t+1)} = \frac{(\mathbf{Y} - \mathbf{1}_n \mu^{(t+1)})^T \Pi_\beta^{(t)} \mathbf{D}_1 - \mathbf{1}_n^T \Pi_\beta^{(t)} (\mathbf{D}_1 \# \mathbf{D}_2) \mathbf{d}^{(t)}}{\mathbf{1}_n^T \Pi_\beta^{(t)} (\mathbf{D}_1 \# \mathbf{D}_1)}, \quad (11)$$

$$d^{(t+1)} = \frac{(Y - \mathbf{1}_n \mu^{(t+1)})^T \Pi_{\beta}^{(t)} D_2 - \mathbf{1}_n^T \Pi_{\beta}^{(t)} (D_1 \# D_2) a^{(t+1)}}{\mathbf{1}_n^T \Pi_{\beta}^{(t)} (D_2 \# D_2)} \quad (12)$$

and

$$\sigma^{2(t+1)} = (1 + \beta)[(Y - \mathbf{1}_n \mu^{(t+1)})^T \{ (Y - \mathbf{1}_n \mu^{(t+1)}) \# (\Pi_{\beta} \mathbf{1}_3) \} - 2(Y - \mathbf{1}_n \mu^{(t+1)})^T \Pi_{\beta}^{(t)} DE^{(t+1)} - E^{(t+1)^T} V^{(t)} E^{(t+1)}] [\mathbf{1}_n^T \Pi_{\beta}^{(t)} \mathbf{1}_3]^{-1}, \quad (13)$$

where

$$V = \begin{bmatrix} \mathbf{1}_n^T \Pi_{\beta} (D_1 \# D_1) & \mathbf{1}_n^T \Pi_{\beta} (D_1 \# D_2) \\ \mathbf{1}_n^T \Pi_{\beta} (D_2 \# D_1) & \mathbf{1}_n^T \Pi_{\beta} (D_2 \# D_2) \end{bmatrix}$$

which is a symmetric matrix. Here  $\#$  denotes Hadamards product, which is the element-by-element product of corresponding elements of two same-order matrices and

$$\Pi_{\beta} = \left\{ \left[ \exp \left\{ -\frac{1}{2} \left( \frac{y_j - \mu_{ji}}{\sigma} \right)^2 \right\} \right]^{\beta} \pi_{ji} \right\}_{n \times 3}$$

which is called the matrix of  $\beta$ -weighted posterior probabilities. For  $\beta=0$ , the matrix  $\Pi_{\beta}$  reduces to the matrix of standard posterior probabilities. It should be noted here that each element of  $n$ -vector  $\mathbf{1}_n$  is 1. The  $E$  and  $M$  steps are iterated until a convergent criterion is satisfied. The converged values of  $a$ ,  $d$ ,  $\mu$  and  $\sigma^2$  are the values of minimum  $\beta$ -divergence estimators. Note that minimum  $\beta$ -divergence estimators (10-13) with  $\beta=0$  reduce to maximum likelihood estimators (MLE) of SIM for QTL analysis.

Under null hypothesis  $H_0: a=0, d=0$ , the minimum  $\beta$ -divergence estimators for the parameters  $\mu$  and  $\sigma^2$  are obtained iteratively as follows

$$\mu^{(t+1)} = [Y W_{\beta}^{(t)}] [\mathbf{1}_n^T w_{\beta}^{(t)}]^{-1} \quad (14)$$

and

$$\sigma^{2(t+1)} = (1 + \beta)(Y - \mathbf{1}_n \mu^{(t+1)})^T [(Y - \mathbf{1}_n \mu^{(t+1)}) \# W_{\beta}^{(t)}] [\mathbf{1}_n^T w_{\beta}^{(t)}]^{-1}, \quad (15)$$

where

$$W_{\beta} = \left[ \exp \left\{ -\frac{\beta}{2} \left( \frac{y_j - \mu}{\sigma} \right)^2 \right\} \right]_{n \times 1}$$

which is called the  $\beta$ -weight vector.

#### 4. SIMULATION RESULTS

To illustrate the performance of the proposed method in a comparison of SIM approach [8] for QTL analysis, we consider  $F2$  intercross population for simulation study. In this study, we assume only one QTL on a chromosome with 10 equally spaced markers, where any two successive marker interval size is 5 cM. Marker positions and their genotypes are generated using R/qt1

software [1], homepage: <http://www.rqtl.org/>). The successive marker interval size 5 is considered. The QTL position is located by the 5<sup>th</sup> marker of chromosome-10. The true values for the parameters in the SIM model are assumed as  $a=0.4$ ,  $d=0.8$ ,  $\mu=0.05$  and  $\sigma^2=1$ . We randomly generated 250 trait values with heritability  $h^2=0.2$  using the SIM model (2). A trait with heritability  $h^2=0.2$  means that 20% of the trait variation is controlled by QTL and the remaining 80% is subject to the environmental effects (random error).

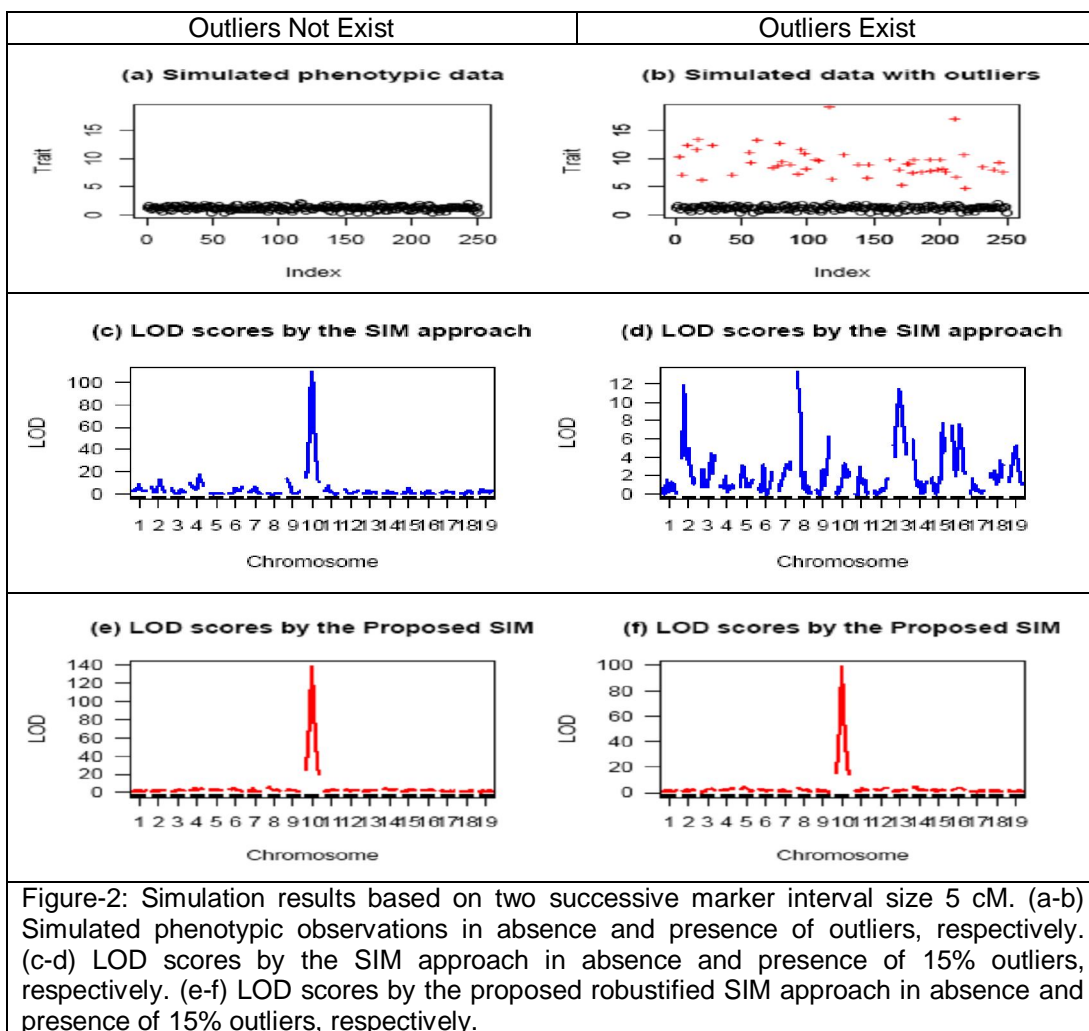


Figure 2(a) represent the scatter plot of a sample of 250 trait values and a covariate. To investigate the robustness of the proposed method in a comparison of the SIM method for QTL mapping, we replaced 15% trait values randomly in each replication of the previous example by outliers (+) so that data contamination rate is 15% in each replication. Figures 2(b) represent the scatter plot of a sample of 250 trait values in presence of outliers.

To determine the QTL position, we compute LOD scores by both the SIM and the proposed robust SIM method. It should be noted here that the name 'LOD scores' is used for convenience of presentation instead of both LRT scores of SIM method and the  $\beta$ -LOD scores of the proposed method. According to the theoretical settings, the largest LOD score should be occurred with the true QTL positions in the entire genome. We computed LOD scores by both SIM and robust SIM approaches. Figures 2(c) and 2(e) represents the LOD scores at every 2 cM position in the chromosomes in absence of outliers by SIM and the proposed method, respectively. Similarly,

figures 2(d) and 2(f) represents the LOD scores at every 2 cM position in the chromosomes in presence of outliers by SIM and the proposed method, respectively. It is seen that the highest and significant LOD score peak occurs with the true QTL position in the chromosome 10 by both methods in absence of outliers, while in presence of phenotypic outliers, highest and significant LOD score peak occurs with the true QTL position by the proposed method only. Therefore, performance of both methods is almost same and good in absence of outliers, while the performance of the proposed method is better than the SIM approach in presence of outliers.

## 5. CONCLUSION

This paper proposes the robustification of the SIM algorithm for QTL mapping by maximizing  $\beta$ -likelihood function using EM like algorithm. The  $\beta$ -likelihood function reduces to the log-likelihood function for  $\beta \rightarrow 0$ . The proposed robust SIM algorithm with the tuning parameter  $\beta=0$  reduces to the traditional SIM algorithm. The value of the tuning parameter  $\beta$  has a key role on the performance of the proposed method for QTL mapping. An appropriate value for the tuning parameter can be selected by cross-validation [10]. However, one can choose  $\beta \in (0.1, 0.5)$ , heuristically. Simulation results show that the robustified SIM algorithm with  $\beta>0$  significantly improves the performance over the SIM approach in presence of phenotypic outliers. It keeps equal performance otherwise.

## 6. REFERENCES

1. K. W. Broman, H. Wu, S. Sen and G. A. Churchill. "R/qtl: QTL mapping in experimental crosses". *Bioinformatics*, Vol. **19**, pp. 889-890, 2003.
2. G. A. Churchill and R. W. Doerge., "Empirical Threshold Values for Quantitative Trait Mapping". *Genetics*, Vol **138**, pp. 963-971, 1994.
3. A. P. Dempster, Laird, and Rubin, D. B.: "Maximum likelihood from incomplete data via the EM algorithm". *J. Roy. Statist. Soc. B*, **39**, pp. 1-38, 1977.
4. Elston, R. C., Stewart, J. "The Analysis of Quantitative Traits for Simple Genetic Models from Parental, F1 and Backcross Data". *Genetics*, **73**, pp. 695-711, 1973.
5. C. S. Haley and S. A. Knott. "A simple regression method for mapping quantitative trait in line crosses using flanking markers". *Heredity* **69**, pp.315-324, 1992.
6. R. C. Jansen, "A general mixture model for mapping quantitative trait loci by using molecular markers". *Theor Appl Genet.*, **85**, 252-260, 1992.
7. C. H. Kao. "On the differences between maximum likelihood and regression interval mapping in the analysis of quantitative trait loci". *Genetics*, **156**, pp.855-865, 2000.
8. E. S. Lander and D. Botstein. "Mapping Mendelian factors underlying quantitative traits using RFLP linkage maps". *Genetics*, **121**, pp. 185-199, 1989.
9. M. N. H. Mollah and S. Eguchi. "Robust Composite interval Mapping for QTL Analysis by Minimum  $\beta$ -Divergence Method". Proceedings of the IEEE International Conference on Bioinformatics and Biomedicine (IEEE BIBM08) , pp. 115-120, Philadelphia, USA, 2008.
10. M. N. H. Mollah, N. Sultana, M. Minami and S. Eguchi. "Robust extraction of local structures by the minimum  $\beta$ -divergence method". *Neural Network*, **23**, pp. 226-238, 2010.
11. A. H. Paterson, S. Damon, J. D. Hewitt, D. Zamir, H. D. Rabinowitch, S.E. Lincoln, E. S. Lander, S.D.Tanksley. "Mendelian factors underlying quantitative traits in tomato: comparison across species, generations and environments". *Genetics*, **127**, pp. 181-197, 1991.
12. J. M. Thoday. "Effects of disruptive selection. III. Coupling and repulsion". *Heredity*, **14**, pp. 35-49, 1960.

# Identification of Obstructive Sleep Apnea from Normal Subjects: FFT Approaches Wavelets

**Abdulnasir Hossen**

*Department of Electrical and Computer Engineering  
College of Engineering  
Sultan Qaboos University  
P.O. Box 33, PC 123, Al-Khoud, Muscat, Oman*

abhossen@squ.edu.om

---

## Abstract

An FFT-based algorithm for Obstructive Sleep Apnea (OSA) patient identification using R-R interval (RRI) data is investigated. The identification is done on the whole record as OSA patient or non-patient (normal). The power spectral density of the three main bands of the RRI data is computed and then three identification factors are calculated from their ratios. The first identification factor is the ratio of the PSD of the low-frequency (LF) band to that of the high-frequency (HF) band. The second identification factor is the ratio of the PSD of the very low-frequency (VLF) band to that of the low-frequency (LF) band, while the third identification factor is the ratio of the PSD of the very low-frequency (VF) band to that of the high-frequency (HF) band. The RRI data used in this work were drawn from MIT database. The three identification factors are tested on MIT trial data. The best factor, which is the (VLF/LF) PSD ratio, is then tested on MIT test data and to evaluate the performance of the identification. The efficiency of identification approaches 87%. The method is then improved by applying FFT on short records and averaging the results to get an efficiency of 93%. Another improvement was done by zero-padding the short records to double its size and then averaging the results to get an efficiency of 93%. This efficiency is compared with a previous work on the same purpose using wavelets which resulted in 90% accuracy.

**Keywords:** Obstructive Sleep Apnea, Non-Invasive Diagnosis, Identification, Spectral Analysis, FFT, Wavelets

---

## 1. INTRODUCTION

Sleep apnea is a common sleep disorder that is defined as a complete or partial cessation of breathing during sleep [1].

Obstructive sleep apnea (OSA) is the common form of apnea that occurs when the upper airway is completely or partially obstructed due to the relaxation of dilating muscles. Hypoapnea occurs when the airway is partially collapsed and causes 50% reduction of air accompanied by oxygen desaturation of 4% or greater [2]. The severity of apnea is measured by a commonly used standard such as the apnea/hypoapnea index (AHI), which is the number of apnea and hypoapnea events per hour [1]. Most clinicians regard an apnea index below 5 as normal, and an apnea index of 10 or more as pathologic.

In the general population, the greatest challenge for primary care providers lies in determining which patients with some symptoms such as snoring warrant further evaluation, as most patients with OSA snore, but most snorers do not have OSA [3]. In developed countries the cost of investigating these symptoms has increased considerably during the last decade as the only reliable method for the diagnosis of OSA until now is overnight sleep studies (Polysomnography) [4], which is a cumbersome, time consuming and expensive procedure requiring specially trained polysomnographers and needs recording of EEG, EOG, EMG, ECG, nasal air respiratory effort and oxygen saturation [1].

Therefore, it is of a great importance and interest to have automatic screening algorithms on a single-lead ECG signals. This will reduce the pressure on sleep laboratories and make it possible to diagnose sleep apnea inexpensively from ECG recordings acquired in the patient's home.

Heart rate variability (HRV) is referred to as the beat-to-beat variation in heart rate. Instantaneous heart rate is measured as the time in seconds between peaks of two consecutive R waves of the ECG signal. This time is referred to as the RRI. The variation of heart rate accompanies the variation of several physiological activities such as breathing, thermoregulation and blood pressure changes [5]. HRV is a result of continuous alteration of the autonomic neural regulation of the heart i.e. the variation of the balance between sympathetic and parasympathetic neural activity. The increase of sympathetic tone or decrease of parasympathetic activity will increase heart rate [5]. Theoretically, in OSA the cessation of breathing will cause the respiration center in the brain to activate its autonomic components (sympathetic and parasympathetic) which send feed back impulses to the heart to compensate for the lack of O<sub>2</sub> and low blood pressure. This interaction between the heart and the brain is reflected into the beat-to-beat variation of heart rate. Therefore the analysis of HRV in time-domain or in frequency-domain should somehow reveal the variations in breathing.

Frequency-domain analysis approaches use one of the signal transformations such as FFT, STFT, wavelet transform to estimate the power spectral density of the RRI data. The frequency spectrum of the RRI data is divided into three main bands:

- The very low-frequency band (VLF):  $f \in (0.0033 - 0.04)$  Hz.
- The low-frequency band (LF):  $f \in (0.04 - 0.15)$  Hz.
- The high-frequency band (HF):  $f \in (0.15 - 0.4)$  Hz.

The LF component reflects the sympathetic tone in heart regulation, while the HF component reflects the parasympathetic tone and is also related to the frequency of respiration [6]. The ratio LF/HF describes the balance between sympathetic and parasympathetic neural activity. However the physiological background of the VLF component is not well unknown but is proposed to be associated with thermoregulation, vasomotor activity, or the rennin-angiotensin system [7].

The LF/HF ratio has been used by some researchers to represent the sympathetic modulation of the heart rate, however this interpretation is not universally accepted. A major limitation of applying the HF component is that it is highly sensitive to differences in ventilation and breathing pattern within and across individuals [8].

In OSA patients, the respiratory modulation of heart rate is not confined to within-breath changes but also takes the form of large cyclical variations that correlate with the episodic apneas. These oscillations generally fall into the VLF band (between 0.01 and 0.04 Hz) [9].

The FFT is used as identification tool of OSA within an efficiency of 87% using the (VLF/LF) PSD ratio as an identification factor on whole records of MIT data [10]. In this work, this technique is improved by applying it on short records and averaging the results for final accuracy. Another improvement is also done by zero-padding the short records and applying the FFT on longer records and averaging for finding the final accuracy.

## 2. MATERIAL AND METHODS

### 2.1. Data Description

The ECG data used in this work were taken from the MIT data base [11]. The data contain 30 trial records and 30 test records. These data sets are single channel ECGs that were extracted from polysomnographic recordings with a sampling rate of 100 Hz for an average duration of 8 hours. The sleep recordings originated from 32 subjects (25 men and 7 women) between 27 and 63 years of age, with weight between 53 and 135 kg. Recordings from 17 of the 32 subjects were represented in the trial set and in the test set; eight subjects were only in the test set, and the remaining seven subjects were only in the trial set. The duration of the recordings varied between 401 and 578 min (average: 492, standard deviation: 32 min).

A total of 40 OSA records and 20 normal records were used in this study. MIT-trial records were used to setup the screen algorithm, which is then applied to the MIT-test records. The ECG data sets are listed in Table 1.

Data	OSA Records	Normal Records
MIT Trial	20	10
MIT Test	20	10

TABLE 1. ECG Data Sets

### 2.2. Pre-Processing of Data

#### 2.2.1 QRS Detection

The accuracy of the identification algorithm depends primarily on the accuracy of the (QRS) detection (R peak detector) that is used to obtain the RRI signal from the raw ECG data. The QRS detection and beat classification (normal or not) is accomplished by the single-lead threshold based ECG wave boundaries detector "Ecgpuwave", which is available on the physionet website [12]. The raw RRI data used in this work are the Normal-to-Normal (NN) intervals obtained directly from the QRS detector without any smoothing and filtering steps; therefore it could contain false intervals, missed and/or ectopic beats.

#### 2.2.2 Outliers Removing and Resampling

The simple approach that is used to exclude false RRI is to bound the RRI with lower and upper limits of 0.4 and 2 seconds respectively [9]. Therefore all RRI samples beyond these limits are excluded. Further removal of outliers is achieved by using of a sliding 41-points moving average filter (MAF) as follows: A local mean is computed for every 41 consecutive RRI excluding the

central interval. The output of the MAF is used as a reference measure to reject or accept the central RRI. If the central RRI is within 20% of the computed local mean, then it is qualified as true RRI otherwise it is an outlier and excluded from the RRI data. Re-sampling at 1 Hz and estimation of missed value are intended to generate equally spaced RRI [13].

### 3. IMPLEMENTATION AND RESULTS

#### 3.1 Evaluation Measures

A classifier is a parameter or a variable, with a suitable optimal threshold, that is used in a classification algorithm. In this study, only binary classification is considered, e.g. classification between two different cases, positive (OSA) and negative cases (normal). The performance of a classifier is evaluated by three main metrics: Specificity, Sensitivity and Accuracy as follows [14]:

$$\text{Specificity} = \frac{\text{TN}}{\text{TN} + \text{FP}} * 100 \quad (1)$$

$$\text{Sensitivity} = \frac{\text{TP}}{\text{TP} + \text{FN}} * 100 \quad (2)$$

$$\text{Accuracy} = \frac{\text{TP} + \text{TN}}{\text{TP} + \text{FP} + \text{TN} + \text{FN}} * 100 \quad (3)$$

Where the entities in the above equation are defined in confusion matrix shown in Table 2, and T is the total number of data under test.

Actual Class <sup>a</sup>	Predicted Class <sup>a</sup>	
	Positive (P)	Negative (N)
Positive (P)	TP	FN
Negative (N)	FP	TN

<sup>a</sup>Positive = OSA, Negative = Normal, T=True, F=False

TABLE 2. The Confusion Matrix

Sensitivity represents the ability of a classifier to detect the positive cases, i.e. OSA cases. Specificity indicates the ability of a classifier to detect negative cases, e.g. normal cases. Accuracy represents the overall performance of a classifier. It indicates the percentage of correctly classified positive and negative cases from the total number of cases.

#### 3.1 FFT Results on long records

The FFT is applied on the whole record of each subject in the trial data. The PSD of the three main bands is found by summing the corresponding FFT results for the different bands. The PSD of the VLF band is taken from 0 to 0.03 Hz, while the PSD of the LF band and the HF band is selected as (0.03 to 0.15 Hz) and (0.15 to 0.4 Hz) respectively. The three identification factors are computed then from the calculated PSD values.

Figures (1-3) show the result of the 3 identification factors on MIT-trial data. The results of identification are shown on Table 3. The metrics used in Table 3 are the sensitivity [14] (accuracy

of identification of apnea cases), and the specificity [14] (accuracy of identification of normal cases) and the efficiency (accuracy of identification of all cases). It is to be concluded from Table 1 that the VLF/LF identification factor is better than the other two factors. The same algorithm is applied using the VLF/LF identification factor with the same threshold on the MIT-test data and results in 16/20 sensitivity and 10/10 specificity and total accuracy of 26/30. Fig.4 shows these results.

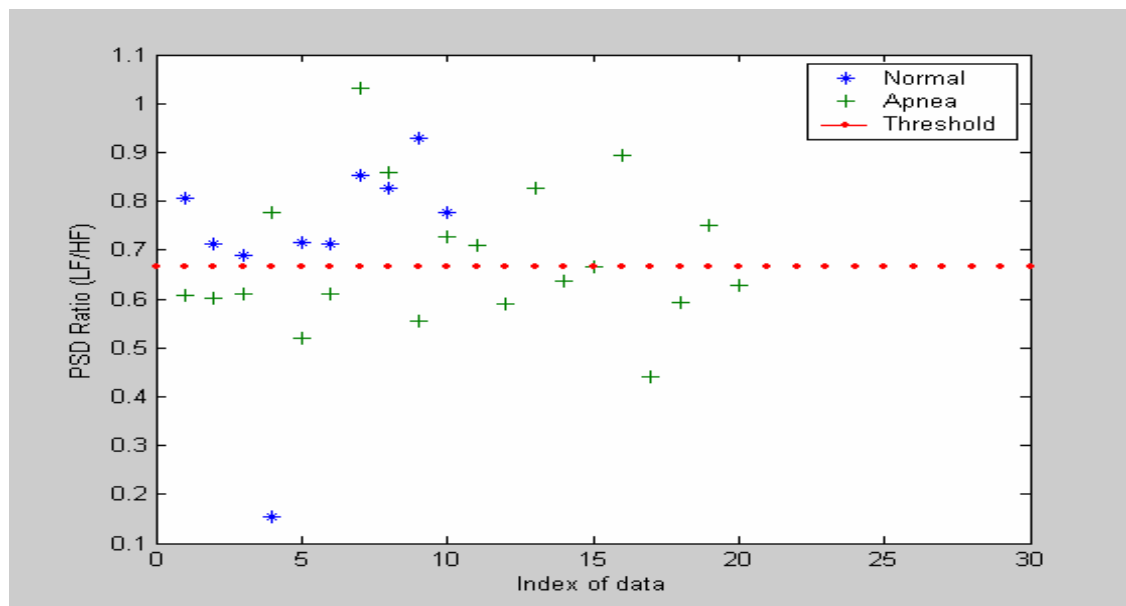


**FIGURE 1:** (LF/HF) PSD Ratio of OSA and Normal Subject of MIT-Trial Data using FFT on Long Record

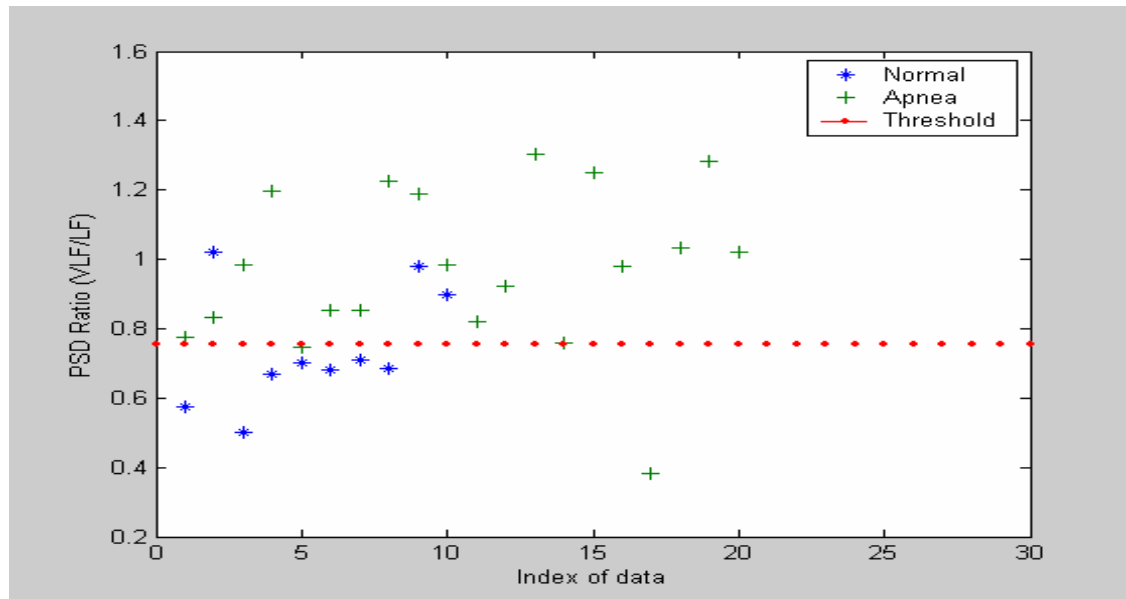


**FIGURE 2:** (VLF/LF) PSD Ratio of OSA and Normal Subject of MIT-Trial Data using FFT on Long Record

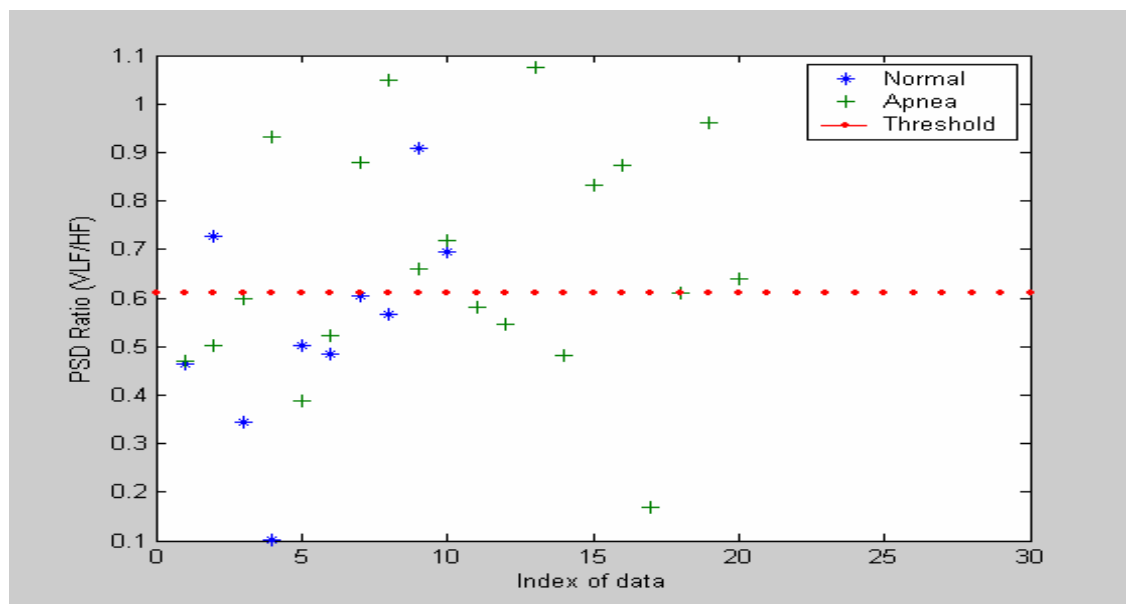


FIGURE 3: (VLF/HF) PSD Ratio of OSA and Normal Subject of MIT-Trial Data using FFT on Long Record

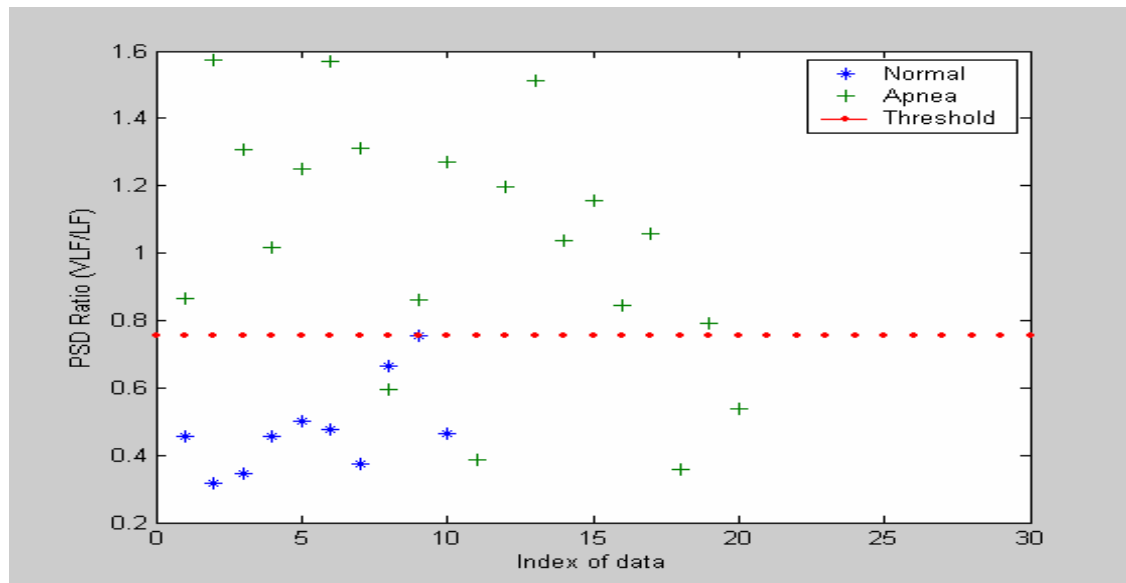


FIGURE 4: (VLF/LF) PSD Ratio of OSA and Normal Subject of MIT-test Data using FFT on Long Record

Identification factor	Specificity	Sensitivity	Accuracy	Threshold
LF/HF	9/10	12/20	21/30	0.666
VLF/LF	7/10	18/20	25/30	0.756
VLF/HF	7/10	11/20	18/30	0.61

TABLE 3: Different Results on MIT-Trial Data

### 3.2 Wavelet Results

A soft decision algorithm for approximate power spectral density estimation for Obstructive Sleep Apnea (OSA) patient classification using R-R interval (RRI) data is investigated in [15]. This algorithm is based on fast and approximate estimation of the entropy (simply logarithmic value of PSD) of the wavelet-decomposed bands of the RRI data. The classification is done on the whole record as OSA patient or non-patient (normal). This technique classifies correctly 28/30 of MIT-test data using Haar wavelet filters [15]. In order to compare the FFT results with wavelet results, the wavelet results are listed in Figures 5 and 6 for both trial and test data. See Table 4 for brief results.

Data	Specificity	Sensitivity	Accuracy
MIT-Trial	7/10	20/20	27/30
MIT-Test	8/10	20/20	28/30

TABLE 4: Different Results using Wavalets

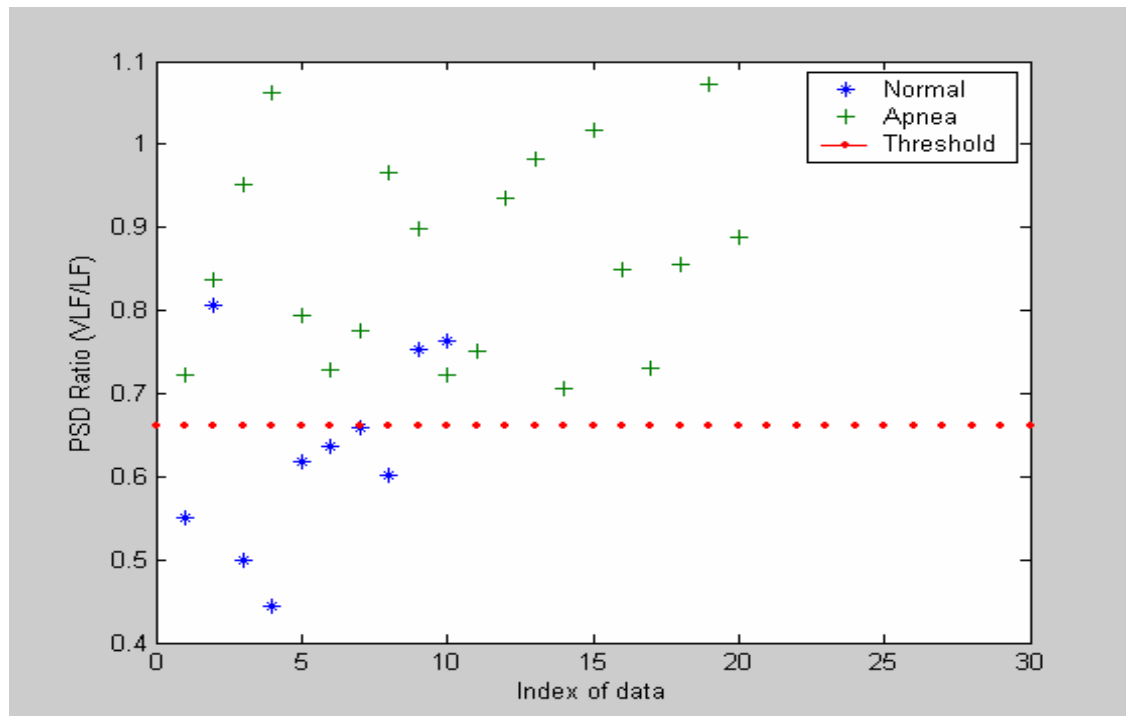
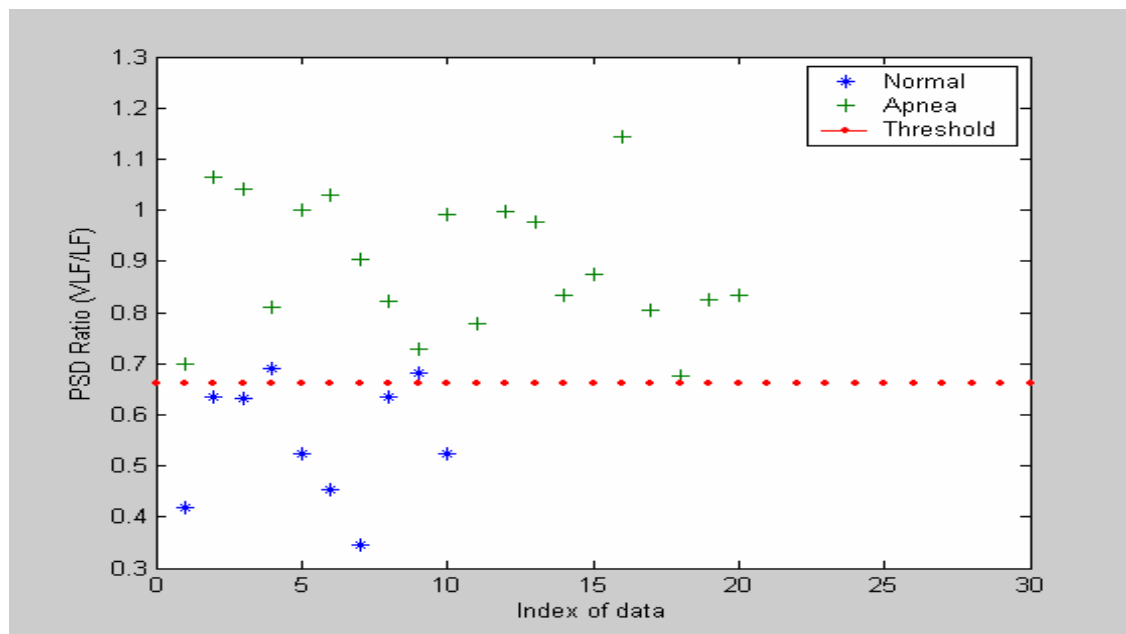
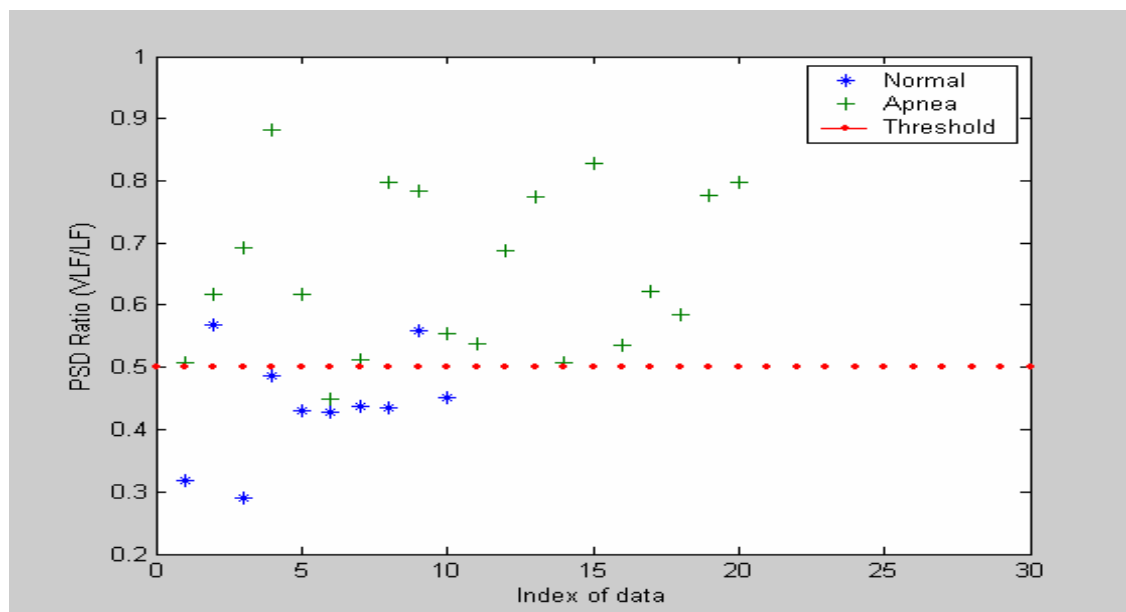


FIGURE 5: (VLF/LF) PSD Ratio of OSA and Normal Subject of MIT-Trial Data using Wavelets

**FIGURE 6:** (VLF/LF) PSD Ratio of OSA and Normal Subject of MIT-Test Data using Wavelets

### 3.3 FFT Short Recording

To enhance the results of FFT spectral analysis the whole record length of RRI data is divided into short records. The FFT is implemented on each short record and PSD ratio of the VLF band to that of the LF band is computed for each short record. The PSD of the whole record is then computed by averaging the results of the short records. Results on MIT trial data and MIT test data are shown in Fig. 7 and Fig. 8 respectively for a short record of length 128. Table 5 shows the MIT-test results using different lengths of short records.

**FIGURE 7:** (VLF'LF) PSD Ratio of OSA and Normal Subject of MIT-Trial Data using FFT Short Records

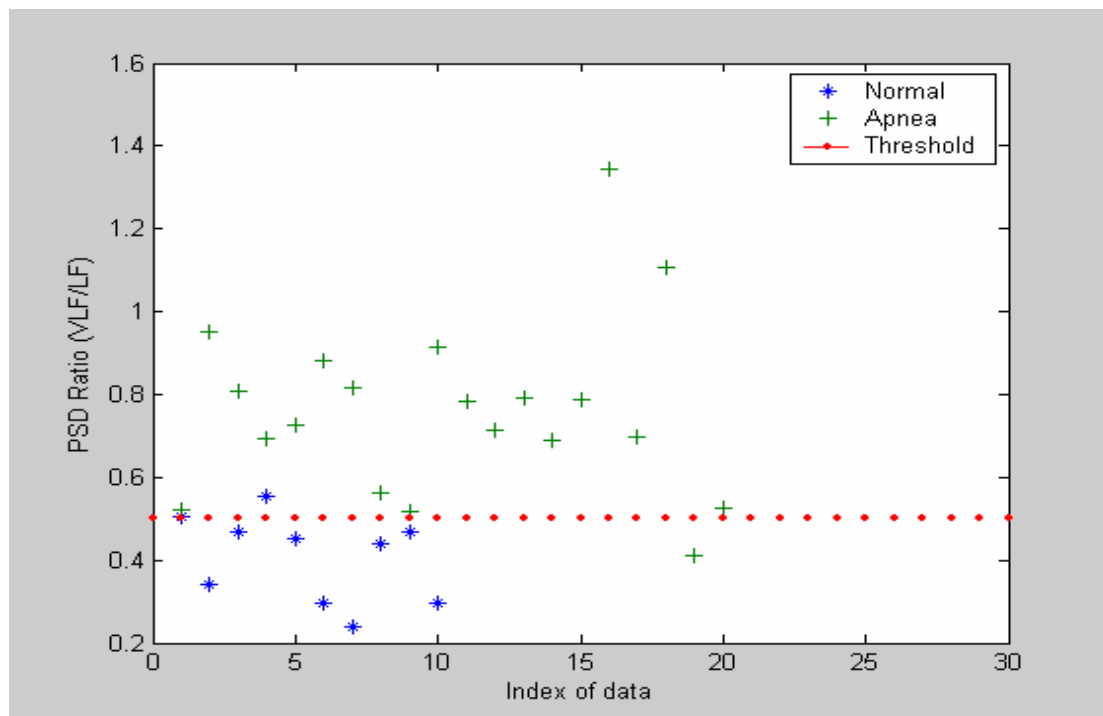


**FIGURE 8:** (VLF/LF) PSD Ratio of OSA and Normal Subject of MIT-Test Data using FFT Short Records

length of FFT	Specificity	Sensitivity	Accuracy
<b>2048</b>	6/10	19/20	25/30
<b>1024</b>	7/10	19/20	26/30
<b>512</b>	8/10	19/20	27/30
<b>256</b>	8/10	19/20	27/30
<b>128</b>	9/10	19/20	28/30

**TABLE 5:** Different Results of MIT-Test Data using FFT Short Records

### 3.4 FFT Short Recording with Zero-Padding

To increase the resolution of any spectral analysis an idea of zero-padding the signal to increase its length can be applied. We improve the results of our FFT spectral identification by adding zeros at the end of the short records to double its length and then the FFT algorithm is applied. The identification factor is found for each zero-padded short record and an average value is obtained then for the whole record. Fig. 9 and Fig. 10 show the results of MIT trail and MIT test data respectively by using a short record with 128 samples which is zero-padded with another 128 zeros. Table 6 lists the results of this improvement using different lengths.

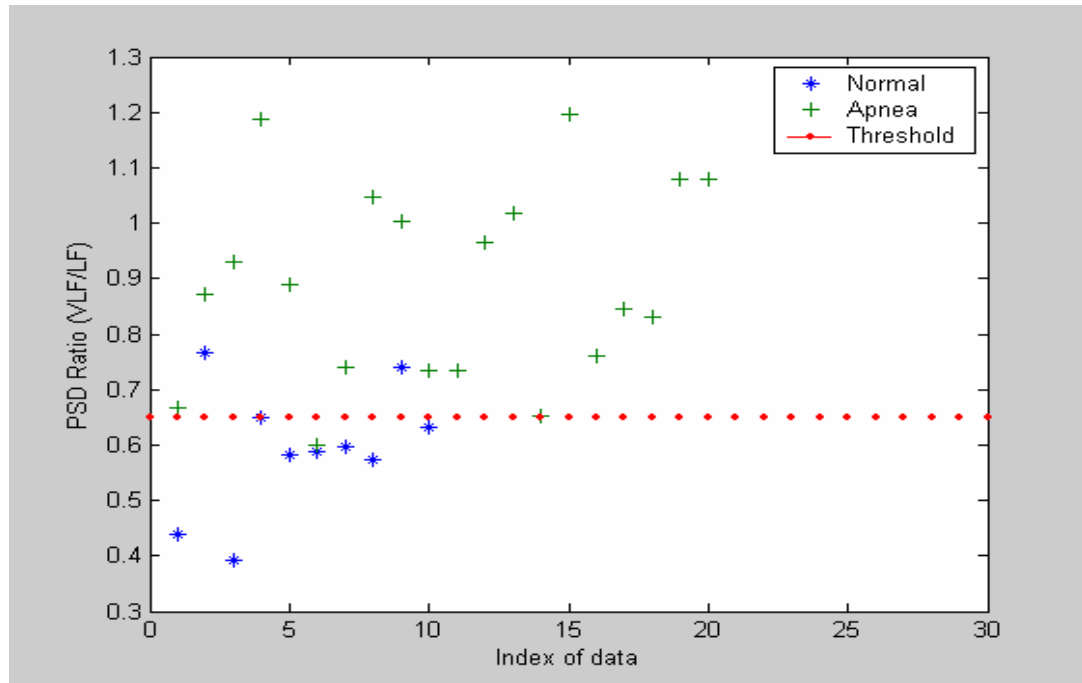


**FIGURE 9:** (VLF/LF) PSD Ratio of OSA and Normal Subject of MIT-Trial Data using FFT Short Records with Zero-Padding

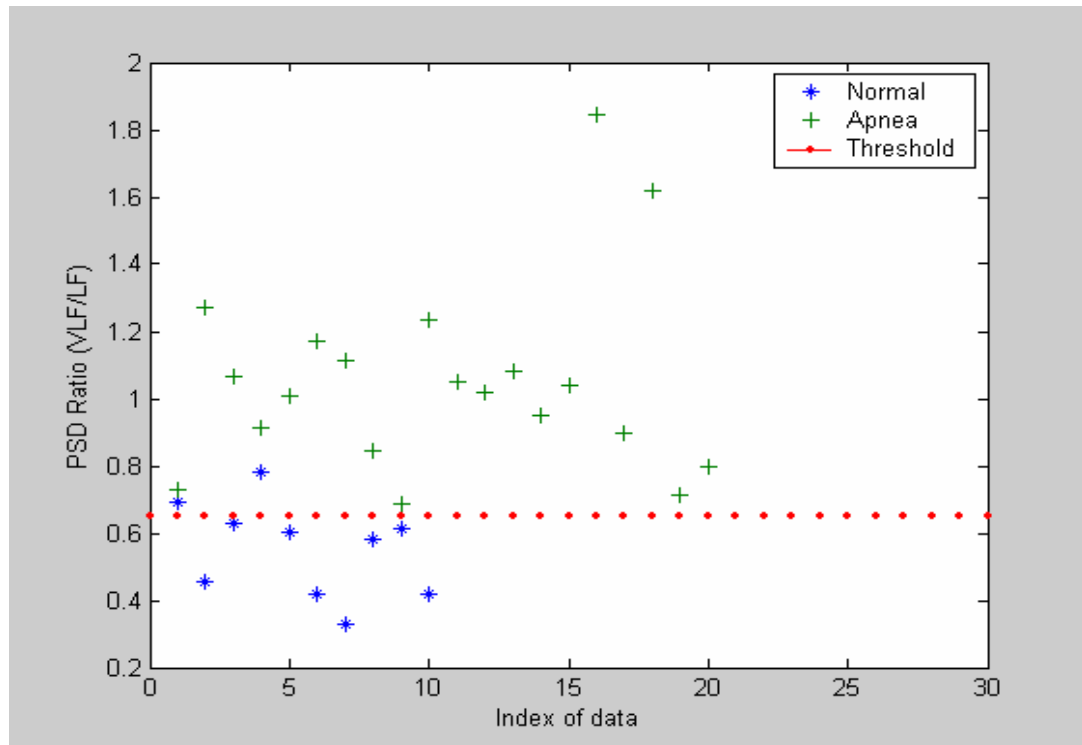


**FIGURE 10:** (VLF/LF) PSD Ratio of OSA and Normal Subject of MIT-Test Data using FFT Short Records with Zero-Padding

<b>length of FFT+ Zeros Padded</b>	<b>Specificity</b>	<b>Sensitivity</b>	<b>Accuracy</b>
<b>1024 + 1024</b>	6/10	20/20	26/30
<b>512 + 512</b>	8/10	19/20	27/30
<b>256 + 256</b>	8/10	20/20	28/30
<b>128 + 128</b>	8/10	20/20	28/30

**TABLE 6:** Different Results on MIT-Test Data using FFT Short Records with Zero-Padding

#### 4. SUMMARY AND CONCLUSIONS

A summary of results of all methods used in this work are listed in Table 7 for better comparison.

<b>Method</b>	<b>Specificity</b>	<b>Sensitivity</b>	<b>Accuracy</b>
<b>Wavelet</b>	8/10	20/20	28/30 = 93%
<b>FFT Long Recording</b>	8/10	19/20	26/30 = 87%
<b>FFT Short Recording</b>	8/10	20/20	28/30 = 93%
<b>FFT Short Recording + Zero Padding</b>	8/10	20/20	28/30 = 93%

**TABLE 7:** Different results on MIT-Test Data using different techniques

The FFT has been implemented in this work as an identification tool in diagnosing of obstructive sleep apnea. The data used is a raw RRI data after simple preprocessing step. The original data has been taken from MIT databases. The FFT spectral analysis of the three main frequency bands (VLF, LF, and HF) and their ratios has been computed for the MIT trail data. The VLF/LF PSD ratio was found as a best identification factor. This identification factor has been tested then on MIT-test data and resulted in almost 87% identification accuracy. The improvement of the technique by using short records raises the identification accuracy up to 93%. The same improvement is obtained by zero-padding the short records and applying FFTs on double length records. The identification accuracy of FFT approaches that accuracy obtained using soft-decision wavelet approach.

## REFERENCES

1. AASM Task Force Report, Sleep-related breathing disorders in adults, recommendations for syndrome definition and measurement techniques in clinical research. *Sleep*, Vol. 22(5), 667-689, 1999.
2. Kentucky Sleep Society, <http://www.kyss.org>.
3. T. Young, PE. Peppard, DJ. Gottlieb, "Epidemiology of obstructive sleep apnea", American Journal of Respiratory and Critical Care Medicine, 165: 1217-1239, 2000.
4. B. Taha, J. Dempsey, S. Weber, M. Badr, J. Skatrud, T. Young, A. Jacques, K. Seow, "Automated detection and classification of sleep-disordered breathing from conventional polysomnography data", *Sleep*, 20 (11): 991-1001, 1997.
5. Task Force of the European Society of Cardiology and the North American Society of Pacing and Electrophysiology, Heart rate variability, standards of measurements, physiological interpretation, and clinical use, *Circulation* 93, 1043-1065, 1996.
6. P. Ranta-aho, "Tool for bio-signal analysis – Application to multi-channel single trial estimation of evoked potentials", Master's Thesis, University of Kuopio, 2003.
7. M. Khoo, V. Belozeroff, R. Berry, C. Sassoon, "Cardiac Autonomic Control in Obstructive Sleep Apnea", American Journal of Respiratory and Critical Care Medicine, 164, 807- 812, 2001.
8. I. Korhonen, "Methods for the analysis of short-term variability of heart rate and blood pressure in frequency domain", Ph.D. Thesis, Tampere University of Technology, 1997.
9. J. Mietus, C. Peng, P. Ivanov, A. Goldberger, "Detection of obstructive sleep apnea from cardiac interbeat interval time series", *Comp. Cardiology*, 27, 753-756, 2000.
10. A. Hossen, "The FFT as an identification tool for obstructive sleep Apnea", WASET, Bangkok, December 2009.
11. <http://www.physionet.org/physiobank/database/apnea-ecg/>.
12. <http://www.physionet.org/physiotools/ecgpuwave>.
13. B. Jr. Thomas, "Overview of RR variability", heart rhythm instruments Inc., 2002.  
Available from <http://www.nervexpress.com/overview.html> .
14. R. M. Rangayyan, "Biomedical Signal Analysis: A Case-Study Approach", IEEE Press, 466-472, 2001.
15. A. Hossen, "A soft-decision algorithm for obstructive patient classification based on fast estimation of wavelet entropy of RRI data", *Technology and Health Care*, 13, 151-165.

## Experimental Design and Predictive Computational Modeling for the Toxicity of Nanomaterials on Human Epidermal Cells

**Natarajan Meghanathan**

natarajan.meghanathan@jsums.edu

*Assistant Professor, Department of Computer Science  
Jackson State University  
Jackson, MS 39217, USA*

**Raphael D. Isokpehi**

raphael.isokpehi@jsums.edu

*Associate Professor, Department of Biology  
Jackson State University  
Jackson, MS 39217, USA*

**Hari Har Parshad Cohly**

hari.cohly@jsums.edu

*Assistant Professor, Department of Biology  
Jackson State University  
Jackson, MS 39217, USA*

---

### Abstract

Nanomaterials are becoming more commonly used in everyday life, where human beings are becoming exposed to such materials. However, the toxicity of the materials being introduced in our environment is not fully studied. We are currently working on a pilot project to develop computation models that can predict the toxicity of nanomaterials on cell types based on empirical data obtained through monoculture experiments and co-culture experiments. Our hypothesis is that computational approach can be utilized to predict the toxicity and model the intercellular interactions in co-culture studies. The uniqueness of this approach is that we propose to employ computational methods to predict the outcome of co-culture experiments and test the validity of the predictions with cellular biology assays results from co-culture experiments. Human skin cell types such as keratinocytes, melanocytes and dendritic cell lines will be used to mimic the cellular elements of the epidermis. Cytotoxicity, genotoxicity and lipid peroxidation assays will be used to measure cytoplasmic, DNA, and lipid membrane damage respectively. The expected results are that the computational approach will use the results from monoculture experiments to generate a preliminary model that will predict the outcome of co-culture experiments. The preliminary model will be further trained using the co-culture experiments conducted to validate the predicted results.

**Keywords:** Computational Modeling, Toxicity, Nanomaterials, Human Epidermal Cells, Co-culture

---

### 1. INTRODUCTION

During the manufacturing process of nanomaterials, several metals (e.g. Iron) are being used as catalysts. Recent studies (e.g. [1]) have shown that if these metals are not completely purged

from the nanomaterials, exposure of human beings to nanomaterials could be toxic to the human skin. Thus, safety is a major concern in the use of nanomaterials. Our research aims at studying and modeling the toxicity of nanomaterials on the cells constituting the epidermal layer of human skin. This study specifically focuses on the following three cells that are part of the epidermis: (i) Keratinocytes (abbreviated as 'K' cells) – epithelial cells constituting a major portion of the basal layer of the epidermis and act as a barrier between the body and environment; (ii) Melanocytes (abbreviated as 'M' cells) – cells that produce a pigment called melanin which is responsible for the color of human skin; and (iii) Dendritic cells (abbreviated as 'D' cells) – cells that are responsible for the generation of microbial antigens as part of the immune system of the skin. We target to study the following types of toxicity using assays that are available for each of them: (i) Cytotoxicity (abbreviated as 'C' toxic) – affecting the cytoplasm of the cells; (ii) Genotoxicity (abbreviated as 'G' toxic) – affecting the genetic makeup (nucleus) of the cells; (iii) Lipid Peroxidation (abbreviated as 'L' toxic) – affecting the cell membrane, which consists mainly of lipids.

The three primary objectives of our research project are:

1. Conduct experiments on various monoculture cell lines of the epidermal layer of the skin
2. Build a computational model using results from monoculture experiments
3. Validate and train the predictability of computational models using data from co-culture experiments

## 2. LITERATURE REVIEW

Nanomaterials have been earlier used in studies involving keratinocytes [2], melanocytes [3] and dendritic cells [4]. It has been also reported that titanium dioxide ( $TiO_2$ )-based nanomaterials when exposed directly to in-vitro cell cultures, exert significant and cell-type dependent effects on such cellular functions as viability, proliferation, apoptosis and differentiation [5]. Studies on the effects of two or more nanomaterials on a particular cell type of skin have been documented [6]. However, co-culture studies involving single nanomaterials on more than one cell type of the skin have not been conducted. A three-dimensional, computational fluid dynamics (CFD) model has been used to simulate inhaled airflow and to calculate nasal deposition efficiency on the rat nasal passages [7]. Computational methods have also been used to investigate human H4 neuroglioma cells exposed to CuO nanomaterials [8].

Very few studies combine computational models with the experimental data related to the effects of nanomaterials on the skin. Our approach is novel and unique, because it employs computational models to predict the outcome of a co-culture experiment, and it then tests the validity of the models using experimental data. The model whose predicted values match closely with the experimental data will be further trained with more co-culture experimental data.

## 3. RESEARCH PLAN

Safety issue in nanomaterials is of primary concern. Skin is the largest organ in the body. Investigation on the toxicity of nanomaterials on the cellular elements of the skin is of great importance. There is a need to develop computational models that would predict the toxicity of nanomaterials on cell culture systems. Individual toxicity of the 3 cell types of the skin including keratinocytes, melanocytes and dendritic cells have been studied earlier [9]. The novelty of our research is that it is translational in nature as it will use the experimental data produced in the laboratory to develop and train computational models that will predict the toxicity of nanomaterials on the epidermal cells of human skin.

Figure 1 illustrates the flow diagram of our research plan. We will use established human cell lines ( $1 \times 10^5$  cells/ml) of keratinocytes (HaCaT), melanocytes (CRL1675), and dendritic cells (THP-1 + A23187). Cells will be grown in Dulbecco's Minimum Essential Medium for HaCaT, RPMI 1640 for THP-1 (dendritic cells), and Vitacell medium for melanocytes (CRL 1675).

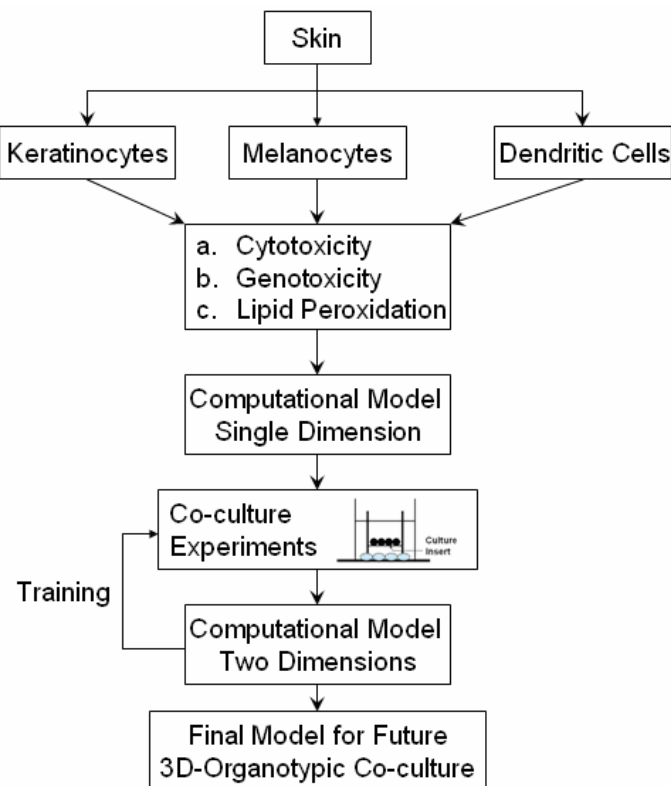


**FIGURE 1:** Flowchart of our Research Plan

The following three assays will be used to study the toxicities of nanomaterials on monocultured epidermal cells:

- Cytotoxicity will be assessed using the Lactate Dehydrogenase assay after 72 hrs of exposure.
- Genotoxicity will be measured through the DNA damage using single cell gel electrophoresis (Comet assay).
- Membrane toxicity will be evaluated using lipid peroxidation.

The results from the toxicity assays for the three different cell types will be used to generate a computational model that will predict the outcome of co-culture experiments. We will additionally use data generated from our labs (Research Center for Minority Institutions, RCMI-funded project by NIH) on the toxicity of arsenic trioxide on skin keratinocytes. Arsenic trioxide can serve as a positive control as it is a known carcinogen and an agent that causes changes in keratinocytes activation and differentiation [10].

#### 4. EXPERIMENTAL DESIGN

##### Nanomaterial Sonification in Different Media

Commercially obtained nanomaterials will be suspended in sterile pyrogen-free phosphate buffer and probe-sonicated for 5 seconds and then incubated with the reaction mixture in a water bath in the dark at 37 °C for 15 min. Nanomaterial stock solutions will be prepared and supplemented with (1, 5 and 10%) FBS containing 1% penicillin and streptomycin in (i) phosphate buffered saline, (ii) Dulbecco's Minimum Essential Medium (iii) RPMI 1640, (iv) Vitacell medium and briefly probe sonicated (15 seconds) [11][12]. Prior to adding the diluted nanomaterials to the cells, the

medium will be aspirated from each well and the nanomaterials in buffer (250 µL) will be gently layered over the cell monolayer; the cells will be allowed to take up the particles in buffer for the period of 10 min, during which the plates will be periodically agitated. After this initial uptake period, medium with 10% FBS will be added back to each well (total of 1 mL). All incubations will be at 37 °C, 5% CO<sub>2</sub>. For the uptake studies, cells will be exposed to the nanomaterials (different shapes and sizes) for 10 min or 24 h. Uptake will be evaluated via EM (Electron Microscopy) and ICP-MS (Inductively Coupled Plasma Mass Spectrometry) analyses.

For EM analyses, the culture supernatant will be removed from each well at the end of the exposure period and glutaraldehyde (2.5%) in Millonig's buffer will be added. Cells will be fixed in this buffer for the period 1 h, after which they will be removed from the culture dishes by scraping and placed in a 15-mL conical tube on its side at 4 °C for 3 more days of fixation. Cells will be rinsed and then post-fixed in phosphate-buffered 1% OsO<sub>4</sub>. After more rinsing, the cells will be trapped in 3% agarose and then cooled so that the material will be cut into 1 mm cubes. These agarose cubes will be stained with 0.25% uranyl acetate in 50% ethanol, dehydrated and infiltrated with araldite resin. The epoxy resin blocks will be sectioned (70 nm) onto 200 mesh grids and the grids will be stained with uranyl acetate and lead citrate.

The grids will be examined for electron-dense particles using a Hitachi 7100 transmission electron microscope; images will be captured digitally. Cell pellets and culture supernatants will be processed for separate analyses of nanomaterial content via ICP-MS analysis. After the 24-h exposure period, cell culture supernatants will be removed and placed in Teflon vials. Each well will be washed 3 times with Hank's balanced salt solution (HBSS), adding each wash to the same vial as the supernatant. The wells will not be acid-washed to remove the nanomaterials that may have adhered to the well material. The cell pellets will be trypsinized to remove them from the culture wells and placed in another Teflon vial. The wells will then be washed 3 times with HBSS, saving the washes in the same vial as the main pellet. The contents of each vial will be dried down and dissolved in aqua regia with heating and this process repeated until the nanomaterial pellet is no longer visible. The dried samples will be re-suspended in 0.5 N HCl/aqua regia and an aliquot of this solution will be spiked with iridium as an internal standard. Nanomaterial concentrations will be determined in a magnetic sector high resolution Thermo-Finnigan Element 1 ICP-MS (Thermo Fisher Scientific, Waltham, MA). ICP-MS certified standards from Inorganic Ventures (Lakewood, NJ) will be used for the external standardization.

### **Electrostatic Potential**

We will also determine the zeta potentials (a widely used measure of the electrostatic potential at the nanomaterial surface double layer) as a feature for each nanomaterial. Nanomaterial sizing will be determined by dynamic light scattering and zeta potential measurement will be determined by laser-Doppler electrophoresis.

### **Cytotoxicity Assay**

Briefly, cells will be counted (20,000 cells/well) and re-suspended in complete medium. Aliquots of 100µL of cell suspension will be placed in wells of microtiter plates, and 100µL of different concentrations of nanomaterials (0 to 200µg/mL) will be used to treat the cells. The plates will be incubated for 24, 48, and 72 hours, respectively. In order to assess cytotoxicity, we will measure the release of lactate dehydrogenase (LDH) into the culture supernatant using a kit from Sigma-Aldrich. The use of THP-1 +A23187 to mimic dendritic cells [13] is due to the fact that dendritic cells will be found in the surface epithelium along with keratinocytes and melanocytes.

### **Cell Treatment for Genotoxicity**

Cells will be counted (10,000 cells/well) and re-suspended in media with 10% FBS. Aliquots of 100µL of the cell suspension will be placed in 96 well plates, treated with arsenic trioxide concentrations at doses of LD<sub>10</sub> and LD<sub>25</sub> determined from the cytotoxicity assay data, and incubated in a 5% CO<sub>2</sub> at 37 °C for 72 hrs. After incubation, the cells will be centrifuged, washed with PBS (Phosphate Buffered Saline), and re-suspended in 100 µL PBS. In a 2 mL tube, 20 µL

of the cell suspension and 200  $\mu\text{L}$  of melted agarose will be mixed and 75 $\mu\text{L}$  pipetted onto a pre-warmed slide. The slides will be placed in a refrigerator at 4°C for 10-20 min and placed in chilled lysis buffer for 45 min. Slides will be washed twice for 5 min with TBE (Tris-Borate-Edta Buffer) and electrophoresed in a horizontal gel apparatus at 25V for 10 min. Slides will be placed in 70% ethanol for 10 min, removed, tapped to remove excess ethanol, and placed in an alkaline solution containing 99mL  $\text{H}_2\text{O}$ , 100 $\mu\text{L}$  of 0.1mM  $\text{Na}_2\text{EDTA}$  (Ethylene Diamine Tetraacetic Acid) and 1g NaOH for 45 min. Slides will be air dried for 2.5 hrs, stained and allowed to set 4 hrs. The slides will be viewed with an Olympus fluorescence microscope and analyzed using LAI's Comet Assay Analysis System software (Loates Associates, Inc. Westminster, MD).

### Liquid Peroxidation

Supernatants from the culture plates will be removed and frozen immediately and stored at -80°C until the assay will be started. For assessment of lipid peroxidation products, the supernatant will be mixed with 20% trichloroacetic acid and 0.67% thiobarbituric acid and then heated for 15 min in boiling water. The concentration of thiobarbituric acid-reactive substances (TBARS) extracted with *n*-butanol will be estimated by absorption at 530 nm. TBARS will be expressed as malondialdehyde (MDA) amounts, using freshly produced MDA as standard prepared from 1,1,3,3-tetramethoxypropane with HCl [14][15].

## 5. PREDICTIVE COMPUTATIONAL MODELING

For a given toxicity assay and concentration  $C\text{-}NM_i$  of a nanomaterial  $NM_i$ , let  $\%Viability_X^{C\text{-}NM_i}$  be the % Viability brought about by  $NM_i$  on a cell type  $X$  mono-culture (where  $X$  can be a Keratinocyte – K or Melanocyte – M or Dendritic Cell - D). Let  $(X/Y)_{\text{co-culture}}$  represent a co-culture where  $X$  is the inactive cell and  $Y$  is the active cell. The concentration of cell  $Y$  is kept constant with the exposure of the nanomaterial, while the different values for the concentration of the inactive  $X$  cell would be  $(1, 2, 4, 8, 10)*10^5$  cells/mL. Let  $nX$  and  $nY$  be the concentrations of the  $X$  and  $Y$  cells respectively in a  $(X/Y)_{\text{co-culture}}$  and  $(ratio)_{X/Y} = nX/nY$  represent the ratio of the concentrations of the two cell types  $X$  and  $Y$  in the  $(X/Y)_{\text{co-culture}}$ . The % Viability of the  $(X/Y)_{\text{co-culture}}$  for a concentration  $C\text{-}NM_i$  of a nanomaterial  $NM_i$  represented as  $\%Viability_{X/Y}^{C\text{-}NM_i}$  is a function of the four variables:  $\%Viability_X^{C\text{-}NM_i}$ ,  $\%Viability_Y^{C\text{-}NM_i}$ ,  $C\text{-}NM_i$ , and the  $(ratio)_{X/Y}$ . Our task is to predict  $\%Viability_{X/Y}^{C\text{-}NM_i}$  using different possible functions of these four variables. Some of the sample functions (F) that are currently being considered for evaluation are as follows:

$$F1: \%Viability_{X/Y}^{C\text{-}NM_i} = \%Viability_X^{C\text{-}NM_i} + \left[ \%Viability_Y^{C\text{-}NM_i} \right] \left\{ \frac{1}{(C\text{-}NM_i)*(ratio) X/Y} \right\}$$

$$F2: \%Viability_{X/Y}^{C\text{-}NM_i} = \%Viability_X^{C\text{-}NM_i} - \left[ \%Viability_Y^{C\text{-}NM_i} \right] \left\{ \frac{1}{(C\text{-}NM_i)*(ratio) X/Y} \right\}$$

$$F3: \%Viability_{X/Y}^{C\text{-}NM_i} = \frac{\%Viability_X^{C\text{-}NM_i}}{\left[ \%Viability_Y^{C\text{-}NM_i} \right] \left\{ \frac{1}{(C\text{-}NM_i)*(ratio) X/Y} \right\}}$$

$$F4: \%Viability_{X/Y}^{C\text{-}NM_i} = \%Viability_Y^{C\text{-}NM_i} + \left[ \%Viability_X^{C\text{-}NM_i} \right] \left\{ \frac{1}{(C\text{-}NM_i)*(ratio) X/Y} \right\}$$

$$F5: \%Viability_{X/Y}^{C\text{-}NM_i} = \%Viability_Y^{C\text{-}NM_i} - \left[ \%Viability_X^{C\text{-}NM_i} \right] \left\{ \frac{1}{(C\text{-}NM_i)*(ratio) X/Y} \right\}$$

F6:

$$\%Viability_{X/Y}^{C-NMi} = \frac{\%Viability_Y^{C-NMi}}{\left[ \%Viability_X^{C-NMi} \right]^{\left\{ \frac{1}{(C-NMi)*(ratio) X/Y} \right\}}}$$

In addition to the above functions, we will also formulate and evaluate several different functions that will predict the % Viability of a  $(X/Y)_{co\text{-culture}}$  for a given concentration of the nanomaterial. The accuracy of the % Viability values predicted by each of these functions will be tested by using the co-culture experimental data obtained from the laboratory. The function whose predictive value matches closely with the experimental value will be chosen for further training in order to develop a more accurate and well-trained 2-dimensional prediction model for a  $(X/Y)_{co\text{-culture}}$  system. We will then develop a 3-dimensional working model for an organotypic  $(X/Y/Z)_{co\text{-culture}}$  system involving all the three cell types. The formulation and training approach for the 3-dimensional working model will be on similar lines as that of the 2-dimensional model.

## 6. EXPECTED RESULTS

A cell is considered toxic if the viability has reached 50%. For a particular type of toxicity, we expect different concentrations of nanomaterials to cause 50% viability. In the co-culture experiments, the varied concentrations of the inactive cells and the released products from the inactive cells will influence the toxicity of the active cell whose concentration is fixed. The computational model developed and trained to predict the % Viability of a co-culture system will capture the intercellular interaction and match closely to the experimental data. Our empirical models will be useful to predict the behavior of multi-dimensional co-culture systems. Figures 2 and 3 illustrate samples of %viability results expected from mono-culture studies and from co-culture modeling and experimental studies respectively.

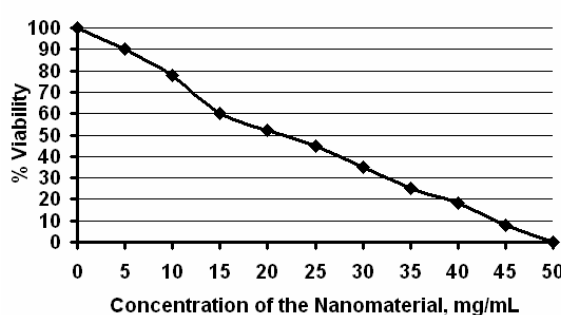


FIGURE 2: Sample Result from Mono-Culture Studies

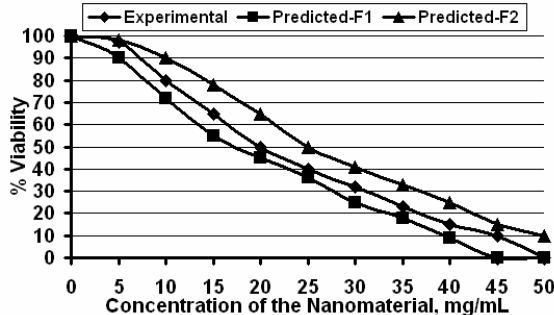


FIGURE 3: Sample Result from Co-Culture Modeling and Experimental Studies

## 7. CONCLUSIONS AND FUTURE WORK

Our research brings together experimental analysis and computational modeling in the context of the toxicity of nanomaterials on human epidermal cells. The significance of this study is that we develop two-dimensional computational models that can extract information from empirical data obtained through monoculture experiments and co-culture experiments. These computational models can be further trained using more experimental data such that the models will form the basis for future 3-dimensional organotypic culture studies. These co-culture studies can predict outcomes that mimic the in vivo paradigm of human skin, which is the largest organ of the body.

## 8. ACKNOWLEDGMENTS

This research has been funded through the National Science Foundation (NSF) – Mississippi EPSCoR grant (EPS-0556308). The views and conclusions contained in this document are those of the authors and should not be interpreted as necessarily representing the official policies, either expressed or implied, of the funding agency.

## 9. REFERENCES

1. A. R. Murray, E. Kisin, S. S. Leonard, S. H. Young, C. Kommineni, V. E. Kagan, V. Castraova and A. A. Shvedova, "Oxidative Stress and Inflammatory Response in Dermal Toxicity of Single-walled Carbon Nanotubes," *Toxicology*, 257(3): 161-171, 2009.
2. E. Sabbioni, S. Fortaner, S. Bosisio, M. Farina, R. Del Torchio, J. Edel and M. Fischbach, "Metabolic Fate of Ultratrace Levels of GeCl<sub>4</sub> in the Rat and In Vitro Studies on its Basal Cytotoxicity and Carcinogenic Potential in Balb/3T3 and HaCaT Cell Lines," *Journal of Applied Toxicology*, 30(1): 34 – 41, 2010.
3. L. Xiao, K. Matsubayashi and N. Miwa, "Inhibitory Effect of the Water-soluble Polymer-wrapped Derivative of Fullerene on UVA-induced Melanogenesis via Downregulation of Tyrosinase Expression in Human Melanocytes and Skin Tissues," *Archives of Dermatological Research*, 299(5-6): 245-257, 2007.
4. V. Manolova, A. Flace, M. Bauer, K. Schwarz, P. Saudan and M. F. Bachmann, "Nanomaterials Target Distinct Dendritic Cell Populations according to their Size," *European Journal of Immunology*, 38(5): 1404-1413, 2008.
5. B. Kiss, T. Biro, G. Czifra, BI Toth, Z. Kertesz, Z. Szikszai, A. Z. Kiss, I. Juhasz, C. C. Zouboulis and J. Hunyadi, "Investigation of Micronized Titanium Dioxide Penetration in Human Skin Xenografts and its Effect on Cellular Functions of Human Skin-derived Cells," *Experimental Dermatology*, 17(8): 659-667, 2008.
6. S. Bastian, W. Busch, D. Kuhnel, A. Springer, T. Meissner, R. Holke, S. Scholz, M. Iwe, W. Pompe, M. Gelinsky, A. Potthoff, V. Richter, C. Ikonomidou and K. Schirmer, "Toxicity of Tungsten Carbide and Cobalt-doped Tungsten Carbide Nanomaterials in Mammalian Cells In Vitro," *Environmental Health Perspectives*, 117(4):530-536, 2009.
7. G. J. Garcia and J. S. Kimbell, "Deposition of Inhaled Nanomaterials in the Rat Nasal Passages: Dose to the Olfactory Region," *Inhalation Toxicology*, 21(14):1165-1175, 2009.
8. F. Li, X. Zhou, J. Zhu, J. Ma, X. Huang and S. T. Wong, "High Content Image Analysis for Human H4 Neuroglioma Cells Exposed to CuO Nanomaterials," *BMC Biotechnology*, 7(66), 2007.
9. B. Graham-Evans, H. H. P. Cohly, H. Yu and P. B. Tchounwou, "Arsenic-Induced Genotoxic and Cytotoxic Effects in Human Keratinocytes, Melanocytes and Dendritic Cells," *International Journal of Environmental Research and Public Health*, 1(2):83 – 89, 2004.
10. C. Huang, Q. Ke, M. Costa and X. Shi, "Molecular Mechanisms of Arsenic Carcinogenesis," *Molecular and Cellular Biochemistry*, 255(1-2):57 – 66, 2004.
11. A. Elder, H. Yang, R. Gwiazda, X. Teng, S. Thurston, H. He and G. Oberdorster, "Testing Nanomaterials of Unknown Toxicity: An Example Based on Platinum Nanomaterials of Different Shapes," *Wiley Advanced Materials*, 19(20):3124 – 3129, 2007.

12. S. Y. Shaw, E. C. Westly, M. J. Pittet, A. Subramanian, S. L. Schreiber and R. Weissleder, "Perturbational Profiling of Nanomaterial Biologic Activity," In Proceedings of the National Academy of Sciences of the United States of America, 105(210):7387 – 7392, 2008.
13. F. Laco, M. Kun, H. J. Weber, S. Ramakrishna and C. K. Chan, "The Dose Effect of Human Bone Marrow-derived Mesenchymal Stem Cells on Epidermal Development in Organotypic Co-culture," Journal of Dermatological Science, 55(3):150-160, 2009.
14. H. Inano, M. Onoda, N. Inafuku, M. Kubota, Y. Kamada, T. Osawa, H. Kobayashi and K. Wakabayashi, "Chemoprevention by Curcumin during the Promotion State of Tumorigenesis of Mammary Gland in Rats Irradiated with Gamma-rays," Carcinogenesis, 20(6): 1011-1018, 1999.
15. J. A. Buege and S. D. Aust, "Microsomal Lipid Peroxidation," Methods in Enzymology, 52: 302-310, 1978.

## Eigenvectors of Covariance Matrix using Row Mean and Column Mean Sequences for Face Recognition

**Dr. H. B. Kekre**

*Senior Professor, Computer Engineering Department  
MPSTME, SVKM'S NMIMS University  
Mumbai 400056, India*

hbkekre@yahoo.com

**Sudeep D. Thepade**

*Ph.D. Research Scholar and Assistant Professor,  
Computer Engineering Department  
MPSTME, SVKM'S NMIMS University  
Mumbai 400056, India*

sudeepthepade@gmail.com

**Akshay Maloo**

*Student, B. Tech (Computer Engineering)  
MPSTME, SVKM'S NMIMS University  
Mumbai 400056, India*

akshaymaloo@gmail.com

---

### Abstract

Face recognition has been a fast growing, challenging and interesting area in real-time applications. A large number of face recognition algorithms have been developed from decades. Principal Component Analysis (PCA) [2][3] is one of the most successful techniques that has been used in face recognition. Four criteria for image pixel selection to create feature vector were analyzed: the first one has all the pixels considered by converting the image into gray plane, the second one is based on taking row mean in RGB plane of face image, the third one is based on taking column mean in RGB plane finally, the fourth criterion is based on taking row and column mean of face image in RGB plane and feature vector were generated to apply PCA technique. Experimental tests on the ORL Face Database [1] achieved 99.60% of recognition accuracy, with lower computational cost. To test the ruggedness of proposed techniques, they are tested on our own created face database where 80.60% of recognition accuracy is achieved.

For a 128 x 128 image that means that one must compute a 16384 x 16384 matrix and calculate 16,384 eigenfaces. Computationally, this is not very efficient as most of those eigenfaces are not useful for our task. Using row mean and column mean reduces computations resulting in faster face recognition with nearly the same accuracy.

**Keywords:**Face recognition, eigenvectors, covariance matrix, row mean, column mean.

---

### 1. INTRODUCTION

The term face recognition refers to identifying, by computational algorithms, an unknown face image. This operation can be done by means of comparisons between the unknown face and faces stored in a database.

Face recognition systems have a wide range of application, especially when dealing with security applications, like computer and physical access control, real-time subject identification and authentication, and criminal screening and surveillance. Biometrical identification based on iris, fingerprint and other attributes all suffer from a series of drawbacks, including need of high precision image acquisition equipment's, difficulty to use with video images and need of

agreement when doing the image acquisition. Systems that use face recognition don't have any of these restrictions.

Face recognition is a difficult task, because it cannot be performed by pixel to pixel comparison of two images. Some aspects of the scene must be irrelevant when doing the recognition, like illumination, pose, position, scale, environment, accessories and small age differences. So, face recognition systems require use of accurate and robust methods. Principal component Analysis is usually used because of its acceptable performance, but it is very time consuming. Particularly, our coefficient selection experiments register an accuracy of over 99.00% in controlled database with using less than 95% coefficients, so reduced computational cost and 80% in non-controlled database.

In the area of human computer interaction, an ultimate goal is for machine to understand, communicate with and react to humans in natural ways. Although there are many other avenues to person identification – gait, clothing, hair, voice, and height are all useful indication of identity of the person, none are as compelling as face recognition.

## **2. PRINCIPAL COMPONENT ANALYSIS (PCA) [6][7]**

The task of facial recognition is discriminating input signals (image data) into several classes (persons). The input signals are highly noisy (e.g. the noise is caused by differing lighting conditions, pose etc.), yet the input images are not completely random and in spite of their differences there are patterns which occur in any input signal. Such patterns, which can be observed in all signals could be in the domain of facial recognition, like the presence of some objects (eyes, nose, mouth) in any face as well as relative distances between these objects. These characteristic features are called eigenfaces in the facial recognition domain (or principal components generally). They can be extracted out of original image data by means of a mathematical tool called Principal Component Analysis (PCA).

The idea of using principal components to represent human faces was developed by Sirovich and Kirby [4] in 1987 and used by Turk and Pentland [2][3] in 1991 for face detection and recognition. The Eigenface approach is considered by many to be the first working facial recognition technology, and it served as the basis for one of the top commercial face recognition technology products. Since its initial development and publication, there have been many extensions to the original method and many new developments [7] in automatic face recognition systems.

By means of PCA one can transform each original image of the training set into a corresponding eigenface. An important feature of PCA is that one can reconstruct any original image from the training set by combining the eigenfaces. But one can also use only a part of the eigenfaces and reconstruct an approximate of the original image[12,13]. However, one can ensure that losses due to omitting some of the eigenfaces can be minimized, by choosing only the most important features (eigenfaces). The jobs which PCA can do are prediction, redundancy removal, feature extraction, data compression, etc. Because PCA is a classical technique which can do something in the linear domain, some applications [14] include signal processing, image processing, system and control theory, communications, etc.

## **3. PCA ALGORITHM [2]**

The various steps to calculate eigenfaces are:

### **A. Prepare the data**

A 2-D facial image can be represented as 1-D vector by concatenating each row (or column) into a long thin vector. Let's suppose we have M vectors of size N (= rows of image  $\times$  columns of image) representing a set of sampled images.

Then the training set becomes:  $\Gamma_1, \Gamma_2, \Gamma_3, \dots, \Gamma_M$ .

### **B. Subtract the mean**

The average matrix  $\Psi$  has to be calculated, then subtracted from the original faces ( $\Gamma_i$ ) and the result stored in the variable  $\Phi_i$ :

$$\Psi = \frac{1}{M} \sum_{n=1}^M \Gamma_n \quad (1)$$

$$\Phi_i = \Gamma_i - \Psi \quad (2)$$

### C. Calculate the co-variance matrix

In the next step the covariance matrix A is calculated according to:

$$A = \Phi^T \Phi \quad (3)$$

### D. Calculate the eigenvectors and eigenvalues of the covariance matrix

In this step, the eigenvectors (eigenvectors)  $X_i$  and the corresponding eigenvalues  $\lambda_i$  should be calculated.

### E. Calculate eigenfaces

$$[\Phi]X_i = f_i \quad (4)$$

where  $X_i$  are eigenvectors and  $f_i$  are eigenfaces.

### F. Classifying the faces

The new image is transformed into its eigenface components. The resulting weights form the weight vector  $\Omega_{new}^T$ . Where  $\omega_k$  is the sum of element wise product of ' $\Gamma_{new}$ ' and ' $f_k$ '.

$$\Omega_{new}^T = [\omega_1 \omega_2 \omega_3 \dots \omega_M] \quad (5)$$

$$\omega_k = \Omega_k^T (\Gamma_{new} | f_k) k = 1, 2, \dots, M \quad (6)$$

The Euclidean distance between two weight vectors  $d(\Omega_i, \Omega_j)$  provides a measure of similarity between the corresponding images i and j. If the Euclidean distance between  $\Gamma_{new}$  and other faces exceeds some threshold value  $\theta$ , one can assume that  $\Gamma_{new}$  is not a face at all,  $d(\Omega_i, \Omega_j)$  also allows one to construct "clusters" of faces such that similar faces are assigned to one cluster.

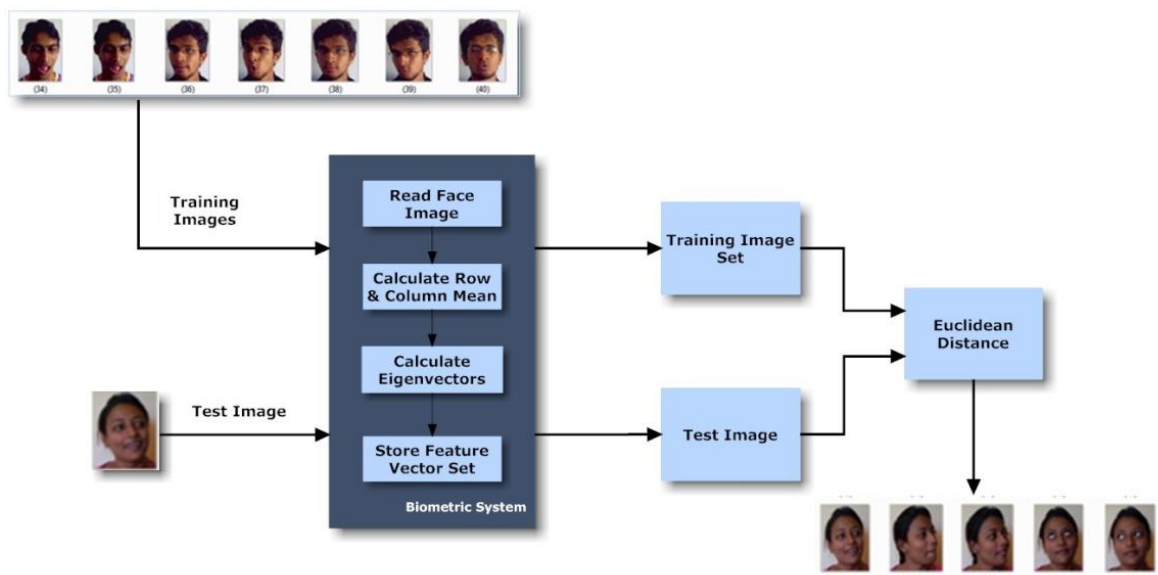


**FIGURE 1:** System using the proposed technique

#### 4. ROW MEAN (RM)/COLUMN MEAN (CM) [5][11]

The row mean vector is the set of averages of the intensity values of the respective rows [8,9,10]. The column mean vector is the set of averages of the intensity values of the respective columns. Fig. 2 is representing the sample image with 4 rows and 4 columns, the row and column mean vectors for this image is given below.

$$\text{Row Mean Vector} = [\text{Avg}(Row 1), \text{Avg}(Row 2), \dots, \text{Avg}(Row n)] \quad (7)$$

$$\text{Column Mean Vector} = [\text{Avg}(Col. 1), \text{Avg}(Col. 2), \dots, \text{Avg}(Col. n)] \quad (8)$$

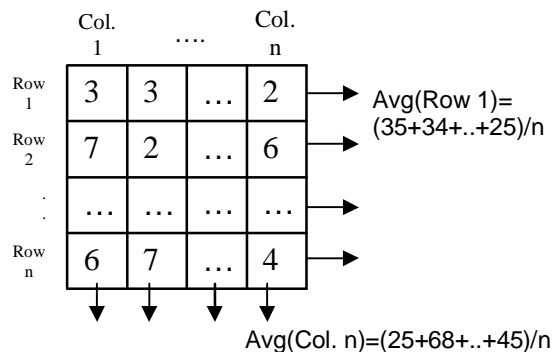


FIGURE 2: Sample Image Template (with size nxn)

#### 5. PROPOSED TECHNIQUES

The various proposed techniques are:

##### A. All image pixels in grey scale

Here the face image is transformed into grey scale and then eigenfaces are generated. Then Euclidean Distance was used to find the best match. This is how PCA is generally implemented we propose new techniques (explained below) to reduce eigenfaces generated so that with nearly the same accuracy faster face recognition techniques are implemented. These calculations are used for comparing proposed techniques with standard PCA technique.

##### B. Row Mean in RGB Plane

Here row mean is calculated of all image pixels in RGB plane. The feature vector is used to generate eigen mean sequences for row mean. Then Euclidean Distance was used to find the best match.

##### C. Column Mean in RGB Plane

Here column mean is calculated of all image pixels in RGB plane. The feature vector is used to generate eigen mean sequences for column mean. Then Euclidean Distance was used to find the best match.

##### D. Row Mean & Column Mean in RGB Plane

Here row&column mean is calculated in red plane, then green and finally blue plane to create a feature vector which is then used to generate eigen row and column sequence. Then Euclidean Distance was used to find the best match.

Partial coefficients	No of image coefficients	No. of elements in Eigen Sequence
All	16384	16384
RM	384	384
CM	384	384
RMCM	768	768

TABLE 1: Complexity analysis for proposed technique for 128\*128 Image

## 6. IMPLEMENTATION

### A. Platform

The experiments were performed using Matlab R2009b, on a machine with Intel Core 2 Duo T8100 (2.1 Ghz) and 2GB ram.

### B. Databases

The experiments were performed on two databases:

- 1) ORL Database[1]: This database has 100 images (each with 180 pixels by 200 pixels), corresponding to 20 persons in five poses each, including both males and females. All the images are taken against a dark or bright homogeneous background, little variation of illumination, different facial expressions and details (open/closed eyes, smiling/non smiling, glasses/no glasses). The five poses of ORL's database are shown in Figure 3.

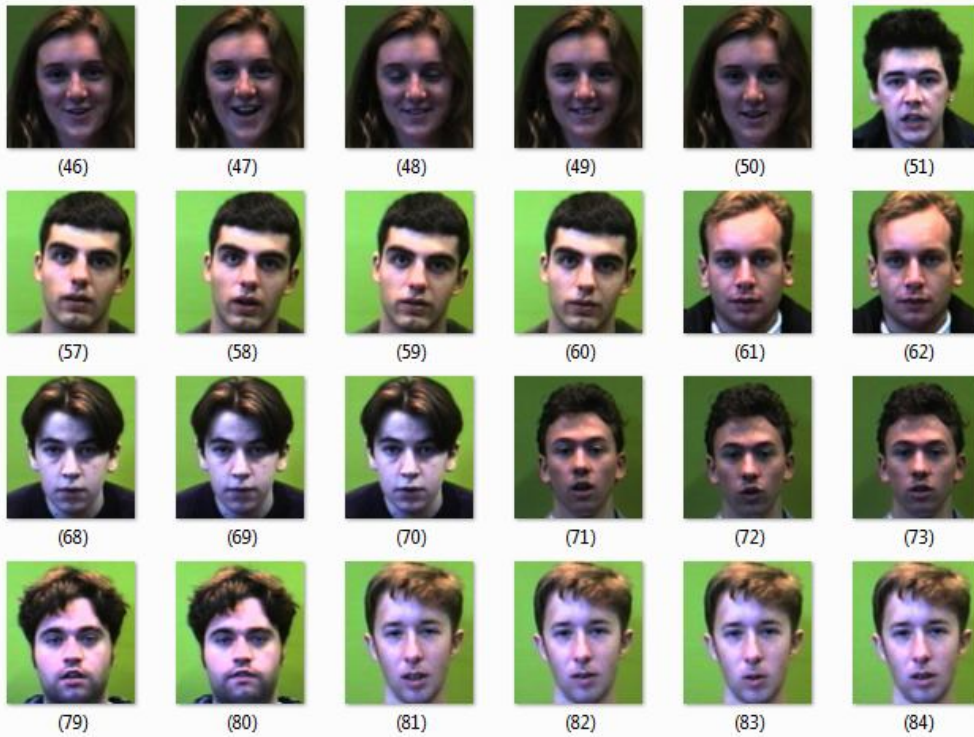
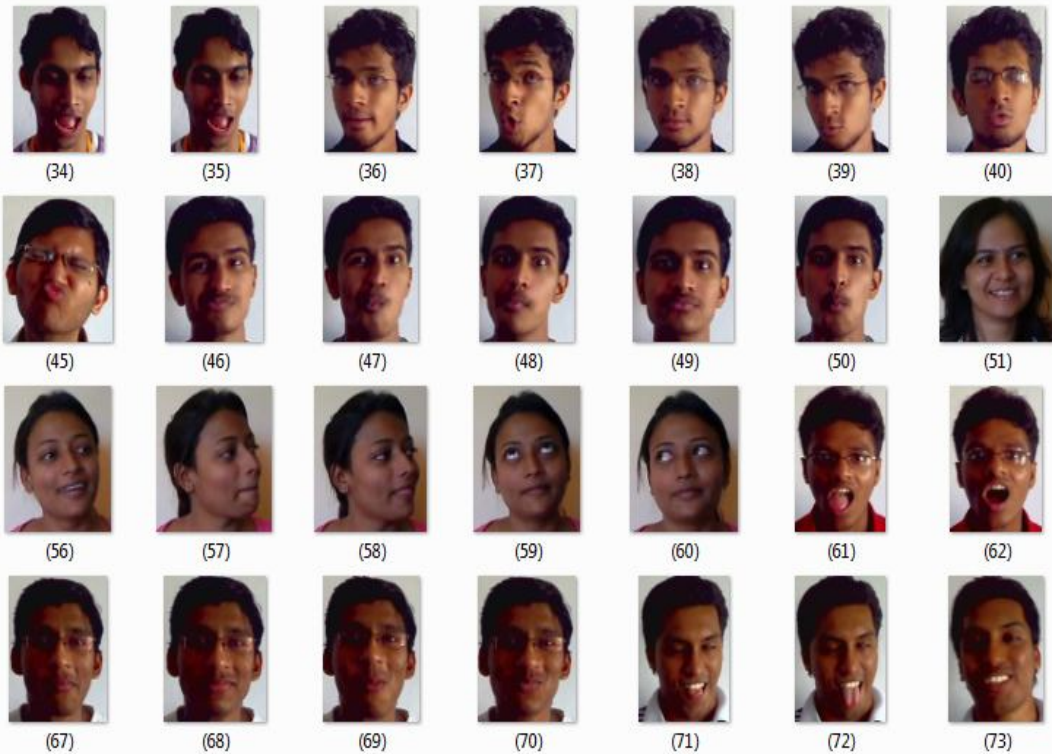


FIGURE 3: Sample Images from ORL Database

- 2) Our Own Database [7]: This database has 85 images (each with 128 pixels by 128 pixels), corresponding to 20 persons in five poses each, including both males and females. All the images are taken against a dark or bright homogeneous background, with variation of illumination, highly different facial expressions and details (open/closed eyes, smiling/non smiling, glasses/no glasses). Our database has many variations in intensity, the image sizes are varying and it is

non-controlled, this was done to test the ruggedness of our algorithm used for face recognition. The five poses of our database are shown in Figure 4.



**FIGURE 4:** Sample Images from Our Own Database

## 7. RESULTS AND DISCUSSIONS

The false acceptance rate (FAR) [16] is the measure of the likelihood that the biometric security system will incorrectly accept an access attempt by an unauthorized user. A system's FAR typically is stated as the ratio of the number of false acceptances divided by the number of identification attempts.

The false rejection rate (FRR) [15] is the measure of the likelihood that the biometric security system will incorrectly reject an access attempt by an authorized user. A system's FRR typically is stated as the ratio of the number of false rejections divided by the number of identification attempts.

During performance testing a test image was considered and five closest matches were displayed, so percentage correct detection is the percentage of relevant images it returned and percentage incorrect detection is the amount irrelevant images it returned.

### 1) ORL Database [1]

In all 100 queries were tested on ORL database for analysing the performance of proposed face recognition techniques. Fig 5 gives the percentage of FAR and FRR for face recognition using variations in PCA based techniques. Here it is observed that PCA on full image and on feature vector of RM and RBCM are nearly giving the same performance, the advantage of using proposed technique over PCA applied on full image is reduced feature vector size which gives faster recognition with nearly the same or better accuracy.

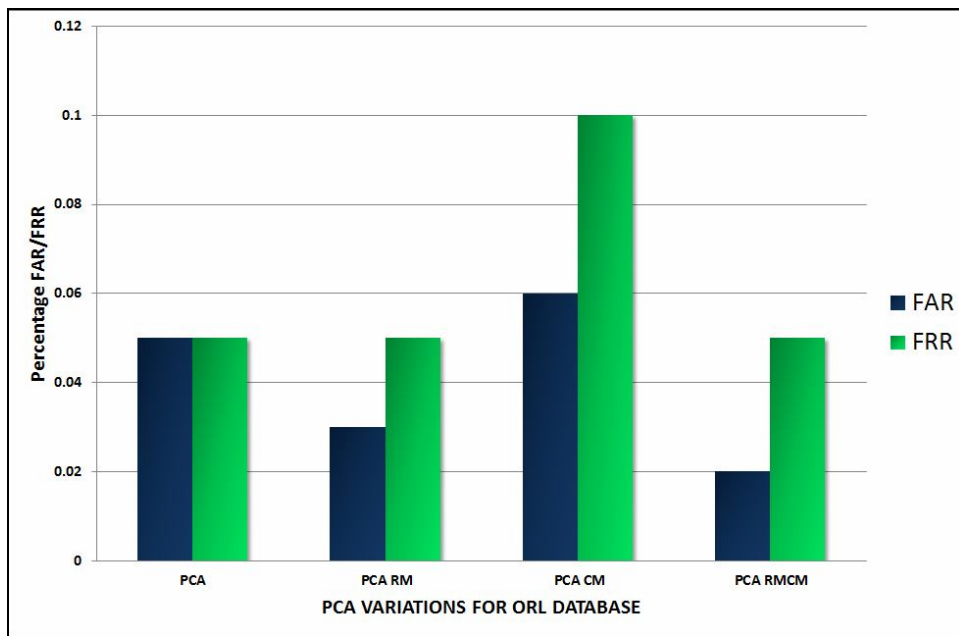


**FIGURE 5:** FAR/FRR using PCA on ORL database

## 2) Own Database [7]

In all 100 queries were tested on Our Own database for analysing the performance of proposed face recognition techniques. Fig 6 gives the percentage of FAR and FRR for face recognition using variations in PCA based techniques. Here it is observed that PCA on full image and on feature vector of RGB RMCM are giving nearly the same performance but the advantage of using the proposed RMCM technique is reduced feature vector size which gives faster recognition (refer table. 4) with nearly the same accuracy.

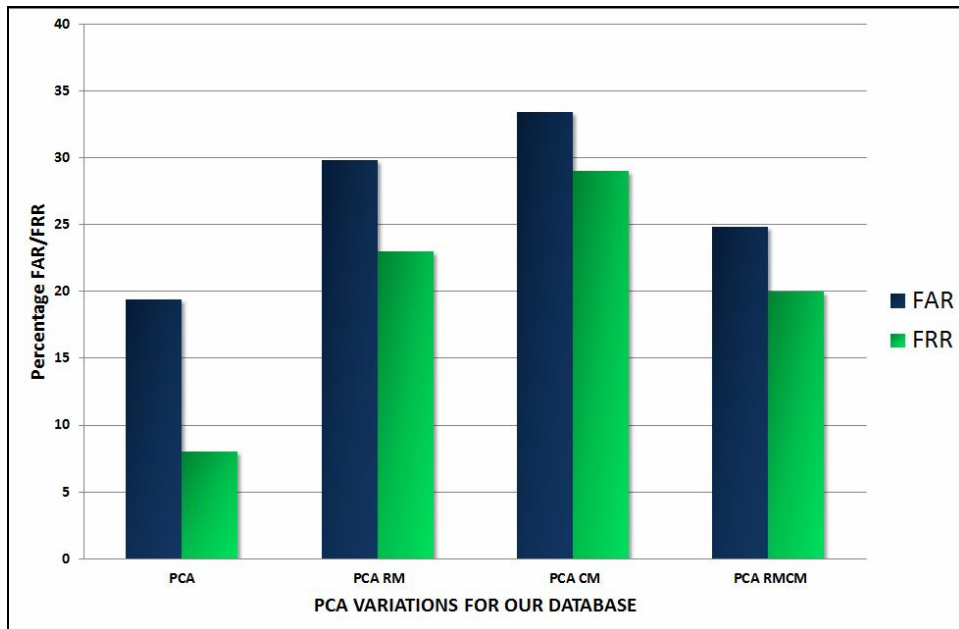


**FIGURE 6:** FAR/FRR using PCA on Our Own Database

In table 2&3 performance comparisons of PCA on both the databases are shown. Here performance of full image and row mean column mean vector is quite similar and row mean column mean is much faster because of less computations required (table 4)as results are based on less number of eigenfaces generated for comparison.

Partial coefficients	Percentage Correct Detection	Percentage Incorrect Detection
All	99.0%	1.0%
Row Mean	99.4%	0.6%
Column Mean	99.2%	0.8%
Row& Column mean	99.6%	0.4%

TABLE 2: Correct/Incorrect Detection Using PCA on ORL Database

Partial coefficients	Percentage Correct Detection	Percentage Incorrect Detection
All	80.0%	20.0%
Row Mean	70.2%	29.8%
Column Mean	66.0%	34.0%
Row& Column mean	75.0%	25.0%

TABLE 3:Correct/Incorrect Detection Using PCA on Our Own Database

PCA applied on	All	Row Mean	Column Mean	Row& Column mean
<b>Feature Extraction</b>				
No of additions	1,61,07,11,040	99,072	99,072	3,94,752
No of multiplications	80,54,53,824	50,304	50,304	1,98,912
<b>Query Execution</b>				
No of additions	1,96,602	1,530	1,530	3,054
No of multiplications	98,304	768	768	1,530

TABLE 4: Complexity analysis for proposed technique for 128\*128 Image

## 8. CONCLUSION

Recognition accuracy, robust method and computational costs are topics that must be taken into account when analyzing a face recognition method.

The proposed method (RMCM technique) is feasible as it achieves a high recognition accuracy (99.6% when using ORL database and correct classification when the five most similar faces are returned), without any pre-processing step. In a 128\*128 face image PCA uses a feature vector of size 16384 coefficients is used and our proposed technique uses only 768 coefficients that is 95.21% less number of coefficients for PCA or eigenvector calculation with nearly the same results.

The proposed method is also suitable for real time applications: in the experimental tests the classification processing time for a face, using 768 coefficients (RMCM technique), is nearly 0.6 seconds in a database of 100 people. The proposed technique so can be used for much real time applications like face recognition in crowded public places where numbers of people moving are high and face recognition is required on the fly, the proposed technique can give guaranteed results instead of using normal PCA with reduced computations and time.

## 9. REFERENCES

- [1] AT&T Laboratories, Cambridge, UK. "The ORL Database of Faces" (now AT&T "The Database of Faces"). Available [Online: [http://www.cl.cam.ac.uk/Research/DTG/attarchive/pub/data/att\\_faces.zip](http://www.cl.cam.ac.uk/Research/DTG/attarchive/pub/data/att_faces.zip) Last referred on 15 September 2007].
- [2] M.Turk and A. Pentland, "Eigenfaces for Recognition", Journal of Cognitive Neuroscience, March 1991.
- [3] M.A. Turk and A.P. Pentland. "Face recognition using eigenfaces". In Proc. of Computer Vision and Pattern Recognition, pages 586-591. IEEE, June 1991b.
- [4] L.Sirovich and M. Kirby (1987). "Low-dimensional procedure for the characterization of human faces". Journal of the Optical Society of America A4: 519–524.
- [5] H.B.Kekre, TanujaSarode, Sudeep D. Thepade, "DCT Applied to Row Mean and Column Vectors in Fingerprint Identification", In Proceedings of Int. Conf. on Computer Networks and Security (IC CNS), 27-28 Sept. 2008, VIT, Pune.
- [6] Prof. Y. VijayaLata, Chandra KiranBharadwajTungathurthi, H. Ram Mohan Rao, Dr. A. Govardhan, Dr. L. P. Reddy, "Facial Recognition using Eigenfaces by PCA", In International Journal of Recent Trends in Engineering, Vol. 1, No. 1, May 2009, Pages 587-590.
- [7] H. B. Kekre, Kamal Shah, Tanuja K. Sarode, Sudeep D. Thepade, "Performance Comparison of Vector Quantization Technique – KFCG with LBG, Existing Transforms and PCA for Face Recognition", Int. Journal of Information Retrieval (IJIR), Vol. 02, Issue 1, pp.: 64-71, 2009.
- [8] H.B.Kekre, Sudeep D. Thepade, ArchanaAthawale, Anant Shah, PrathmeshVerlekar, SurajShirke, "Walsh Transform over Row Mean and Column Mean using Image Fragmentation and Energy Compaction for Image Retrieval", International Journal on Computer Science and Engineering (IJCSE), Volume 2S, Issue1, January 2010, (ISSN: 0975-3397). Available online at [www.enggjournals.com/ijcse](http://www.enggjournals.com/ijcse).
- [9] H.B.Kekre, Sudeep D. Thepade, ArchanaAthawale, Anant Shah, PrathmeshVerlekar, SurajShirke, "Energy Compaction and Image Splitting for Image Retrieval using Kekre Transform over Row and Column Feature Vectors", International Journal of Computer Science and Network Security (IJCSNS), Volume:10, Number 1, January 2010, (ISSN: 1738-7906) Available at [www.IJCSNS.org](http://www.IJCSNS.org).
- [10] H.B.Kekre, Sudeep D. Thepade, ArchanaAthawale, Anant Shah, PrathmeshVerlekar, SurajShirke, "Performance Evaluation of Image Retrieval using Energy Compaction and Image Tiling over DCT Row Mean and DCT Column Mean", Springer-International Conference on Contours of Computing Technology (Thinkquest-2010), BabasahebGawde Institute of Technology, Mumbai, 13-14 March 2010, The paper will be uploaded on online Springerlink.
- [11] H.B.Kekre, Sudeep D. Thepade, AkshayMaloo "Performance Comparison for Face Recognition using PCA, DCT & Walsh Transform of Row Mean and Column Mean", ICGST International Journal on Graphics, Vision and Image Processing (GVIP), Volume 10, Issue II, Jun.2010, pp.9-18, Available online at <http://209.61.248.177/gvip/Volume10/Issue2/P1181012028.pdf>.
- [12] D. L. Swets and J. Weng, "Using discriminant eigenfeatures for image retrieval", IEEE Transactions on Pattern Analysis and Machine Intelligence, vol. 18, pp. 831–836, 1996.
- [13] C. Liu and H. Wechsler, "Evolutionary pursuit and its application to face recognition", IEEE Transactions on Pattern Analysis and Machine Intelligence, vol. 22, no. 6, pp. 570–582, June 2000.
- [14] A. M. Martinez and A. C. Kak, "PCA versus LDA", IEEE Transactions on Pattern Analysis and Machine Intelligence, vol. 23, no. 2, pp. 228–233, 2001.May
- [15] [http://www.webopedia.com/TERM/F/false\\_rejection.html](http://www.webopedia.com/TERM/F/false_rejection.html)
- [16] [http://www.webopedia.com/TERM/F/false\\_acceptance.html](http://www.webopedia.com/TERM/F/false_acceptance.html)

## Gouraud Shading to Improve Appearance of Neuronal Morphology Visualization

**Norhasana Razzali**

*ViCube Lab*

*Department of Computer Graphics and Multimedia  
Faculty of Computer Science and Information System  
Universiti Teknologi Malaysia  
Johor, 81310, Malaysia*

hasanarazzali@gmail.my

**Mohd Shafry Mohd Rahim**

*ViCube Lab*

*Department of Computer Graphics and Multimedia  
Faculty of Computer Science and Information System  
Universiti Teknologi Malaysia  
Johor, 81310, Malaysia*

shafry@utm.my

**Rosely Kumoi**

*ViCube Lab*

*Department of Computer Graphics and Multimedia  
Faculty of Computer Science and Information System  
Universiti Teknologi Malaysia  
Johor, 81310, Malaysia*

rosely@utm.my

**Daut Daman**

*ViCube Lab*

*Department of Computer Graphics and Multimedia  
Faculty of Computer Science and Information System  
Universiti Teknologi Malaysia  
Johor, 81310,*

daut@utm.my

*Malaysia*

---

### Abstract

This study is focused on Gouraud Shading's approach to improve appearance of neuron visualization. Neuron visualization is a computational tool that is able to describe, generate, store and render large set of three-dimensional neuronal morphology in a format that is compact, quantitative, and readily accessible to the neuroscientists. This tool enlightens its ability as a powerful computational modeling of neuronal morphology to explore greater understanding in neuron developmental processes and structure-function relationships. However, after a thorough investigation, one of the problems discovered in neuron structure prediction is related to misleading in generating digitalized neuron raw data toward realistic neuron morphology visualization. For that reason, many approaches have been proposed in previous studies in order to perform such visualization based on stochastic sampling data of morphological measures from digital reconstructions of real neuron cells. Therefore, comparison among these approaches has been conducted to recognize a suitable approach. It is still at a preliminary stage in research development. This exercise reveals a constraint to

reconstruct neuron model towards greater realism efficiently is still remains as an essential challenge in biological computing and visualization to provide a broad appearance of neuron knowledge distribution. As a result, the areas of comparative neuron analysis can be aided through presenting the knowledge of realism virtual neuron morphology. As a proposal, Gouraud Shading's approach is applied for this purpose. Gouraud Shading is a visualization shading technique to perform a smooth lighting on the polygon surface without heavy computational requirement in calculating lighting for each pixel but at vertices only. The conclusion is summarized based on verification exercise between our framework's results with existing results from three neuron visualization applications. The comparison analysis is done in term of reliability and smoothness of surface neuron presentation. Roughly the proposed framework achieved the objective to solve the problem encountered in presenting virtual neuron data.

**Keywords:** Neuron morphology data, visualization, Gouraud Shading

---

## 1. INTRODUCTION

Basically, the neuron visualization application depends on the product information and neuron structure presentation criteria to simplify and contribute to an extensive study of brain's functions and/or dysfunctions. By applying such applications especially in lab-experimenting, it potentially facilitates scientist's life to do thorough analysis in determining the relations between neuron's connection and its function. Thus, apparently, extraction and accuracy is an important aspect in generating the reconstruction neuron morphology visualization.

The development of digital neuron visualization is rapidly increases as a significant prerequisite in the quantitative exploration of cellular neuroanatomy. Recently, neuron morphology data has been gathered and published in digital databases offering variety of dendritic structure. One of the famous databases is known as Duke Southampton [23]. However, the approach that is applied in this database presents static image of neuron. As such, there is a certain situation where neuron structure is unable to be extracted in details because of no interaction facility to manipulate the neuron's presentation. It requires specific tool to apply this useful data for knowledge distribution.

Based on the above review, a lot of approaches have been proposed by previous researchers. Findings from these studies showed that the core rationale of these executions were prominence on tool for constructing and generating the anatomical neuron network model. These established applications' approaches are able to provide facility to access simulation of neuron morphological but they remain to offer a greater biological realism of virtual neuron model. Finally, in our proposed framework, we are able to produce comparable neuron model as per existing application's output as well as toward realistic presentation in order to be applied by a group of scientists who are involved in neuron analysis study.

The reminder of the paper consists of a detailed explanation on the proposed approach, description of neuron computational environment and data used in material and method to improve appearance of neuronal morphology visualization, the result and discussion of proposed approach, and the conclusions of the achieved results.

## 2. PRELIMINARIES

The practice of medicine and biologic investigations lies in direct, fully immersive, real-time multisensory fusion of real and virtual information data streams into online, real-time available during actual clinical procedures or biological experiments had offered the potential for revolutionary innovation in biomedical application. These goals are able to be materialized and realized with major facilitation progress of current high-performance computing, advanced image processing and high-fidelity rendering capabilities. With these advances offered in the current technology, there are several significant applications of three-dimensional visualization established to perform an impact to the practice of medicine and biological research.

The study of biology always dependent on visualizations tools to explore the relationship of an anatomic structure [22] to biologic function to detect and treat disease that disturb or threaten normal life processes. The value of biomedical images i.e neuron cells largely depend on the context from which they are obtained either for the scientific or medical interest and goals that motivate their production and use. However, the valuable potential of 3D visualization in neuron cells remains mostly unexploited and practical tools remain undeveloped. The most recent requirement is to continue advances in visualization technology to the level of utilization, so that they can provide new tools and procedures that physicians can apply to treat their patients and empower scientists in neurology studies of structure-to-function relationships.

As such, a particular challenge in imaging science for biomedical applications need to be focused is to provide realistic displays, interactive manipulation and simulation and accurate and reproducible measurements. This is because an adequate description of neuronal morphology is significantly for investigating the influence of morphology in information processing of neurons.

### **Neuron Data Acquisition**

Basically neuroanatomical experiments result in chemically processed tissue accumulated on a microscope slide. This corresponding observable microscope image can only be further manipulated in a limited way. It involves the computer acquisition or digitization as a key step toward the flexible, quantitative, an extensive analysis and modeling of these data. The result from digital files is represented by data in numerical (machine-readable) format. A major benefit of digital representation of neuronal morphological is a virtually and geometrically feature captured by the cylindrical-based description can be measured statistically and analyzed quickly, reliably, and precisely [19].

This digitally neuron raw data have been stored in different format in several published databases for easy sharing and allowing for visualizing and capturing purposes. There are three (3) popular digital adopted formats to describe neuron morphology which are 'SWC', 'Neurolucida' and 'Eutectic' format. Even though it is provided in a different format, it is still used in the basic structure of neuron data [2]. These files can range from 500 lines for small and simple cell to 10,000 or more lines for large and complex cells. In this purpose, 'SWC' format will be applied and details explanation about its basic structure will discuss. This neuron morphology data was acquired from Duke-Southampton website. This database provides neuron cell images for rat hippocampus that consists of CA1 pyramidal cell, DG granule cell and CA3A pyramidal cell in different age as per example in Figure 1. Generally, before neuron can be visualized by the extractor, digitalized neuron data will be loaded into the system.

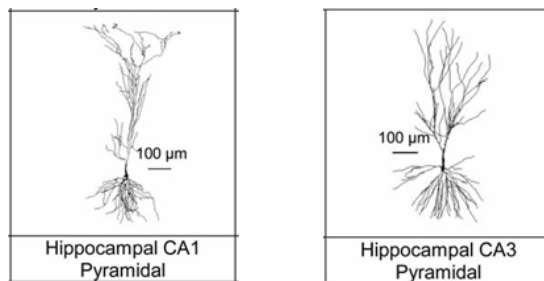


**FIGURE 1:** Sample cell of neuronal morphology used as data for this study [11].

'SWC' format is for describing the structure of neuron in the simplest way and has been designed to emphasize on compactness and uses the minimum amount of information and number of fields to fully describe the branching structure [17]. Basically in 'SWC' format, each neuron dendritic segments is represented by an identification number (ID, the number reported next to the branches in the picture), a type of distinguish basal (T), Cartesian positions (X,Y,Z in micrometers), radius (R), and end-point connection (C, presenting the label of the parent) [2,12,23] as per stated in Figure 2, refer to the right panel. As shown in Figure 2, each tracing point is represented as a row of seven numbers [2,12,23] that describes the properties of a single compartment, an arbitrarily sized piece of a segment.

ID	T	X	Y	Z	R	C
1	1	-1.5	-8.2	1.3	3.8	-1
2	3	0.8	4.2	1.4	2.3	1
3	3	21.1	41.1	1.4	1.3	2
4	3	89.2	115.1	-5.3	1.1	3
5	3	153.6	163.5	3.0	0.6	4
6	3	184.9	218.1	-2.3	0.5	5
7	3	220.9	238.7	-13.7	0.3	6
8	3	159.9	183.9	-23.6	1.1	4
9	3	211.9	270.9	-35.2	0.7	8
10	3	0.6	58.1	-2.6	1.1	2
11	3	-0.5	75.9	-18.6	1.1	10
12	3	-40.5	180.0	-55.3	1.0	11
13	3	-156.4	281.8	-65.9	0.8	12
14	3	0.3	186.8	-7.0	0.8	12
15	3	-51.5	235.7	-27.0	0.8	14
16	3	-85.2	297.6	-41.5	0.5	15
17	3	75.3	198.3	-54.6	0.8	10
18	3	130.6	228.6	-81.3	0.5	17

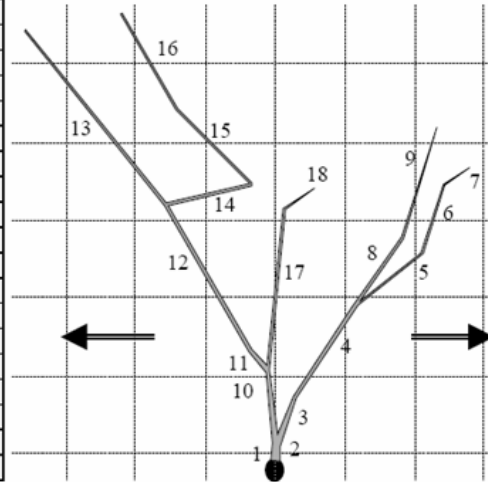


**FIGURE 2:** Digital representation of neuron morphology from 'SWC' format data (left panel) [12].

This segment may either branch into further segment at a bifurcation or end at a terminal (both of these segments are also represented as compartments), make up the entire neuron shapes. These varieties of neuron shapes attain through a development process called of elongation and branching of axonal and dendrites extensions [1,2,3,4].

Such digital reconstruction files are efficient and allow extensive morphometric analysis to be produced from implementation of biophysical virtual neuron models as allowing 'pseudo-3D' rendering and animation in modern computer graphics [12]. In general, this digital format consists of a plain text file that each line describing the cylindrical geometry of neuronal segment and its connection to derive any morphological measurement.

### Reconstructing and Modeling

The tracing process involves converting described neuronal morphology from Cartesian data into a digital three-dimensional (3D) coordinates and branch connectivity of the corresponding trees. In this process, the link segment of digitized neuron data is traced automatically from identified format data mentioned previously and followed by generating a branching of cylindrical neuron compartments. The system will scan the uploaded data in order to differentiate between HEADER

part and CARTESIAN data. This process will recognize the first character represented by “#” in the HEADER. After all the “#” character has been emphasized and the HEADER part has been traced, the system will read and translate the neuron CARTESIAN data line by line. The simulated neuron branching from CARTESIAN data is generated by continuous compartment as shown in Figure 3

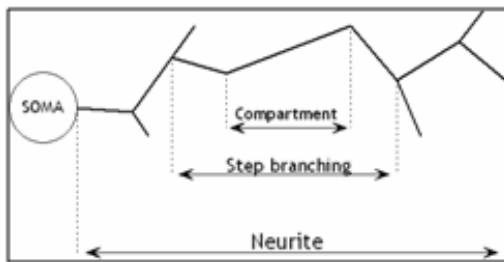


**FIGURE 3:** A part of simulated neurons.

The traced data is visualized via reconstruction model aims at finding minimal algorithms for generating trees which reproduce the statistical properties of observed neuronal shapes [2]. Reconstruct virtual neuron applying dissimilar color to represent different type of neuronal segment. The first soma was indicated by sphere and cylindrical to represent neuron connection consist of dendritic and axon. As summarized, the reconstruction process is illustrated as per Figure 4.

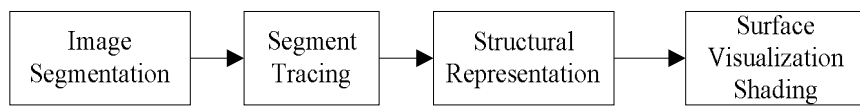


**FIGURE 4:** A summary of neuronal morphology reconstruction pipeline.

#### Surface visualization shading approaches

According to J.C Fiala [19], the most reliable method is computer aided tracing profiles on neuron segments followed by rendering it with appropriate shading. Shading technique is the process of assigning colors to the pixels. The implementation with a smooth shading and lighting is understood can assist in reconstructing neuron morphologies toward realistic visualization. The purpose of shading algorithms is to smooth the appearance of polygonal model by reducing the impact of sharp edge in order to give the eye the impression of a smooth curved surface.

In this part, Gouraud shading (GS) technique is applied to neuron surface visualization in order to perform a smooth lighting on the polygon surface without the heavy computational requirement of calculating lighting for each pixel but at vertices only. This approach was applied because it able to provide the objects i.e the series of cylindrical that as neuron connection towards realistic surface. The comparison between curved surfaces rendered using flat shade polygons and curved surface rendered using Gouraud Shading is shown in Figure 5.

GS also called intensity interpolation provides a way to display smooth shaded polygons by defining the RGB color components of each polygon vertex based on the color and illumination to eliminate intensity discontinuities. GS is the simplest rendering method and it computed faster than Phong Shading. It does not produce shadows and reflections. GS smoothes the appearance of the object by linearly interpolating intensities along scan lines.

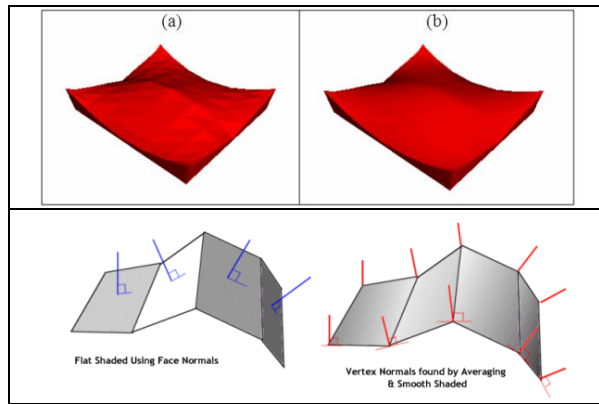


**FIGURE 5:** A comparison between curved surface using (a) flat shaded and (b) Gouraud shaded.

The purpose of GS is to eliminate Mach bands, discontinuities in intensity along polygon edges. It reduces the visibility of polygonal edges by blurring the intensity across the boundaries of adjacent polygons. The underlying strategy is to compute the intensities for the pixels in 3 steps:

- Calculate the intensities at the individual vertices of the polygon
- Interpolate these vertex intensities along the edges of the polygon
- Interpolate these edge intensities along scan lines to the pixels in the interior of the polygon (as per illustrated in Figure 6)

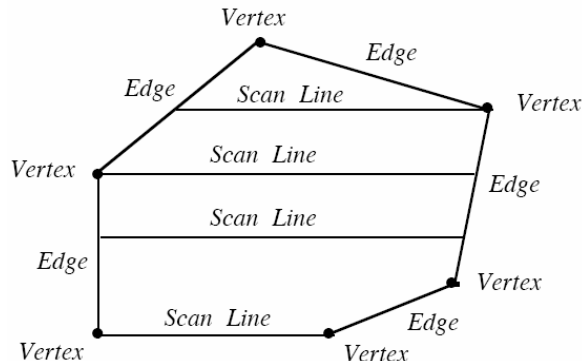


**FIGURE 6:** Gouraud shading mechanisms.

In order to compute the intensity at a vertex, we require to obtain the unit normal vector at the vertex. Since each vertex may belong to many polygons, we first use Newell's formula (equation 1.1) to calculate the unit normal for each polygon containing the vertex.

$$N = \sum_{k=0}^n P_k \times P_{k+1}. \quad \{P_{n+1} = P_0\} \quad (1.1)$$

We then calculate the unit normal vector by averaging the unit normal of the polygons containing the vertex:

$$N_{vertex} = \frac{\sum_{vertex \in Polygon} N_{polygon}}{\left| \sum_{vertex \in Polygon} N_{polygon} \right|}. \quad (1.2)$$

Finally, we apply equation 1.3 to compute the intensity at the vertex.

$$I_{uniform} = \underbrace{I_a k_a}_{ambient} + \underbrace{I_p k_d (L \cdot N)}_{diffuse} + \underbrace{I_p k_s (R \cdot V)^n}_{specular}, \quad (1.3)$$

Once we have the intensities at the vertices, we can apply linear interpolation to compute intensities first along edges and then along scan lines.

Notice that for adjacent polygons, intensities necessarily agree along common edges because the intensities agree at common vertices. Moreover, on both sides of an edge, the value of the intensity near the edge is close to the value of the intensity along the edge. Thus linear interpolation of intensities along scan lines blurs the difference in intensities between adjacent polygons. This blurring eliminates Mach bands and provides the appearance of smooth curved surfaces.

The Gouraud Shading algorithm is an example of a scan line algorithm. A scan line algorithm is an algorithm that evaluates values at pixels scan line by scan line, taking advantage of the natural coordinate system induced by the orientation of the scan lines.

### 3. CONSLUSION & FUTURE WORK

#### Comparative Discussion

In this study, the system is developed to visualize neuron structure focuses on rat hippocampus cells, generate digitalized data from 'SWC' format and rendered its surface using Gouraud Shading approach. This is a new simplified prototype for constructing neuron structure model with properties closely matches with 3D neuronal morphology and connectivity.

The 3D scene is created using an OpenGL graphics window for previewing the 3D representation neuron. When a neuron is loaded to the scene, a 3D representation is generated from the object's component traces. The scene is rendered with the fidelity of the computers' OpenGL implementation and this generally allows the diffuse, ambient, emissive and transparency properties of objects to be specified. An OpenGL has been chosen to create the 3D model since it significantly speeds up the rendering and the real-time visualization.

Due to result raised from analyzing constraints of neuron structure prediction, a proposed area of comparative neuron study will be aided by performing the knowledge of virtual neuron connection structure. This study is focus to two main constraints where the first scope is related to misleading in generating digitalized neuron raw data toward realistic neuron morphology visualization. Previously, this data is represented as static view in archive database and certain developed neuron visualization system requires programming expertise to apply it. When the structure is restricted to achieve, this framework is introduced to visualize neuron raw data by integration of reconstruction model and surface rendering technique aim to produce neuron morphology toward realistic structure presentation. From this proposed approach, the framework's result was validated based on comparison with produced result from three selected existing program. The validation is measured in term of visualization quality towards greater realistic biological performance and accuracy of presentation virtual neuron. The development from our proposed framework was produced a neuron model as accurate as existing application.

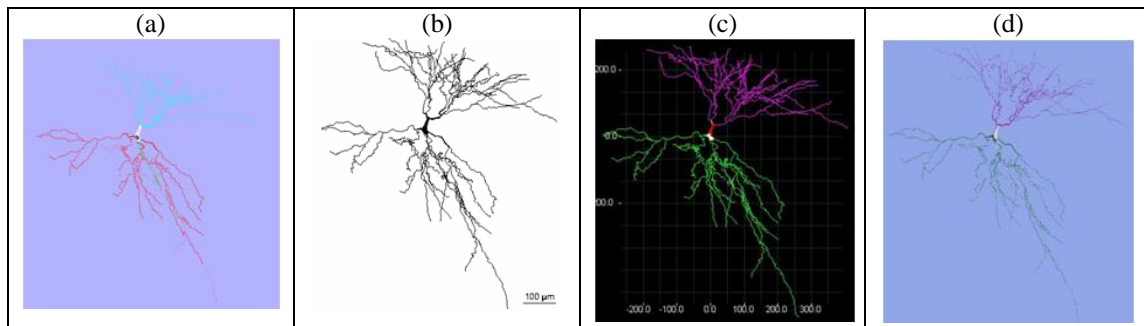


**FIGURE 7:** Validation and comparison result of visualizing neuron model of digital file between (a) our proposed framework and existing application, (b) result from Duke-Southampton which only presented static neuron model, (c) result achieved from CVapp program which having time constraints to fetch list of neuron selection and (d) result produced from neuroConstruct program which still presented a less realistic neuron especially for solid presentation type and slow in re-perform the neuron model after displaying other type of visualization mode.

Figure 7 shown the result discovered from comparison exercise for one of neuron sample. In this effort, Gouraud shading techniques has been embedded in our proposed neuron visualization application. The major contribution by introducing such shading algorithms in this framework is able to furnish smooth appearance of polygonal model by reducing the impact of sharp edge in order to give eyes the impression of a smooth curved surface. In CVapp, its application is for editing and converting morphology files either read or write the data from variety format i.e neurolucida .ascii, SWC, genesis .p and neuron .hoc. Still, each compartment presented in CVapp is listed as a line with its coordinates, parent compartment, and diameter. neuroConstruct also one of application that the creation, visualization, and analysis of networks of multicompartmental neurons in 3D space. It provides a number of functions to facilitate the clear display of large networks, cells with complex morphologies and individual synaptic connections. These include showing the dendrite and axon as lines or just showing ball-shaped somata rather than the full 3D structure of each cell. Even both applications able visualize neuron reconstruction model, however they still not emphasize on the appearance of neuron model which rendered the model by default without applied any shading. The priorities for those developments are only focus on ability to generate accurate network models wit properties that closely match the 3D neuronal morphology and connectivity of different brain regions. Still, in neuroConstruct [8] envisioned in its extensions will allow greater biological realism. Only in late 1990, one development [21] had applied volume rendering techniques with shading to reconstruct and visualize a 3D volumetric model of a dendritic. The shading helps accentuate the 3D shape of the dendrite but can represent the 3D shape of the model with accuracy limited only.

This shading implementation understood to assists in reconstructing neuron morphologies toward realistic visualization. Nevertheless, while smooth lighting was well captured to the polygon surface, others resulted constraint was occur in the neuron connection. The application encountered disconnect neuron segment whilst presented in the virtual environment. Even implementation of this algorithm has produced useful displays of 3D neurons images but also prove to be cumbersome, especially when the algorithm is used to detect and display soft issues for example this such neuron cells. The time required to segment the volume, isolate the desired surface (as is required by any 3D surface display). As such, even though shading application manage to provide smooth and realistic surface, it seem less suitable to be applied by its own for anatomical structure visualization i.e neuronal morphology. Thus, as the way forward, in this paper introduce an algorithm to overcome such problem to enhance the neuron connection towards smoother surface visualization. It will be valuable by integrating the shading technique with other application approach that will produce better image presentation virtual neuron morphology.

Currently, this program is focus in generating neuron connectivity phase and from this execution, we facing the second constraint which related to discontinue neuron connection between each

neuron segment in our generated virtual neuron result. To solve this encountered constraint we will propose to apply bounding curve interpolation, the algorithm returns points along a curve that passes exactly through the points at specific instants and forms a smooth curve for points in between in the next implementation phase. In this development phase, the evaluation is done based on comparison between our resulted virtual neuron with others three existing applications.

Subsequently, in the future, it will be an important task to enhance such neuron connection. As such, for the future work, the plan for combining current result with curve interpolation technique is required to improve neuron connection. It also would be more comprehensive and efficient by retrieving generation of neurons against another digital files database and format such as 'Neurolucida' for assisting the comparison analysis.

### Conclusion

Neuroanatomy is leading the pack of success stories in neuroinformatics [20]. An important aims in computational anatomy at the single-cell level consists of creating algorithms to generate virtual neuron structures that are morphologically corresponding to real neuronal dendrites. This goal may contribute a powerful knowledge distribution for the creation of large-scale, low-level model of neuron structure, activity and function. Virtual experiments can be carried out quickly, reliably, safely and inexpensively to allow the exploration of a large number of promising questions, and optimal experimental conditions. Virtual experiments can also examine the theoretical effect of each model parameter separately by precisely reproducing all other initial conditions.

Along with a numbers of on-going projects in categorizing the types of neuronal structures or mapping the neuronal networks, these facilities will provide valuable information to understand and manipulate neuronal morphology. In this article, we has reviewed some of these developments comprises of neuronal reconstruction in modeling digital morphological files and in databasing of neuronal morphologies.

The most important note that has been highlighted in this paper is the impact of neuronal morphology databases and its presentation. It depends on the availability of simple software tools that can extract flexibility a variety of user-defined morphological parameters from the archives database. As such, our priority in proposed reconstructing program is emphasizes to simplify the virtual function to be impacted for the signal transformation properties. Therefore, it will allow to be thoroughly analyzing to determine the relation between neuron's function and its relevant disease.

Roughly the proposed framework achieved the objective to solve the constraint encountered in presenting virtual neuron morphology data. Hopefully, these variations will be used in future work to improve the appearance of the neuron morphology connection in this proposed algorithm. We anticipate that the presented facts can be helpful and useful for the researchers in this field and the general audiences who may keen interests in exploring the ideas of neuron reconstruction visualization.

## 4. REFERENCES

1. Jaap van Pelt & Harry B.M. Uylings. "*Modeling Biology – Structures, Behaviors, Evolution: Modeling Neuronal Growth and Shape.*" The MIT Press, Cambridge, Massachusetts, 2007
2. Jaap van Pelt, Arjen van Ooyen & Harry B.M. Uylings. "*The need for integrating neuronal morphology databases and computational environments in exploring neuronal structure and function.*" Springer-Verlag, 2001.

3. Jaap van Pelt, Arjen van Ooyen, Harry B.M. Uylings. "Computational Neuroscience: Realistic Modeling for Experimentalists – Modelling dendritic geometry and the development of nerve connections." CRC-Press, Boca Raton, USA. 2001.
4. Jaap van Pelt & Andreas Schierwagen. "Morphological analysis and modeling of neuronal dendrites." Science Direct: Mathematical Biosciences, 2004.
5. Orit Shefi, Amir Harel, Dmitri B. Chklovskii, Eshel Ben-Jacob & Amir Ayali, "Biophysical constraints on neuronal branching." Science Direct: Neurocomputing, 2004.
6. G. Ascoli & J.L Krichmar. "L-Neuron: a modeling tool for the efficient generation and parsimonious description of dendritic morphology." ScienceDirect: Neurocomputing, 2000.
7. J.P. Eberhard, A. Wanner & G. Wittun. "NeuGen: A tool for the generation of realistic morphology of cortical neurons and neural networks in 3D". ScienceDirect: Neurocomputing, 2006.
8. Padraig Gleeson, Volker Steuber & R. Angus Silver. "neuroConstruct: A tool for modeling networks of neurons in 3D space." Cell Press; Neuron Neurotechnique, 2007.
9. Nivaldi Calonego Jr., Regina Celia Coelho & Luis Augusto Consularo. "3D neuron growth visualization." 2007.
10. J. Kozloski, K. Sfyarakis, S. Hill, F.Schurman, C. Peck & H. Makram. "Identifying, tabulating and analyzing contacts between branched neuron morphologies." International Business Machines Corporation. Volume 52. March 2008.
11. Duncan E. Donohue & Giorgio A. Ascoli. "A comparative computer simulation of dendritic morphology." PLoS Computational Biology. June 2008
12. Giorgio A. Ascoli, Jeffrey L. Krichmar, Slawomir J. Nasuto and Stephen L. Senft, "Generation, description and storage of dendritic morphology data." The Royal Society. 2001.
13. Ben Torben\_Nielsen, Karl Tuyls, Eric Postma,. "EvOL-NEURON: Neuronal morphology generation". ScienceDirect: Neurocomputing. 2008
14. Hylke Buisman, Manuel Gomez-Rodriguez & Saeed Hassanpour, "3D Reconstruction of Brain Tissue." Department of Computer Science & Electrical Engineering, Stanford University. 2007.
15. Susanne Schonknecht, Carsten Duch, Klaus Obermayer & Michael Sibila. "3D Reconstruction of Neurons from Confocal Image Stacks and Visualization of Computational Modeling Experiments." Arizona State University. 2007.
16. Kerry M. Brown, Duncan E. Donohue, Giampaolo D'Alessandro. "A Cross-Platform of Freeware Tool for Digital Reconstruction of Neuronal Arborizations from Image Stacks." Humana Press Inc: Neuroinformatics. 2005.
17. Bruce P Graham & Arjen van Ooyen. "Mathematical modelling and numerical simulation of the morphological development of neurons." BMC Neuroscience. 2006.
18. J. F. Evers, S. Schmitt, M. Sibila & C. Duch. "Progress in Functional Neuroanatomy: Precise Automatic Geometric Reconstruction of Neuronal Morphology from Confocal Image Stacks." Neurophysiology: Innovative Methodology. 2005.

19. J. C. Fiala,. “*Reconstruct: a free editor for serial section microscopy. Journal of Microscopy.*” 2005.
20. Giorgio A. Ascoli & Ruggero Scorcioni. “*Neuron and Network Modeling.*” George Mason University. 2006.
21. Ingrid Carlbom, Demetri Terzopoulos & Kristen M. Harrits. “*Reconstructing and Visualizing Models of Neuronal Dendrites.*” Digital Equipment Corporation Cambridge Research Lab. December, 1990.
22. Richard A. Robb. *3-D Visualization in Biomedical Applications.* Annual Reviews Biomedical. Mayo Foundation/Clinic, Rochester, Minnesota. 1999.
23. R.C. Cannon<sup>1,2</sup>, F.W. Howell<sup>2</sup>, N.H. Goddard<sup>2</sup> & E.De Schutter<sup>1</sup>. *Non-accurate Distributed Databases for Experimental Data & Models in Neuroscience.* Network: Computing Neural System. <sup>1</sup>University of Antwerp, Belgium & <sup>2</sup>University of Edinburgh, Scotland. 2002.

## Detection of Some Major Heart Diseases Using Fractal Analysis

**Nahina Islam**

eshika\_11@yahoo.com

*Department of Electrical and Electronic Engineering,  
Bangladesh University of Engineering and Technology (BUET)  
Dhaka, Bangladesh*

**Nafiz Imtiaz Bin Hamid**

nafiz\_24@iut-dhaka.edu

*Department of Electrical and Electronic Engineering,  
Islamic University of Technology (IUT)  
Dhaka, Bangladesh*

**Adnan Mahmud**

adnan903@iut-dhaka.edu

*Department of Electrical and Electronic Engineering,  
Islamic University of Technology (IUT)  
Dhaka, Bangladesh*

**Sk. M. Rahman**

s0163345@cqu.edu.au

*Department of Business and Informatics,  
Central Queensland University (CQU),  
Queensland, Australia*

**Arafat H. Khan**

sagar\_buet@yahoo.com

*Department of Electrical and Electronic Engineering,  
Bangladesh University of Engineering and Technology (BUET)  
Dhaka, Bangladesh*

---

### Abstract

This paper presents a new method to analyze three specific heart diseases namely Atrial Premature Beat (APB), Left Bundle Branch Block (LBBB) and Premature Ventricular Contraction (PVC). The problem is introduced from the discussion of Fractal Dimension. Further, the fractal dimension is used to distinguish between the Electrocardiogram (ECG) signals of healthy person and persons with PVC, LBBB and APB from the raw ECG data. The work done in this paper can be divided into few steps. First step is the determination of the rescaled range of an ECG signal. Then there comes the necessity of calculating the slope of the rescaled range curve. Through this methodology we have established a range of fractal dimension for healthy person and persons with various heart diseases. The way towards determining the range of fractal dimension for those ECG data taken from MIT-BIH Arrhythmia Database has been explained. Again, the obtained range of fractal dimension is also presented here in a tabular fashion with proper analysis

**Keywords:** Rescaled Range Analysis, PVC, APB, LBBB

---

## 1. INTRODUCTION

Premature Ventricular Contraction, also known as extra systole is a relatively common condition where the heart beat is initiated by the heart ventricles rather than the sino atrial node, the normal heartbeat initiator.

The term atrial premature beat describes beat arising from the atrium and occurring before the expected sinus beats. Premature beats can occur randomly or in a pattern. P-wave morphology differs from sinus beats and varies, depending on the origin of the impulse in the atria. In general beats arising in the high atria have upright P-waves in leads II, III and a VF and those originating in the low atria have inverted P-waves in those leads. Depending on the prematurity of the atrial impulse and refractoriness of the AV node and His-Purkinje system, the P-wave may conduct with normal or prolonged PR interval with narrow or aberrant QRS complex or may block and not be followed by a QRS complex. It has been empirically noted that alcohol in excess, fatigue, cigarettes, fever, anxiety and infectious diseases of all sort may result in atrial premature beats and elimination of these factors may correct the disorder. APB also occurs in some patients with CHF and in some with myocardial ischemia. They may also be noted in patients with underline myocardial disease, in those with pulmonary disease and systemic hypoxia. Premature beats are usually perceived by patients as "palpitations", and sometimes are of concern to patients who noticed skipped beats or fluttering that is frightening. Often atrial premature beats cause no symptoms and are not recognized by the patients. Then APB requires no specific therapy. If they are a source of aggravation or concerned to the patient and one of the above mentioned factors can be identified and should take immediate Medicare.

Premature and abnormal P-wave morphology as compared to the sinus P-wave activity (the premature P-wave may be obscure or it may be buried in the P-wave).

Premature P-wave may or may not be conducted and when conducted would be followed by a QRS wave that often has a normal duration but sometimes it is prolonged.

In a bundle branch block (either left or right) a block of excitation in one of the branches will cause the effective side to be excited i.e. depolarized later and this fact will be revealed in a prolongation of the duration of the QRS. So in BBB, the ventricles will be excited serially, the effected side being excited lastly. Excitation first appears on the surface of the thin walled right ventricles owing to the nature of the conduction system and differing thickness of ventricular myocardium. In the ECG signal the right sided V leads show a large, broad, downward wave. Left sided V leads show a large broad upward wave. QR is prolonged and downward in V5-V6.

So detecting APB, PVC and LBBB precisely have important clinical significance.

## 2. RELATED WORKS

Frequently a time varying signal is required to analyze to extract characteristic of interest. For example, medical diagnosis often requires the analysis of time varying cardiac, respiratory or brain signals in order to detect cardiac, pulmonary, or mental problems. In general, most temporal processes are analyzed using Fourier transform technique (frequency domain); chaos dynamic (position-velocity phase plane) and other complex mathematical techniques have been applied to signal analysis [4].

Heart failure patients can also be identified by computing certain statistics of the sequence of heart beats such as the Allan factor (AF) and its generalization [1]. One method has been applied in [5] for the diagnosis of neuromuscular diseases and can be suitably applied for microcomputer-based on-line analysis of EMG signals. In [7] an electrocardiogram (ECG) beat classification system based on wavelet transformation and probabilistic neural network (PNN) is proposed to discriminate six ECG beat types. With observations it opted for computer-aided diagnosis of heart diseases based on ECG signals. In [8] a functional model of ANN is proposed to aid existing diagnosis methods which investigates the use of Artificial Neural Networks (ANN) in predicting

the Thrombo-embolic stroke disease. For ascertaining the robustness of the proposed algorithm; evaluation of the entire MIT-BIH arrhythmia database has been attempted in [9], but the view and purpose was way too different from that of ours. With the best of our effort we couldn't come up with similar works using ECG signal for detailed fractal analysis.

### 3. SIGNIFICANCE OF OUR WORK

A common drawback of the related methods described above is that they are often complex, not easily amenable to analyze and require some data preprocessing procedures, such as filtering etc. Thus there remains a need for simple and practical method for analyzing such time varying electrical signals.

ECG signal is a self-similar object. So, fractal analysis can be implemented here for proper utilization of the gathered info. It obviously opens scope to analyze the MIT-BIH Arrhythmia Database with different view points. Scope for further medical research and clinical advancement remain wide open through this.

## 4. WHAT IS FRACTAL AND FRACTAL ANALYSIS

Fractals are of rough or fragmented geometric shape that can be sub divided in parts, is of which are reduced copy of the whole [2]. Fractal dimension is number very often non integer, often it is the only one measure of fractals. It measures the degree of fractal boundary fragmentation or irregularity over multiple scales. It determines how fractal differs from Euclidian objects.

Images and shapes within images which cannot be represented by Euclidian geometry have been analyzed by fractal geometry. Unlike conventional geometry, which deals with lines, triangles, circles, spheres and cones, fractal geometry is concerned with broken or fractured shapes as so commonly found in nature.

A collection of mathematical procedure used to determine fractal dimension (or any other fractal characteristic) or set of fractal dimensions with smallest error.

### 4.1 Self similarities and fractal analysis

Fractal is strictly self similar if it can be expressed as a union of sets, each of which is an exactly reduced copy of the full set (Sierpinski triangle, Koch flack). The most fractal looking in nature does not display this precise form.

Natural objects are not union of exact reduced copies of whole. A magnified view of one part will not precisely reproduce the whole object, but it will have the same qualitative appearance. This property is called statistical self-similarity or semi-self similarity.

As ECG signal of a human heart is a self similar object. So it must have a fractal dimension. So we have used fractal analysis. And to determine the fractal dimension rescaled range method has been used here.

### 4.2 Rescaled range analysis

Hurst developed the rescaled range analysis, a statistical method to analyze long records of natural phenomena [3]. There are two factors used in this analysis; firstly the range R, this is the difference between the minimum and the maximum accumulated values of cumulative sum of X(t, τ) of the natural phenomenon at discrete integer-valued time t over a time span τ, and secondly, the standard deviation is S, estimated from the observed values X<sub>i</sub>(t). Hurst found that the ratio R/S is very well described for a large number of natural phenomena by the following empirical relation.

$$[R(\tau) / S(\tau)] \propto \tau^H$$

Where  $\tau$  is the time span and  $H$  is the Hurst component. The coefficient  $C$  is taken equal to 0.5 by Hurst.  $R$  and  $S$  are defined as:

$$R(\tau) = \max_{1 \leq t \leq \tau} X(t, \tau) - \min_{1 \leq t \leq \tau} X(t, \tau)$$

$$S(\tau) = \left\{ \frac{1}{\tau} \sum_{t=1}^{\tau} [\zeta(t) - (\zeta)_\tau]^2 \right\}^{1/2}$$

Where,

$$(\zeta)_\tau = \frac{1}{\tau} \sum_{t=1}^{\tau} \zeta(t)$$

and,

$$X(t, \tau) = \sum_{u=1}^t [\zeta(u) - (\zeta)_\tau]$$

#### 4.3 Relation between the rescaled range and fractal dimension

The relation between the Hurst exponent and the fractal dimension is simply  $D=2-H$ . We have calculated the individual calculations for each interval length. A straight line is fitted in the log-log plot.

$\log [R(\tau)/S(\tau)] = c + H \log (\tau)$  Where  $H$  = slope.

So fractal dimension,  $D=2-H$ . With the help of these equations we can easily evaluate fractal dimension in the rescaled range analysis.

The results for the R/S analysis depend on the number of sub-interval, the minimum and maximum lags. It is not clear how important the number of sub interval is. Mandel Brot and Wallis noted that the smallest lags (under 30) cannot be expected to be on the line and should not be in the procedure. In the analysis, we choose not to use overlapping sub intervals so that extra dependency between these sub-intervals occurs to find the fractal dimension.

#### 4.4 Analysis of the procedure in brief

We have implemented the rescale range by using MATLAB codes. The source of the ECGs included in the MIT-BIH arrhythmia database is a set of over 4000 long term Holter recording that were obtained by the Beth Israel Hospital Arrhythmia laboratories between 1975 and 1979 [6]. Here, a sample of the analysis procedure is shown through PVC patient. At first we are showing the ECG signal of a patient with Premature Ventricular Contraction (PVC).

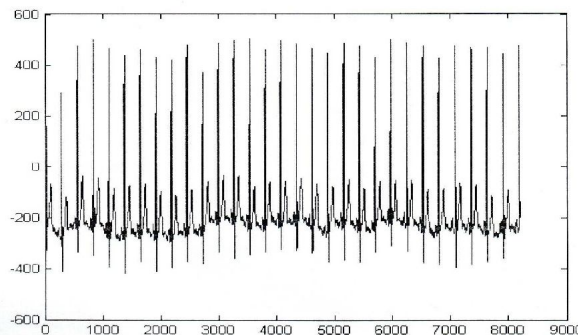


**FIGURE 1:** ECG Signal of a PVC Patient.

Then we determined the rescaled range of this ECG signal for different slot size (analogous to the sub-interval) utilizing MATLAB code. After that, we got the following table:

Slot Size, T	$\log_2(T)$	$\log_2(R/S)$
1024	10	12.0865
512	9	11.4365
256	8	10.8452
128	7	10.3248
64	6	9.9850
32	5	9.3542

**TABLE 1:** Rescaled Range of ECG Signal for Different Slot Size

From this table we have got the following graph:

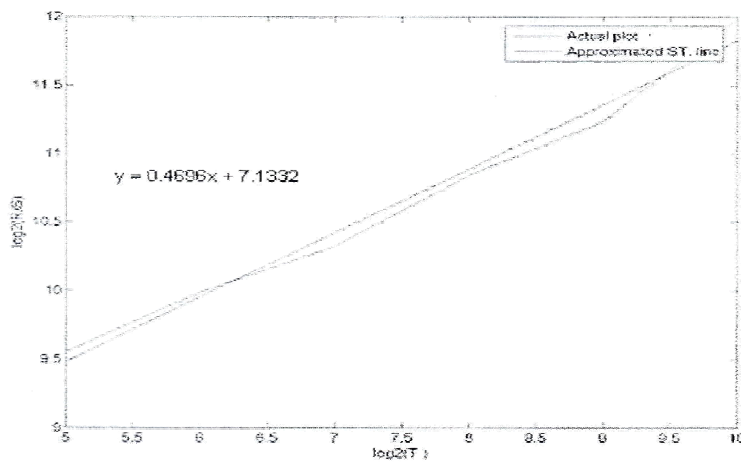


**FIGURE 2:** Fitted Straight Line by Log-Log Plot

Slope being,  $H=0.5164$ , fractal dimension thus remains,  $D=2-H=1.4836$

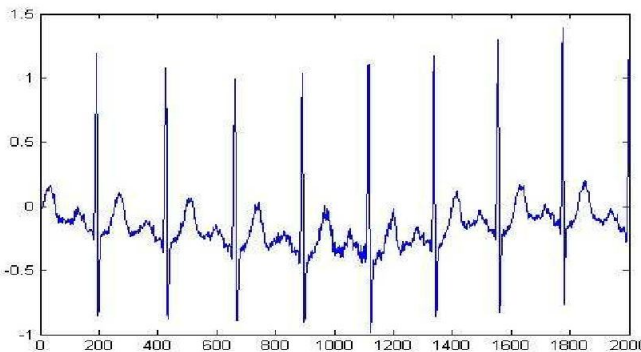


**FIGURE 3:** ECG signal of APB patient (MIT-BIH 209)

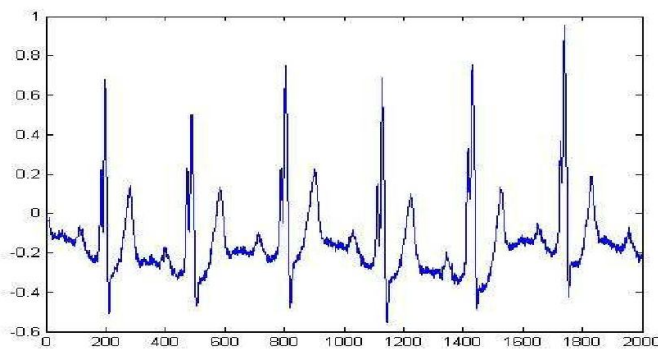


**FIGURE 4:** ECG signal of LBBB patient (MIT- BIH 111)

Like the example shown above, this approach was applied to MIT-BIH Arrhythmia database file 209 for patient with Atrial Premature Beat (APB) in Fig 3 & Left Bundle Branch Block (LBBB) in Fig 4. Again, it can also be successfully used to tell about the fractal dimension range for the other database files.

Thus, our above mentioned methodology can be suitably applied to MIT-BIH database and in this way a distinct range of fractal dimension was found out for the cases mentioned.

#### 4.5 Obtained result and discussion

Here, we have determined the range of fractal dimension for patients with premature ventricular contraction, left bundle branch block, atrial premature beats along with healthy persons.

Like the shown example, our methodology was applied to other MIT-BIH Arrhythmia database for providing a thorough analysis. Again, it can successfully tell about the fractal dimension range using the other database files of MIT-BIH for PVC patient like 106, 116, 119, 200, 201, 203, 207, 208, 210, 213, 214, 215, 217, 221, 223, 228, and 233. In the same way, for APB case it also accomplishes its goal of reaching a proper fractal dimension range analyzing the samples like 207,209,222,232 etc.

Thus, our above mentioned methodology can be suitably applied to MIT-BIH database and thus a distinct range of fractal dimension was found out for the cases mentioned. The ranges are tabulated here below:

Sample ECG signal	Range
Healthy Person	1.65-1.67
Patients with PVC	1.48-1.53
Patients with APB	1.54-1.58
Patients with LBBB	1.71-1.74

**TABLE 2:** Distinct range of fractal dimension for sample ECG signal

## 5. CONSLUSION

In this paper it has been tried to present a different method for the detection of heart diseases from a newer perspective. ECG signal being a self-similar object; can well be considered for fractal analysis. We have used rescaled range method to determine the specific range of fractal dimension for each specific disease. And we found that the range of fractal dimension for healthy person is 1.65-1.67, for PVC patients it is 1.48-1.53, for APB patients it is 1.54-1.58 and finally for LBBB patients the range is 1.71-1.74. So, the methodological analysis does provide a significant clinical advantage.

## 6. FUTURE WORK

This paper went for fractal analyzing the MIT-BIH arrhythmia database for heart disease detection. Such an approach should further encourage the researchers in algorithm development on these as it is a widely used database. So, suitably ranging the MIT-BIH arrhythmia database on the basis of fractal dimension should obviously encourage and smooth further research.

## 7. REFERENCES

1. Malvin C. Teich, "Fractal behavior of the Electrocardiogram: Distinguishing Heart Failure and Normal Patients using Wavelet Analysis.", IEEE-EMBS-18-1128-1996.pdf
2. "Fractals and Fractal Dimension", <http://www.vanderbilt.edu/AnS/psychology/cogsci/chaos/workshop/Fractals.html>
3. P. Vanouplines, "Rescaled range analysis and the fractal dimension of pi". University Library, Free University Brussels, Pleinlaan 2, 1050 Brussels, Belgium.
4. Daoming Zhang, Guojun Tan, Jifei Hao, "Fractal random walk and classification of ECG signal" International Journal of Hybrid Information Technology, Vol. 1, No. 1, Jan 2008.
5. M. Bodruzzaman,J. Cadzow, R. Shiavi, A. IGroy, B. Dawant and M. Wilkes,"Hurst's Rescaled-Range (R/S) Analysis and Fractal Dimension of Electromyographic (EMG) Signal" Southeastcon '91., IEEE Proceedings.
6. MIT-BIH Arrhythmia Database from PhysioBank- physiologic signal archives for biomedical research.

7. Sung-Nien Yu and Ying-Hsiang Chen-"Electrocardiogram beat classification based on wavelet transformation and probabilistic neural network"-ScienceDirect:Pattern Recognition Letters; Volume 28, Issue 10, 15 July 2007, Pages 1142-1150
8. D.Shanthi, Dr.G.Sahoo and Dr.N.Saravanan-"Designing an Artificial Neural Network Model for the Prediction of Thrombo-embolic Stroke"- International Journals of Biometric and Bioinformatics (IJBB): Volume (3), Issue (1)
9. Jinkwon Kim, Hang Sik Shin, Kwangsoo Shin and Myoungho Lee-"Robust algorithm for arrhythmia classification in ECG using extreme learning machine"BioMedical Engineering Online,2009.  
<http://www.biomedical-engineering-online.com/content/8/1/31>

## Effective Morphological Extraction of True Fingerprint Minutiae based on the Hit or Miss Transform

**Roli Bansal**

*Dept. of Comp. Science  
University of Delhi, Delhi (India)  
110001.*

rolibansal1@rediffmail.com

**Priti Sehgal**

*Reader, Deptt. of Comp. Science  
Keshav Mahavidyalaya,  
University of Delhi, Delhi (India)  
1100035.*

psehgal@keshav.du.ac.in

**Punam Bedi**

*Associate Professor,  
Dept. of Comp. Science  
University of Delhi, Delhi (India)  
110001.*

pbedil@cs.du.ac.in

---

### ABSTRACT

Fingerprints are the most widely used parameter for personal identification amongst all biometrics based personal authentication systems. As most Automatic Fingerprint Recognition Systems are based on local ridge features known as minutiae, marking minutiae accurately and rejecting false ones is critically important. In this paper we propose an algorithm for extracting minutiae from a fingerprint image using the binary Hit or Miss transform (HMT) of mathematical morphology. We have developed and tested structuring elements for different types of minutiae present in a fingerprint image to be used by the HMT after preprocessing the image with morphological operators. This results in efficient minutiae detection, thereby saving a lot of effort in the post processing stage. The algorithm is tested on a large number of images. Experimental results depict the effectiveness of the proposed technique.

**Keywords :** Biometrics, fingerprint image, minutiae extraction, Hit or Miss transform, mathematical morphology

---

### 1. INTRODUCTION

In today's advanced digital technology world, there is an increased requirement of security measures leading to the development of many biometrics based personal authentication systems. Biometrics is the science of uniquely recognizing humans based upon one or more intrinsic physical (e.g., fingerprint, iris, face, retina etc.) or behavioral (e.g., gait, signature etc.) traits. Fingerprints are the most widely used parameter for personal identification amongst all biometrics. The reason behind the popularity of fingerprint-based recognition among the biometrics-based security systems is the unchangeability of fingerprints during the human life span and their uniqueness [7]. However to meet the performance requirements of high security applications, multimodal biometrics [1, 5] is also used as it helps to minimize system error rates.

Fingerprint identification is commonly employed in forensic science to aid criminal investigations etc. A fingerprint is a unique pattern of ridges and valleys on the surface of finger of an individual. A ridge is defined as a single curved segment, and a valley is the region between two adjacent ridges. Most Automatic Fingerprint Recognition Systems are based on local ridge features known as minutiae. Sir Francis Galton (1822-1922) was the first person who observed the structures and permanence of minutiae. Therefore, minutiae are also called "Galton details".

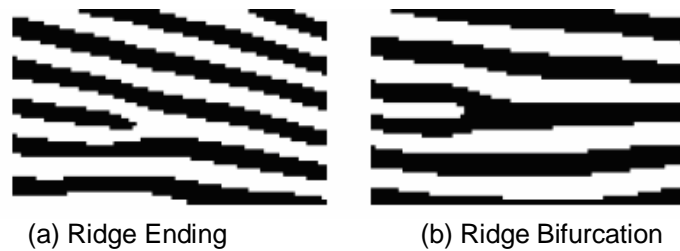


**Figure 1:** Example of a ridge ending and a bifurcation.

They are used by forensic experts to match two fingerprints. There are about 150 different types of minutiae [2] categorized according to their configuration. Among these minutia types, "ridge ending" and "ridge bifurcation" are the most commonly used, since the other types of minutiae can be seen as combinations of "ridge endings" and "ridge bifurcations" (figure 2). Figure 1 illustrates the two most basic types of minutiae: ridge endings and bifurcations. It is these minutiae points which are used for determining uniqueness of a fingerprint.

Automated fingerprint recognition systems can be categorized as: verification or identification systems. The verification process either accepts or rejects the user's identity by matching against an existing fingerprint database. In identification, the identity of the user is established using fingerprints. Since accurate matching of fingerprints depends largely on ridge structures, the quality of the fingerprint image is of critical importance. However, in practice, a fingerprint image may not always be well defined due to elements of noise that corrupt the clarity of the ridge structures.

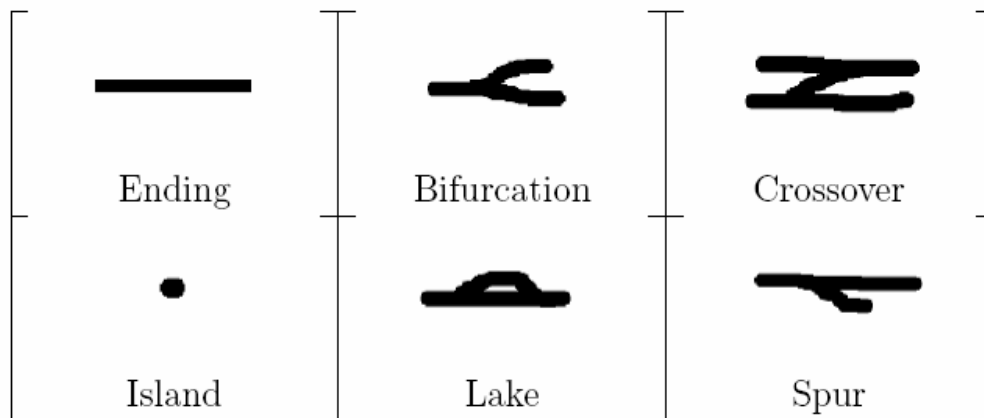


**Figure 2 :** Some common minutiae types.

This corruption may occur due to variations in skin and impression conditions such as scars, humidity, dirt, and non-uniform contact with the fingerprint capture device. Many algorithms [2, 16, 26, 27, 28] have been proposed in the literature for minutia analysis and fingerprint classification for better fingerprint verification and identification. Some algorithms classify the fingerprint pattern into different groups at the time of enrollment [30]. Their results also depend largely on the quality of the input image. Thus, image enhancement techniques are often employed to reduce the noise and to enhance the definition of ridges against valleys so that no spurious minutiae are identified. Several methods have been proposed for enhancement of fingerprint images which are based on image normalization and Gabor filtering (Hong's algorithm) [11], Directional Fourier filtering

[3], Binarization Method [23], Directional Filter Based Analysis [25], Fingerprint image thinning using PCNNs [9] etc. The Hong's algorithm inputs a fingerprint image and applies various steps for enhancement. Several other fuzzy techniques for image enhancement are also available [4, 20, 21, 32, 33].

Once the fingerprint image is enhanced minutiae points can be extracted. There are a lot of minutiae extraction algorithms available in the literature like direct gray scale ridge tracking strategy [7, 31] which work on gray scale images directly, minutiae extraction by run length encoding method [34] which does not require the fingerprint image to be thinned and other techniques based on extracting minutiae from skeletonised images using the crossing number algorithm [8, 10, 14, 15, 18, 19, 24]. The crossing number technique extracts ridge endings and bifurcations from a binarized skeletonised image by examining the local neighbourhood using a 3X3 window of each pixel and counting the number of 0 to 1 transitions in it. This method of extraction extracts a very large number of spurious minutiae together with true ones, thereby relying heavily on enormous post processing procedures including one by one minutia validation and invalidation[8, 14, 15].

In this paper we propose a novel algorithm for extracting minutiae from a fingerprint image using the binary Hit or Miss transform (HMT) of mathematical morphology. Morphological operators are basically shape operators and their composition allows the natural manipulation of shapes for the identification and the composition of objects and object features. We have developed and tested structuring elements for different types of minutiae present in a fingerprint image to be used by the HMT to extract valid minutiae, after preprocessing the image with such morphological operators. As mentioned earlier, the problem with other techniques is the generation of a large number of spurious minutiae together with true ones whereas our algorithm results in efficient minutiae detection, thereby saving a lot of effort in the post processing stage. The algorithm is tested on a large number of images. Experimental results depict the effectiveness of the proposed technique.

The rest of the paper is organized as follows: Section 2 introduces basic concepts and operations of mathematical morphology to be used in this paper. Section 3 describes the proposed algorithm. Experimental results are reported in Section 4. Section 5 concludes the paper.

## 2. MATHEMATICAL MORPHOLOGY

Mathematical morphology finds its place in computer vision as it emphasizes in shape information. It refers to a branch of nonlinear image processing and analysis that concentrates on the geometric structure within an image, it is mathematical in the sense that the analysis is based on set theory, topology, lattice, random functions, etc. Mathematical morphology is considered to be a powerful tool to extract information from images. We briefly discuss some mathematical morphology transformations [22] in this section.

### 2.1 Erosion and Dilation.

Erosion and dilation are considered the primary morphological operations. Erosion shrinks or thins object in a binary image where as Dilation grows or thickens objects. Erosion and Dilation constitute the basis for more complex morphological operators and can be defined as follows:

Let A:  $z^2 \rightarrow z$  be an image and B:  $z^2 \rightarrow z$  be a structuring element. The erosion of A by B denoted by  $(A \ominus B)$ , is expressed as

$$(A \ominus B) = \{ z | (B)_z \cap A^c \neq \emptyset \} \quad (1)$$

The dilation of A by B, is denoted by  $(A \oplus B)$ , and is expressed as

$$(A \oplus B) = \{ z | (B)_z \cap A \neq \emptyset \} \quad (2)$$

In other words dilation of A by B is the set of all structuring element origin locations where the reflected and translated B overlaps at least some portion of A.

### 2.2 Opening and Closing.

Closing and opening are two examples of elementary combinations of erosion and dilation. Visually, opening smoothes contours, break narrow isthmuses and eliminates small islands. The gray-scale opening of A by B, denoted by  $A \circ B$ , is simply erosion of A by B, followed by dilation of the result by B as,

$$(A \circ B) = (A \ominus B) \oplus B \quad (3)$$

On the other hand, closing smoothes the contours, fills narrow gulfs and eliminate small holes. The gray-scale closing of A by B, denoted by  $A \bullet B$  is a dilation followed by an erosion, as

$$(A \bullet B) = (A \oplus B) \ominus B \quad (4)$$

### 2.3 The Hit or Miss Transformation(HMT)

The morphological Hit or Miss Transform is the localization operator in mathematical morphology. It finds occurrences of an object and its nominal surroundings in a set or an image. It is a natural operation to select out pixels that have certain geometric properties, such as corner points, isolated points or border points and performs template matching.

The Hit or Miss Transformation of A by B is denoted by  $A \otimes B$ . Here B is a structuring element pair  $B = (B_1, B_2)$ , rather than a single element as before. The hit and miss transformation is defined in terms of these two structuring elements as

$$A \otimes B = (A \ominus B_1) \cap (A^c \ominus B_2) \quad (5)$$

Erosion with  $B_1$  determines the location of foreground pixels and erosion of the complement with  $B_2$  determines the location of the background pixels. Performing intersection of these two operations outputs an image which consists of all locations that match the pixels in  $B_1$  (a hit) and that have none of the pixels in  $B_2$  (a miss). In this paper HMT has been used as a building block for complex morphological operators like spur removal, bridge removal, thinning and minutiae detection.

## 3. PROPOSED TECHNIQUE

In this paper we propose a minutiae extraction algorithm which extracts minutiae using the morphological Hit or Miss Transform. But, as discussed earlier, the success of any minutiae extraction technique depends on the quality of the input image, the image needs to be enhanced before processing it for minutiae extraction. Given in figure 3 is the schematic diagram of the proposed technique. The details of the various steps are explained in the following subsections

### 3.1 Image Enhancement

The performance of any minutiae detection algorithm relies heavily on the quality of the input fingerprint image. For a fingerprint image of low quality, a large number of false minutiae are extracted during minutiae extraction. Hence, it is important to enhance the input fingerprint before performing minutiae extraction to cater to the following two aspects:

- Noise
- Broken ridges.

A lot of fingerprint enhancement methods based on input image quality have been proposed in the literature [4, 9, 11, 12, 20, 23, 32]. We have used the Hong's algorithm [11] for the enhancement of our input fingerprint image, which is based on the convolution of the image with Gabor filters tuned to the local ridge orientation and frequency. Firstly, the image is segmented to extract it from the background. Next, it is normalized so that it has a prespecified mean and variance. After calculating the local orientation and ridge frequency around each pixel, the Gabor filter is applied to each pixel location in the image. As a result the filter enhances the ridges oriented in the direction of local orientation. Hence the filter increases the contrast between the foreground ridges and the background, while effectively reducing noise [figure 4].

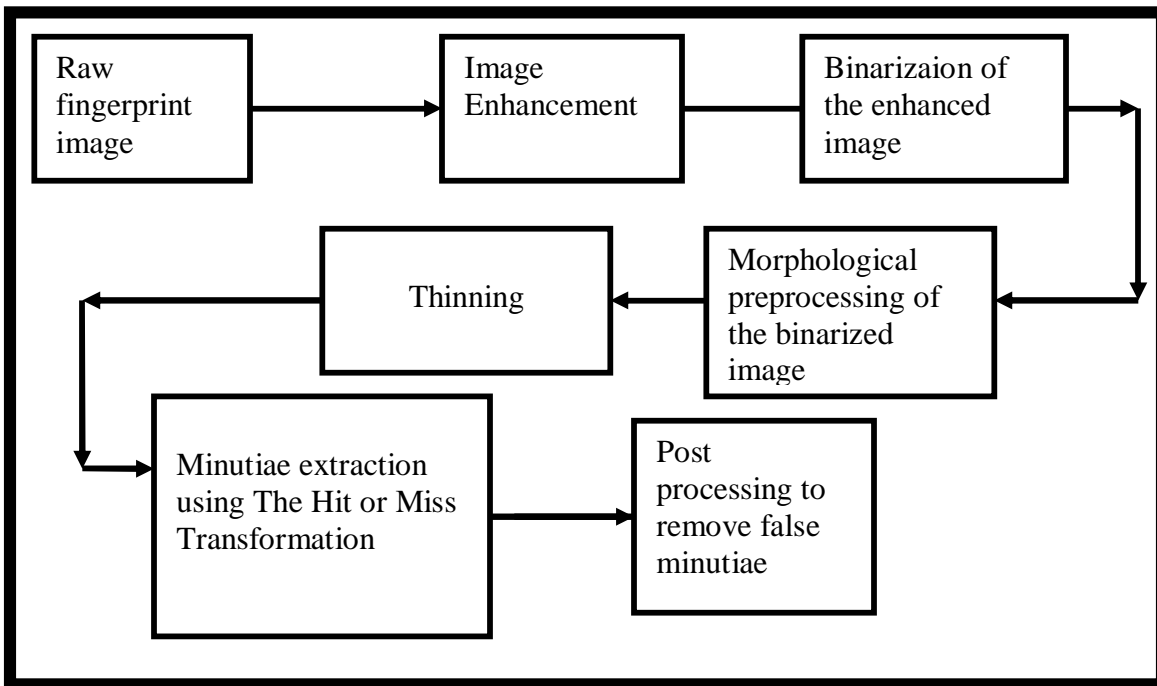


**Figure 3 :** Block diagram of the proposed Algorithm.

### 3.2 Binarization

Image binarization converts a 256 gray level image to a binary image (i.e. with only two levels – black and white [figure 4]). The simplest way to use image binarization is to choose a threshold value, and classify all pixels with values above this threshold as white, and all other pixels as black. The problem is how to select the correct threshold. In many cases, finding one threshold compatible to the entire image is very difficult, and in many cases even impossible. Therefore, adaptive image binarization is needed where an optimal threshold is chosen for each image area [6]. There are other methods also available for image binarization [17].

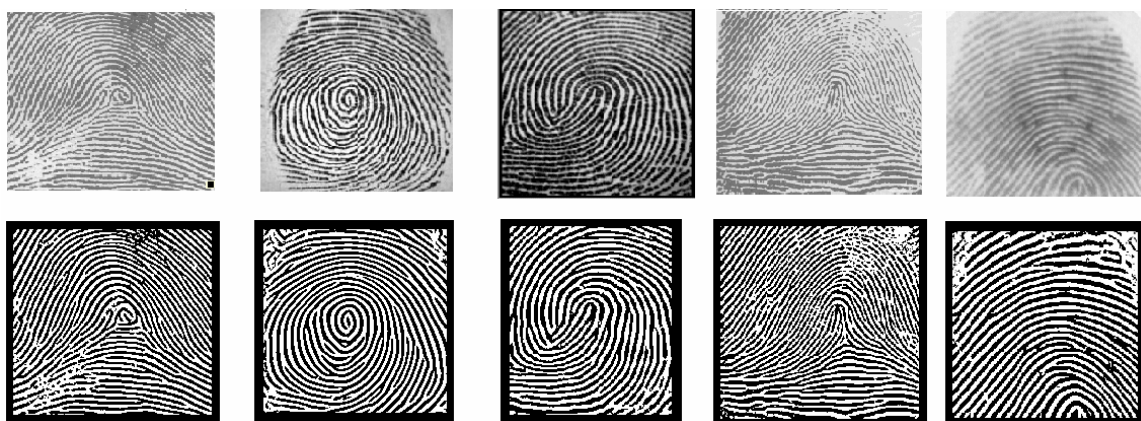


**Figure 4 :** The first row shows the original images. The second shows the enhanced and binarized images correspondingly.

### 3.3 Morphological Preprocessing

After close examination of the binarized image, it can be seen that the misconnections and isolated regions (dots, holes, islands etc.) in a binary image may introduce a number of spurious minutiae in thinned images. Therefore some morphological operators are applied to the binarized image as follows:

#### 1. Spur removal

Spurs are short length irregularities in the boundary of the original object. They can be removed by a process called pruning. The spur operator is shown in figure 5.

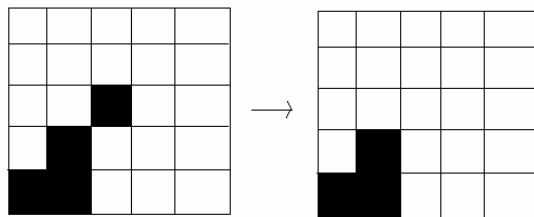


**Figure 5:** Spur operator.

#### 2. Spurious bridge removal

Some linked parallel valleys may be separated to eliminate spurious bridges(figure 6) in the skeleton image.

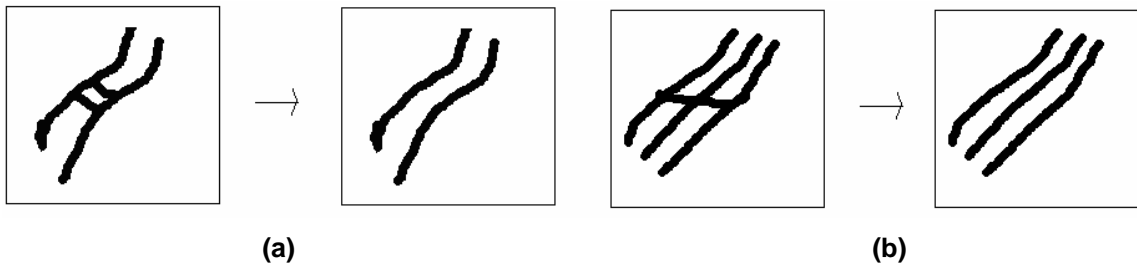


**Figure 6(a) and (b) :** Spurious bridges removal.

#### 3. Spurious holes removal .

Spurious holes are regions (figure 7) with an area (number of pixels) below a threshold  $w_1$ . The threshold value has to be selected appropriately so that it is not so small that it does not remove the spurious hole and not so large that it distorts the actual image. These regions are identified and filled so that the subsequent thinning operation does not produce spurious closed loops.

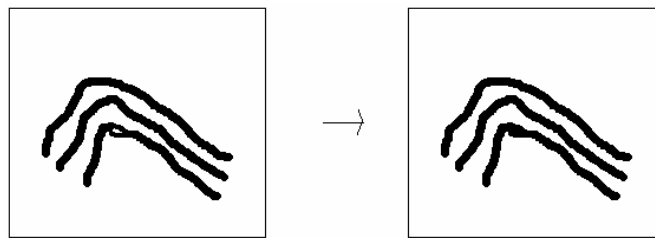


**Figure 7 :** Spurious holes removal.

#### 4 Isolated islands removal

Islands (figure 8) are short lines with an area below a threshold  $w_2$ . Removing these areas eliminates any spurious dots and islands from the binarized image.

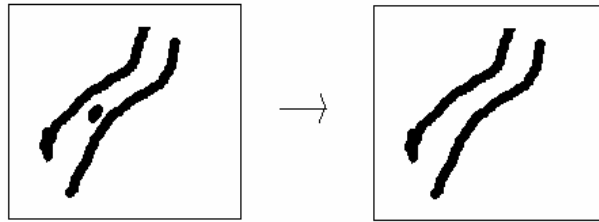


**Figure 8 :** Islands removal

### 3.4 Thinning

The next step is to thin the processed binary image using the morphological thinning operation. The thinning algorithm removes pixels from ridges until the ridges are one pixel wide[29]. In this paper, it is related to the hit or miss transform and can be expressed quite simply in terms of it . The thinning of an image  $I$  by a structuring element  $J = (J_1, J_2)$  is given by :

$$\text{Thin}(I, J) = I - (I \otimes J) \quad (6)$$

where, the subtraction is the logical subtraction defined by:

$$X - Y = X \cap \text{Not } Y \quad (7)$$

The operation is repeatedly applied until it causes no further changes to the image(i. e., until convergence). The structuring element sequence  $J$  used by us is shown in figure 9. Structuring elements from (i) to (viii) show the sequence for  $J_1$  and from (ix) to (xvi) show the sequence for  $J_2$ (complement of  $J_1$ ). The image is thinned using the structuring element pairs  $(J_1^i, J_2^i)$ ,  $i = 1..8$  in sequence. Doing so produces a connected skeleton of the image. The process is repeated in cyclic fashion until the operation produces any further change in the image (figure 10).

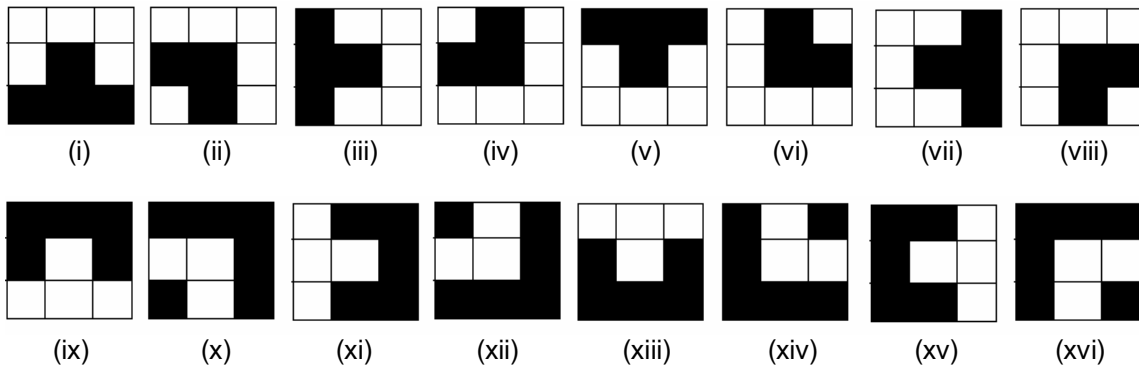


**Figure 9 :** (i) to (viii) The structuring element sequence  $J_1 = (J_1^1, J_1^2, J_1^3, J_1^4, J_1^5, J_1^6, J_1^7, J_1^8)$ . (ix) to (xvi) The structuring element sequence  $J_2 = (J_2^1, J_2^2, J_2^3, J_2^4, J_2^5, J_2^6, J_2^7, J_2^8)$ .

### 3.5 Minutiae Extraction Using HMT

In this step, we shall extract the two basic types of minutiae points (ridge terminations and ridge bifurcations) from the thinned image obtained from the previous step using the Hit or Miss Transformation. For this purpose, we have developed structuring elements to for different types of minutiae present in the fingerprint image, to be utilized by the HMT. Although this computes all the minutiae points, some false minutiae may occur due to some superfluous information in the thinned image. They are removed in the last step of the algorithm. However, it can be seen from the final results that the number of false minutiae is lesser as compared to other techniques as the image is already preprocessed with morphological operators before thinning.

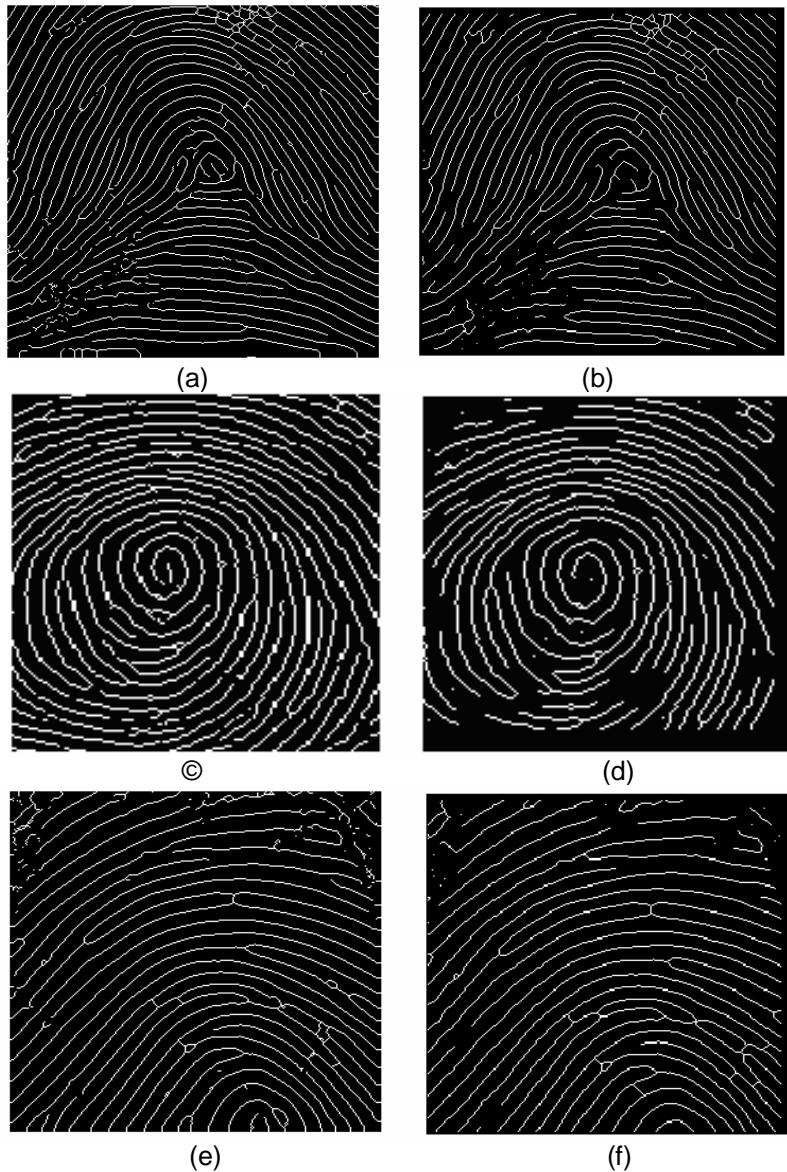


**Figure 10 :** (a), (c) and (e) show the thinned image after applying the thinning operator directly to the binarized images. (b), (d) and (f) show the thinned image after applying the thinning operator to the corresponding morphologically processed binarized images.

### 3.5.1 Extracting Ridge Terminations

Ridge endings are those pixels in an image which have only one neighbour in a 3X3 neighbourhood. The minutiae image M1 containing ridge terminations is given by applying Hit or Miss transform on I by J as follows:

$$M1 = I \otimes J \quad (8)$$

where, I is the thinned image and J is the sequence of structuring element pairs (J<sub>1</sub>, J<sub>2</sub>) .

Applying eq. 5,

$$I \otimes J = (I \ominus J_1) \cap (I^c \ominus J_2) \quad (9)$$

The structuring element sequence J that we have designed for determining endpoints in an image in this paper is shown in figure 11. The structuring elements have been designed in such a way so as to select all pixels from

image I that have a single neighbour in a 3X3 neighbourhood and leave all pixels that have more than one neighbour. Each of the structuring element pairs  $(J_1^i, J_2^i)$ ,  $i = 1..8$ , is applied in sequence and the collective output gives the ridge endpoints in the fingerprint image.

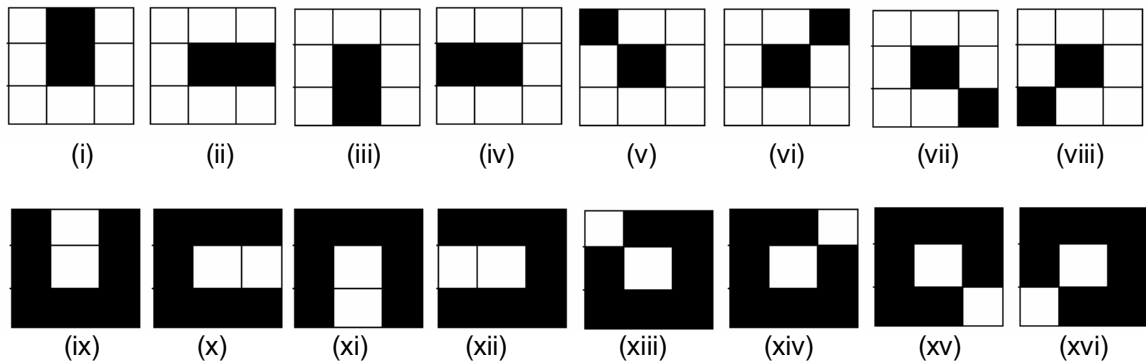


**Figure 11 :** (i) to (viii) The structuring element sequence  $J_1 = (J_1^1, J_1^2, J_1^3, J_1^4, J_1^5, J_1^6, J_1^7, J_1^8)$ . (ix) to (xvi) The structuring element sequence  $J_2 = (J_2^1, J_2^2, J_2^3, J_2^4, J_2^5, J_2^6, J_2^7, J_2^8)$ .

### 3.5.2 Extracting Ridge Bifurcations

Ridge bifurcations are those pixels in an image which have only three neighbours in a 3X3 neighbourhood and these neighbours are not adjacent to each other. The minutiae image M2 containing ridge terminations is given by:

$$M2 = I \otimes J \quad (10)$$

where, I is the thinned image and J is the sequence of structuring element pairs ( $J_1, J_2$ ). Applying eq. 5,

$$I \otimes J = (I \ominus J_1) \cap (I^c \ominus J_2) \quad (11)$$

The structuring element sequence J that we have designed for determining endpoints in an image in this paper is shown in figure 12. Structuring elements from (i) to (viii) show the sequence for  $J_1$  and from (ix) to (xvi) show the sequence for  $J_2$  (complement of  $J_1$ ). The structuring elements are designed as per an actual bifurcation point in a fingerprint image, where each pixel has exactly three neighbours which are not next to each other. Each of the structuring element pairs  $(J_1^i, J_2^i)$ ,  $i = 1..8$ , is applied in sequence and the collective output gives the ridge bifurcations in the fingerprint image.

When the Hit or Miss structuring elements are small, a faster way to compute the HMT is to use a lookup table [21].

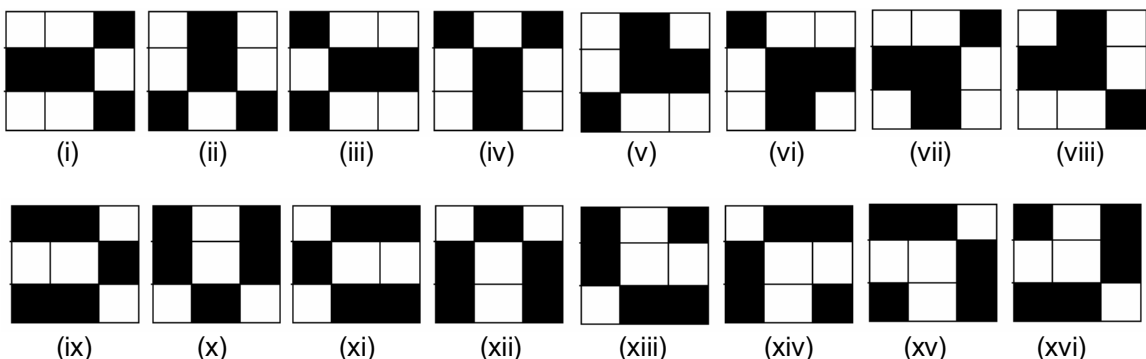


**Figure 12 :** (i) to (viii) The structuring element sequence  $J_1 = (J_1^1, J_1^2, J_1^3, J_1^4, J_1^5, J_1^6, J_1^7, J_1^8)$ . (ix) to (xvi) The structuring element sequence  $J_2 = (J_2^1, J_2^2, J_2^3, J_2^4, J_2^5, J_2^6, J_2^7, J_2^8)$ .

### 3.6 Post Processing.

The minutiae set extracted in the previous step contains many false or spurious minutiae. The following simple post processing steps remove them.

1. If the distance between two bifurcations is less than a threshold  $T$  and they are in the same ridge, remove both of them (merge, bridge, ladder, lake in figure 13).
2. If the distance between two terminations is less than a threshold  $T$  and the difference between their angles of orientation is very small, then the two minutiae are regarded as false (break, multiple breaks in figure 13) and are removed.

If the distance between a bifurcation and a termination is less than a threshold  $T$  such that  $T$  is the average inter ridge width, then they are removed (spur, break and merge in the figure).

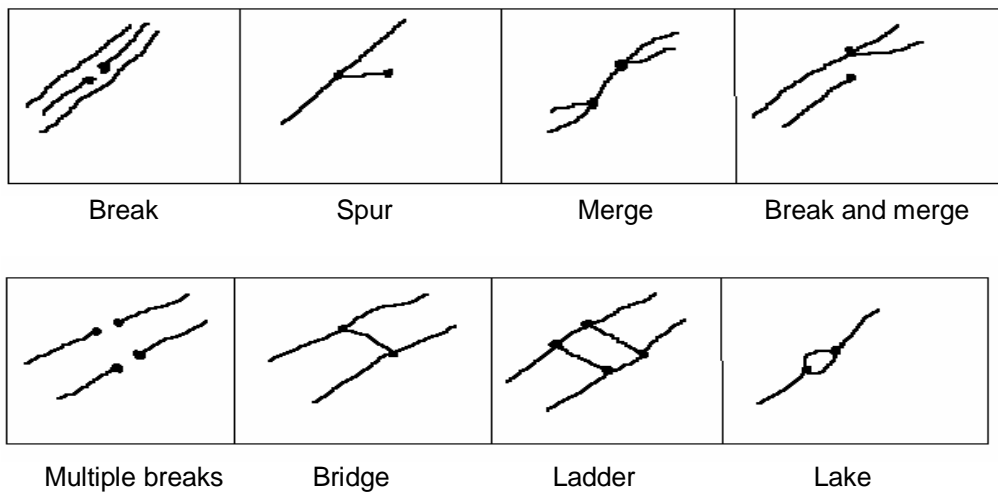


**Figure 13:** Some common false minutiae points (black dots).

## 4. EXPERIMENTAL RESULTS

In our experimental work, we have tested the above algorithm on FVC(2002) fingerprint database. The database contains 40 different fingers and eight impressions of each finger, which makes it a total of  $40 \times 8 = 320$  fingerprints. Minutiae are extracted at four stages from the images as follows and the results are tabulated.

- 1). Original raw images.
- 2). Enhanced and then thinned (repairing broken ridges etc.).
- 3). Preprocessed thinned images (Removal of spurs, spurious bridges, filling holes etc.).
- 4). Post processing the minutiae to get rid of the spurious ones.

We have tested the proposed algorithm using two quantity measures namely Sensitivity and Specificity which indicate the ability of the algorithm to detect the genuine minutiae and remove the false minutiae for fingerprint image [13]. The performance of the proposed algorithm has been measured based on the missing and the spurious minutiae after each stage (figure 14).

$$\text{Sensitivity} = 1 - \frac{\text{Missed Minutiae}}{\text{Ground Truth Minutiae}} \quad (12)$$

$$\text{Specificity} = 1 - \frac{\text{False Minutiae}}{\text{Ground Truth Minutiae}} \quad (13)$$

Table 1 shows the total number of minutiae together with the number of ridge endings and bifurcations separately at each stage. It also shows the reduction in ridge endings and bifurcations after each stage. It also shows the ground truth minutiae in each case. The found truth minutiae have been calculated by manually inspecting the fingerprint image.

Image	Ground Truth Minutiae	Stage	Total minutiae	Ridge endings	Ridge bifurcations	Total Red. (%)	End. Red. (%)	Bif. Red. (%)
I1	59(36+23)	Original	347	201	146	-	-	-
		Enhanced	315	180	135	9.2	10.4	7.5
		Preprocessed	215	101	114	31.7	43.9	15.6
		Post processed	62	38	24	71.1	62.4	78.9
I2	23(12+11)	Original	114	75	39	-	-	-
		Enhanced	88	56	29	22.8	25.3	25.6
		Preprocessed thinned	61	42	19	30.7	25.0	34.5
		Post processed	23	11	12	62.2	73.8	36.8
I3	23(9+14)	Original	201	106	95	-	-	-
		Enhanced	73	30	43	63.7	71.7	54.7
		Preprocessed thinned	54	20	34	26.0	33.3	20.9
		Post processed	22	8	14	57.4	60.0	58.8
I4	32(13+19)	Original	360	110	250	-	-	-
		Enhanced	121	52	89	66.3	52.7	64.4
		Preprocessed thinned	76	24	52	37.2	53.9	41.6
		Post processed	33	14	17	56.6	41.7	67.3

**Table 1 :** Total, endings and bifurcations with % reduction in false minutiae after each stage.

Table 2 lists the total, missed and false number of minutiae before and after the post processing stage together with the sensitivity and specificity values. The high values of sensitivity and specificity in the end, suggest the effectiveness of the proposed technique. Since our technique works on thinned binarized images, the most widely used technique applicable to such images in the literature is the crossing number technique. Hence, we have compared both of them and table 3 shows the comparative results of our technique with the much used crossing number technique. It can be clearly seen that the results of the proposed algorithm are better at both before and after post processing stages. This is so because most crossing number techniques rely on complicated and extensive post processing algorithms to improve their result.

Image	Before Post processing			After Post processing			Final Sensitivity %	Final Specificity %
	Total	Missed	False	Total	Missed	False		
I1	215	1	157	62	1	4	98.3	93.2
I2	61	1	40	23	1	1	95.7	95.7
I3	64	1	43	22	1	0	95.7	100
I4	76	2	45	31	2	1	93.6	96.9

**Table 2 :** Total, missed and false number of minutiae before and after the post processing stage together with the sensitivity and specificity in the proposed technique.

Stage	Image	Proposed Technique			Crossing Number Technique		
		Total	Endings	Bifurcations	Total	Endings	Bifurcations
Before Post processing	I1	215	101	114	589	303	286
	I2	61	42	19	189	109	80
	I3	54	20	34	183	69	114
	I4	76	24	52	189	85	104
After Post processing	I1	62	38	24	145	67	78
	I2	23	11	12	38	24	14
	I3	22	8	14	78	26	52
	I4	33	14	17	41	15	26

**Table 3 :** Total minutiae together with endings and bifurcations before and after the post processing stage in the proposed as well as the crossing number technique.

## 5. CONCLUSIONS

The proposed technique depicts the successful usage of the Hit or Miss Transform on thinned fingerprint images for efficient minutiae extraction. It clearly shows that preprocessing a fingerprint image with morphological operators before thinning removes superfluous information and extracts a clear and reliable ridge map structure from the input fingerprint image thereby giving better results in minutiae extraction. This also reduces a lot of effort in the post processing stage as the number of spurious minutiae is comparatively

lesser. The high values of Sensitivity and Specificity in the end and the comparative results with the crossing number technique illustrate the encouraging performance of our method. Our future work would be to consider fuzzy morphology for minutiae detection.

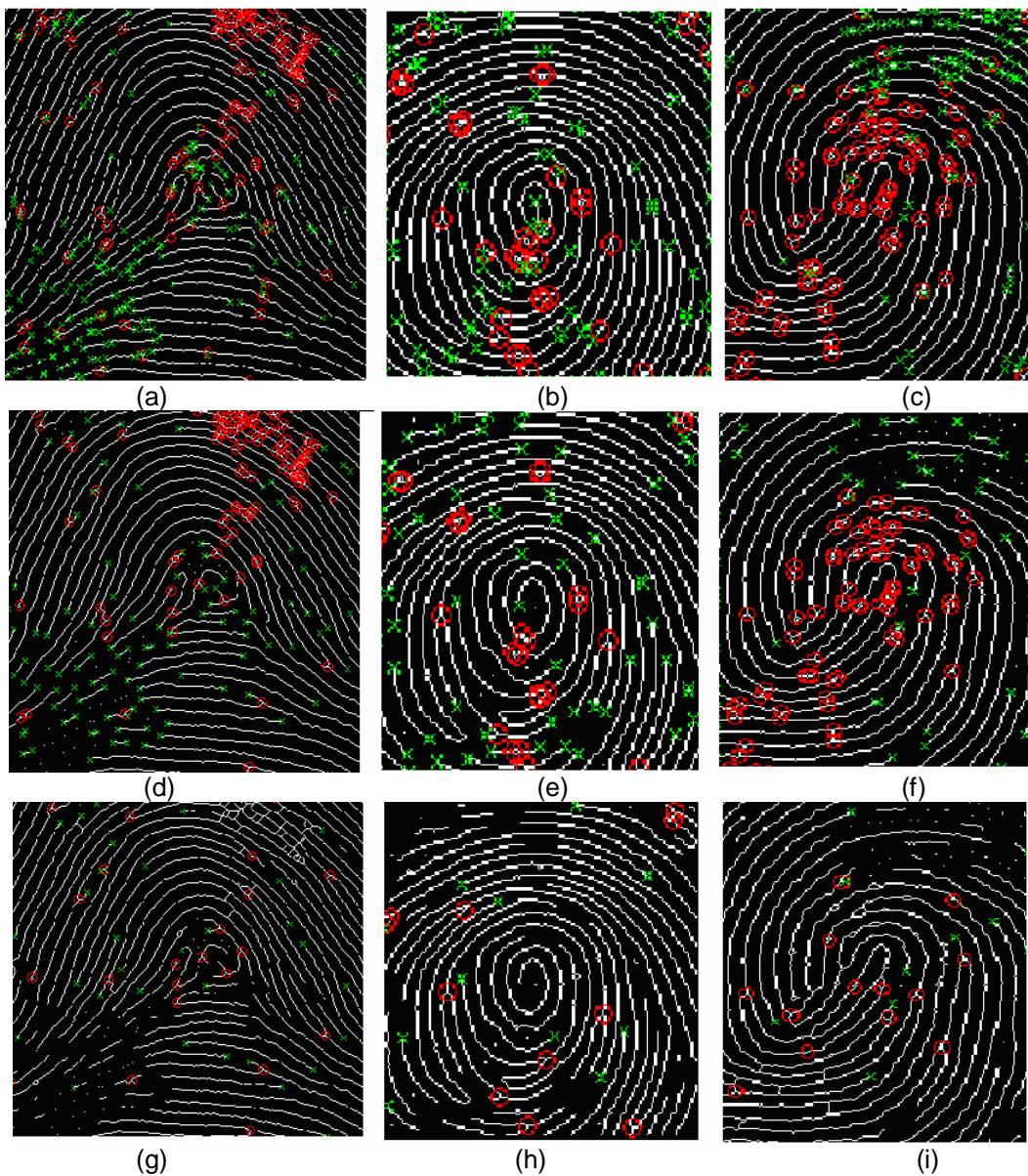


Figure 14(a), (b), (c) show minutiae on enhanced images I1, I2 and I3 respectively, which have been thinned but not morphologically preprocessed. (d), (e), (f) show minutiae on enhanced and thinned images I1, I2 and I3 respectively, which have been morphologically preprocessed. (g), (h) and (i) show the finally post processed minutiae on images I1, I2 and I3 respectively. In all the images endings are shown as x and bifurcations are shown as o.

## REFERENCES

- [1] A. George, "Multi-Modal Biometrics Human Verification Using LDA and DFB", International Journal of Biometrics and Bioinformatics, vol. 2, issue 4, 2008.

- [2] A. Jain, L. Hong, "Online Fingerprint Verification", IEEE Transactions on Pattern Analysis and Machine Intelligence 19, 4 (1997), 302–314.
- [3] B.G. Sherlock, D. M. Monro, K. Millard, " Fingerprint Enhancement by Directional Fourier Filtering", IEE Proc. Image Signal Process, Vol. 141, No. 2, April 1994.
- [4] C. S. Lee, Y. H. Kuo, "Adaptive fuzzy filter and its application to image enhancement," in Fuzzy techniques in Image Processing , 1 edition E. E. Kerre and M. Nachtegael , Eds. , Heidelberg, germany: Physica Verlag, 2000 , vol. 52, pp. 172-193.
- [5] D. V. Jadhav, V.M.Mane, "Review of Multimodal Biometrics: Applications, Challenges and Research Areas", International Journal of Biometrics and Bioinformatics, vol. 3, issue 5, 2009.
- [6]D. Trier, T. Taxt,(1995) "Evaluation of binarisation methods for document images", IEEE Transactions on Pattern Analysis and Machine Intelligence, Vol. 17, No. 3, pp.312–315.
- [7] D. Maltoni, D. Maio, A. K. Jain, and S. Prabhakar, Handbook of Fingerprint Recognition. Springer, 2003.
- [8] Feng Zhao, Xiaou Tang, "Preprocessing and post processing for skeleton-based fingerprint minutiae extraction", Pattern Recognition 40, p.no. 1270-1281, 2007.
- [9] J. Luping, Y. Zhang , S. Lifeng, P. Xiaorong, "Binary Fingerprint Image Thinning using PCNNs", IEEE Trans. On Systems, Man and cybernetics, Part B, vol. 7 , No. 5, October 2007.
- [10] J. C. Amengual, A. Juan, J. C. Prez, Prat, F., Sez, S., and Vilar, J. M. Real-time minutiae extraction in fingerprint images. In Proc. of the 6th Int. Conf. on Image Processing and its Applications (July 1997), pp. 871–875.
- [11] L.Hong, Y. Wan, A. K. Jain "Fingerprint Image Enhancement: Algorithm and Performance Evaluation" IEEE Transaction on pattern analysis and machine intelligence, Vol 20 No. 8, p.p. 777-789, 1998.
- [12] M. A. Oliveira, N. J. Leite, "A multiscale directional operator and morphological tools for reconnecting broken ridges in fingerprint images", Pattern Recognition 41, p.no. 367-377 , 2008.
- [13] M. Tico, M. Vehvilainen, J. Saarinen, "A method of fingerprint image enhancement based on second directional derivatives" (ICASSP '05). IEEE International Conference on Acoustics, Speech, and Signal Processing, 2005. Proceedings. Volume 2, March 18-23, PP:985 – 988, 2005
- [14] M. Tico and P. Kuosmanen, " An algorithm for fingerprint image postprocessing", In Proceedings of the Thirty-Fourth Asilomar Conference on Signals, Systems and Computers (November 2000), vol. 2, pp. 1735–1739.
- [15] M. Usman Akram , A. Tariq, Shoaib A. Khan, "Fingerprint image : pre and post processing", Int. Journal of Biometrics, Vol. 1, No.1, 2008.
- [16] M. Kaur, M. Singh, P.S. Sandhu, "Fingerprint Verification system using Minutiae Verification Technique", Proceedings of world Academy of Science, Engineering and Technology, vol. 36, Dec. 2008.
- [17] N. Otsu, "A threshold selection method from gray level histograms", IEEE Transactions Analysis and machine intelligence, June 1990.
- [18] N. Ratha, S. Chen, and A. Jain, Adaptive flow orientation based feature extraction in fingerprint images. Pattern Recognition 28, 11 (1995), 1657–1672.

- [19] Q. Xiao and H. Raafat, "Fingerprint image postprocessing: a combined statistical and structural approach" Pattern Recognition 24, 10 (1991), 985–992.
- [20] R. Bansal, P. Sehgal, P. Bedi, "Fingerprint Image Enhancement Using Type-2 fuzzy sets", IEEE International Conference on Fuzzy Systems and Knowledge Discovery(FSKD'2009), August 2009.
- [21] R. Bansal, P. Sehgal, P. Bedi, "A novel framework for enhancing images corrupted by impulse noise using type-II fuzzy sets", IEEE International Conference on Fuzzy Systems and Knowledge Discovery(FSKD'2008), vol. 3, pp 266-271, October 2008.
- [22] R. C. Gonzalez, R. E. Wood, "Digital Image Processing", Second Edition, Prentice Hall,2006.
- [23] S. Greenberg, M. Aladjem, D. Kogan and I. Dimitrov "Fingerprint Image Enhancement using Filtering Techniques" ,Electrical and Computer Engineering Department, Ben-Gurion University of the Negev, Beer-Sheva, Israel, 2000.
- [24] S. Kasaei, M. D., and B. Boashash, Fingerprint feature extraction using block-direction on reconstructed images. In IEEE region TEN Conf., digital signal Processing applications, TENCON (December 1997), pp. 303–306.
- [25] S.K. Oh, J.J. Lee, C.H. Park, B.S. Kim, K.H. Park, "New Fingerprint Image Enhancement Using Directional Filter Bank", School of Electrical Engineering, Kyungpook National University SEOUL, Daegu, Korea, School of Internet Engineering, Dongseo University SEOUL , Daegu, Korea.
- [26] S. Prabhakar, J. Wang, A. K. Jain, S. Pankanti, and Bolle, R. "Minutiae Verification and classification for fingerprint matching". In Proc. 15th International Conference Pattern Recognition (ICPR) (September 2000), vol. 1, pp. 25–29.
- [27] S. M Mohsen, S. M. Zamshed, M. M. A. Hashem, "Automated Fingerprint Recognition : Using Minutiae Matching Technique for the large Fingerprint Database", III International conference on Electrical and Computer Engineering ICECE 2004, 28-30 December, 2004,Dhaka, Bangladesh.
- [28] S. Shah, P. S. Sastry, " Fingerprint Classification Using a Feedback –Based Line Detector", IEEE Trans. On Systems, Man and Cybernetics, Part B, vol. 34, no.1, February 2004.
- [29] V. Espinosa, "Mathematical Morphological approaches for Fingerprint Thinning", IEEE, 2002.
- [30] Chander Kant, R. Nath, "Reducing Process Time for Fingerprint Identification System", International Journal of Biometrics and Bioinformatics, vol. 3, issue 1, 2009.
- [31] X. Jiang, W.-Y. Yau, and W. Ser, "Detecting the fingerprint minutiae by adaptive tracing the gray-level ridge", Pattern Recognition, 34(5):999–1013, 2001.
- [32] Y.S. Choi and R. Krishnapuram , " A robust approach to image enhancement based on fuzzy logic", IEEE Trans. Image Process., vol 6, no. 6, pp 808-825, Jun 1997.
- [33] M. T. Yildrim, A. Basturk, " A Detail Preerving type-2 Fuzzy Logic Filter for Impulse Noise Removal from Digital Images", Fuzzy Systems Conference, FUZZ-IEEE, 2007.
- [34] Zenzo, L. Cinque, and S. Levialdi, "Run-Based Algorithms for Binary Image Analysis and Processing," IEEE Trans. PAMI, vol. 18, no. 1, pp. 83-88, January 1996.

## Incremental PCA-LDA Algorithm

**Issam Dagher**

*Department Of Computer Engineering  
University of Balamand  
POBOX 100,Elkoura,Lebanon*

dagheri@balamand.edu.lb

---

### Abstract

In this paper a recursive algorithm of calculating the discriminant features of the PCA-LDA procedure is introduced. This algorithm computes the principal components of a sequence of vectors incrementally without estimating the covariance matrix (so covariance-free) and at the same time computing the linear discriminant directions along which the classes are well separated. Two major techniques are used sequentially in a real time fashion in order to obtain the most efficient and linearly discriminative components. This procedure is done by merging the runs of two algorithms based on principal component analysis (PCA) and linear discriminant analysis (LDA) running sequentially. This algorithm is applied to face recognition problem. Simulation results on different databases showed high average success rate of this algorithm compared to PCA and LDA algorithms. The advantage of the incremental property of this algorithm compared to the batch PCA-LDA is also shown.

**Keywords:** Recursive PCA-LDA, principal component analysis (PCA), linear discriminant analysis (LDA), face recognition.

---

### 1. INTRODUCTION

A large number of face recognition techniques use face representations found by unsupervised statistical methods. Typically, these methods find a set of basis images and represent faces as a linear combination of those images. For the same purpose, this paper merges sequentially two techniques based on principal component analysis and linear discriminant analysis.

The first technique is called incremental principal component analysis (IPCA) which is an incremental version of the popular unsupervised principal component technique. The traditional PCA algorithm [13] computes eigenvectors and eigenvalues for a sample covariance matrix derived from a well known given image data matrix, by solving an eigenvalue system problem. Also, this algorithm requires that the image data matrix be available before solving the problem (batch method). The incremental principal component method updates the eigenvectors each time a new image is introduced.

The second technique is called linear discriminant analysis (LDA) [14]. LDA is a data separation technique. The objective of LDA is to find the directions that will well separate the different classes of the data once projected upon. The set of human faces is represented as a data matrix  $X$  where each row corresponds to a different human face.

Each image  $x$ , represented by a  $(n,m)$  matrix of pixels, will be represented by a high dimensional vector of  $n \times m$  pixels. Turk and Pentland [22] were among the first who used this representation for face recognition.

2-dimensional principal component analysis (2dPCA) [31] was proposed which directly computes the eigenvectors of the covariance matrix without matrix to vector conversion.

2-dimensional LDA [32,33] computes directly the directions which will separate the classes without matrix to vector conversion as well.

Higher recognition rate was reported for both cases.

Both of these algorithms work in batch mode, all the image data must be present a priori.

It should be noted that incremental face recognition systems are studied in [3,7,8,9,10,11,12], incremental LDA was studied in [1,2,4,5,6].

While the incremental PCA methods update the eigenspace model (the covariance matrix), the incremental LDA methods update the fisherspace model (the within class scatter matrix and the between class scatter matrix). The incremental PCA-LDA updates directly the eigenvectors using the general eigenvalue problem and the complementary space. It also updates the fisherspace model based on the projected PCA data and an update of the inverse of the within class scatter matrix.

The PCA/LDA-based face recognition systems suffer from the scalability problem. To overcome this limitation, an incremental approach is a natural solution. The main difficulty in developing the incremental PCA/LDA is to compute covariance matrix and to handle the inverse of the within-class scatter matrix.

These techniques have been applied to 3D object recognition [17], sign recognition [18], and autonomous navigation [19] among many other image analysis problems [16,26,27,28]. However, the batch method no longer satisfies an up coming new trend of computer vision research [20] in which all 2-d filters are incrementally derived from very long online real-time video stream. Online development of 2-d filters requires that the system perform while new sensory signals flow in. When the dimension of the image is high, both the computation and storage complexity grow dramatically. Thus, the idea of using a real time process becomes very efficient in order to compute the principal components for observations (faces) arriving sequentially

It should be noted that the incremental PCA-LDA has the following advantages:

1. Low memory demands: No need to store all the images (mainly due to the incremental structure of the PCA). All you need to store are the eigenvectors. Given a new image or a new class, the eigenvectors will be updated using only the stored eigenvectors. From a practical point of view, there is no need to store any face database (store the unrecognized eigenvectors) and some image data could not be presently available. It should be noted that 2dPCA, 2dLDA, and SVD work in batch mode.
2. Low computational complexity: the batch PCA-LDA needs to compute all the eigenvectors of all the data then gets the first  $k$  eigenvectors. The incremental PCA-LDA operates directly on the first  $k$  eigenvectors (unwanted vectors do not need to be calculated). The processing of IPCA\_LDA is restricted to only the specified number of  $k$  directions and not on all the directions.
3. Better recognition accuracy and less execution time.
4. Updating the inverse of the within class scatter matrix without calculating its inverse.

## 2. DERIVATION OF THE ALGORITHM

Given that large number of  $d$ -dimensional vectors,  $\mathbf{u}(1); \mathbf{u}(2); \dots$ , which are the observations from a certain given image data, are received sequentially. The class of each image is determined. Without loss of generality, a fixed estimated mean image  $\mu$  is initialized in the beginning of the algorithm. It should be noted that a simple way of getting the mean image is to present sequentially all the images and calculating their mean. At the same time, the mean  $\mu_j$  and the

number of data  $n_j$  of each class are determined. The mean image can be subtracted from each vector  $\mathbf{u}(n)$  in order to obtain a normalization vector of approximately zero mean. Let  $C = E[\mathbf{u}(n)\mathbf{u}^T(n)]$  be the dxd covariance matrix.

The proposed algorithm takes the number of input images (n), the dimension of the images, and the number of desired PCA (k) directions as inputs and returns the c-1 LDA vectors (c-1 directions that will well separate the different classes of the data once projected upon.) and the image coordinates with respect to these vectors as outputs. It works like a linear system that predicts the next state vector from an input vector and a current state vector. All the components will be updated from the previous values and from a new input image vector by processing sequentially the PCA and LDA algorithms. While incremental PCA returns the estimated eigenvectors as a matrix that represents subspaces of data and the corresponding eigenvalues as a row vector, incremental LDA searches for the directions where the projections of the input data vectors are well separated.

The obtained vectors will form a basis which describes the original data set without loss of information. The face recognition can be done by projecting the input test image onto this basis and comparing the resulting coordinates with those of the training images in order to find the nearest appropriate image.

#### A. Batch PCA-LDA algorithm :

Given [21] the image data  $U_i$ ,  
 (Steps 1-4 compute the k PCA eigenvectors. Step 5 computes the projected LDA data on those eigenvectors. Steps 6-8 compute the LDA directions which separate the data.)

1. Subtract the sample mean from the data:  

$$Y_i = U_i - \mu \quad i = 1, 2, \dots, n$$
2. Compute the scatter matrix S:  $S = \sum_{i=1}^n Y_i Y_i^T$
3. Compute eigenvectors  $\{ \mathbf{v}_1, \mathbf{v}_2 \dots \mathbf{v}_k \}$  corresponding to the largest k eigenvalues of S.
4. Let  $\mathbf{v}_1, \mathbf{v}_2 \dots \mathbf{v}_k$  be the columns of eigenvector matrix  $A = [\mathbf{v}_1, \mathbf{v}_2 \dots \mathbf{v}_k]$ .
5. The new projected LDA data are:  $Z_i = A^T Y_i \quad i = 1, 2, \dots, n$
6. Compute the sample mean  $\mu_z$  of the LDA data and the sample mean  $\mu_{zi}$  of each class.
7. Compute the between class scatter matrix  $S_b$  and the within class scatter matrix  $S_w$ .  

$$S_b = \sum_{i=1}^c n_i (\mu_{zi} - \mu_z)(\mu_{zi} - \mu_z)^T; \quad S_w = \sum_{i=1}^c \sum_{\text{class } k} (Z_k - \mu_{zi})(Z_k - \mu_{zi})^T$$
8. Solve  $S_b w = \lambda S_w w \Rightarrow [w_1, w_2, \dots, w_{c-1}]$

#### B. Incremental PCA equations:

By definition [10], an eigenvector  $\mathbf{x}$  with a corresponding eigenvalue  $\lambda$  of a covariance matrix C satisfies:

$$\lambda \cdot x = C \cdot x \quad (1)$$

By replacing in (2) the unknown C with the sample covariance matrix  $\frac{1}{n} \sum_{i=1}^n u(i)u^T(i)$  and using  $v = \lambda \cdot x$ , the following equation is obtained:

$$v(n) = \frac{1}{n} \sum_{i=1}^n u(i)u^T(i)x(i) \quad (2)$$

where  $v(n)$  is the nth step estimate of  $v$  after entering all the n images.

Since  $\lambda = \|v\|$  and  $x = v/\|v\|$ ,  $x(i)$  is set to  $v(i-1)/\|v(i-1)\|$  (estimating  $x(i)$  according to the given previous value of  $v$ ). Equation (2) leads to the following equation:

$$v(n) = \frac{1}{n} \sum_{i=1}^n u(i)u^T(i) \cdot \frac{v(i-1)}{\|v(i-1)\|} \quad (3)$$

Equation (3) can be written in a recursive form:

$$v(n) = \frac{n-1}{n} v(n-1) + \frac{1}{n} u(n)u^T(n) \frac{v(n-1)}{\|v(n-1)\|} \quad (4)$$

where  $\frac{n-1}{n}$  is the weight for the last estimate and  $\frac{1}{n}$  is the weight for the new data.

To begin with, Let's set  $v(0) = u(1)$ , the first direction of data spread. The IPCA algorithm will give the first estimate of the first principal component  $v(1)$  that corresponds to the maximum eigenvalue:

$$v(1) = \frac{1}{n} u(1)u^T(1) \frac{v(0)}{\|v(0)\|}$$

Each time a new image is introduced, the eigenvectors will be updated. They are presented by the algorithm in a decreasing order with respect to the corresponding eigenvalue (the first eigenvector will correspond to the largest eigenvalue). The other higher order vectors are estimated following what *Stochastic Gradient Ascent* SGA does: Start with a set of orthonormalized vectors, update them using the suggested iteration step, and recover the orthogonality using *Gram-Schmidt Orthonormalization* GSO. For real-time online computation, avoiding time-consuming GSO is needed. Further, the vectors should be orthogonal to each other in order to ensure the independency. So, it helps to generate "observations" only in a complementary space for the computation of the higher order eigenvectors. For example, to compute the second order vector, first the data is subtracted from its projection on the estimated first order eigenvector  $v_1(n)$ , as shown in (6):

$$u_2(n) = u(n) - u_1^T(n) \frac{v_1(n)}{\|v_1(n)\|} \frac{v_2(n)}{\|v_2(n)\|} \quad (5)$$

where  $u_1(n) = u(n)$ . The obtained residual,  $u_2(n)$ , which is in the complementary space of  $v_1(n)$ , serves as the input data to the iteration step.

In this way, the orthogonality is always enforced when the convergence is reached, although not exactly so at early stages. This, in effect, better uses the sample available and avoids the time-consuming GSO.

After convergence, the vectors will also be enforced to be orthogonal, since they are estimated in complementary spaces.

### C. Incremental LDA equations :

At iteration k (corresponding to the data  $U_k$ ):

Given the projected LDA data  $Z_k = AY_k$

$$\text{and the sample mean of class } j \quad \mu_{zj} = \frac{\sum Z_k}{n_j} = A \frac{\sum Y_k}{n_j} = A \frac{\sum (X_k - \mu)}{n_j} = A(\mu_j - \mu)$$

and the general following formula :  $(D + BC)^{-1} = D^{-1} - D^{-1}B(I + CD^{-1}B)^{-1}CD^{-1}$

The update formulas for  $S_w$  is given by :

$$S_w = S_w + (Z_k - \mu_{kj})(Z_k - \mu_{kj})^T = S_w + A(Y_k - (\mu_j - \mu))(Y_k - (\mu_j - \mu))^T A^T$$

Using the previous 2 equations the update formula for the inverse of  $S_w$  is :

$$S_{wi} = S_{wi} - \frac{S_{wi} A(Y_k - (\mu_j - \mu))(Y_k - (\mu_j - \mu))^T A^T S_{wi}}{1 + (Y_k - (\mu_j - \mu))^T A^T S_{wi} (Y_k - (\mu_j - \mu))A}$$

Because A is not yet completely specified, the following update matrices will be used :

$$S_{w1} = S_{w1} + (Y_k - (\mu_j - \mu))(Y_k - (\mu_j - \mu))^T$$

$$S_{wi1} = S_{wi1} - \frac{S_{wi1}(Y_k - (\mu_j - \mu))(Y_k - (\mu_j - \mu))^T S_{wi1}}{1 + (Y_k - (\mu_j - \mu))^T S_{wi1} (Y_k - (\mu_j - \mu))}$$

And at the end of the nth iteration:

$$S_w = AS_{w1}A^T$$

$$S_{wi} = AS_{wi1}A^T$$

$$S_b = \sum_{i=1}^c n_i (\mu_{zi} - \mu_z)(\mu_{zi} - \mu_z)^T =$$

$[w_1, w_2, \dots, w_{c-1}]$  = eigenvectors of  $(S_{wi} S_b)$

It should be noted that the above equations are considered to be a contribution of this paper

### D. Algorithm Summary:

Assume n different images  $u(n)$  are given.

$\mu$  is the sample mean of all the images,  $\mu_j$  is the sample mean of each class,

and  $n_j$  is the number of data of each class.

Combining IPCA and LDA algorithms, the new algorithm can be summarized as follows:

(Input one image at a time. Update the k eigenvectors ( $v$ ) according to that image. Update the fisherspace model based on the projected data and update the inverse of the within class scatter matrix. Compute the LDA directions ( $w$ ))

Initialize  $S_w$  to zero elements and  $S_{wi}$  to random big numbers.  
 For i=1:n  
 $u(i) = img;$   
 $\text{for } j=1:k$   
 $\quad \text{if } j == i, \text{ initialize the eigenvector as:}$   
 $\quad \quad v_j(i) = u(i);$   
 $\quad \text{else}$   
 $\quad \quad v_j(i) = \frac{i-1}{i} v_j(i-1) + \frac{1}{i} u(i) u^T(i) \frac{v_j(i-1)}{\|v_j(i-1)\|};$  (vector update)  
 $\quad \quad u(i) = u(i) - u^T(i) \cdot \frac{v_j(i)}{\|v_j(i)\|} \frac{v_j(i)}{\|v_j(i)\|};$  (To ensure orthogonality)  
 $\quad \text{end}$   
 $\text{end}$

$$Y_i = img - \mu;$$

$$S_{w1} = S_{w1} + (Y_k - (\mu_j - \mu))(Y_k - (\mu_j - \mu))^T$$

$$S_{wi1} = S_{wi1} - \frac{S_{wi1}(Y_k - (\mu_j - \mu))(Y_k - (\mu_j - \mu))^T S_{wi1}}{1 + (Y_k - (\mu_j - \mu))^T S_{wi1}(Y_k - (\mu_j - \mu))}$$

*end*

$S_w = AS_{w1}A^T$   
 $S_{wi} = AS_{wi1}A^T$   
 $S_b = A(\sum_{i=1}^c n_i (\mu_i - \mu)(\mu_i - \mu)^T)A^T$   
 $[w_1, w_2, \dots, w_{c-1}] = \text{eigenvectors of } (S_{wi}S_b)$

**E . Comparison with PCA-LDA Batch algorithm:**

The major difference between this algorithm and the PCA-LDA batch algorithm [21],[29], is the sequential flow of input data. Incremental PCA-LDA doesn't need a large memory to store the whole data matrix that represents the incoming images. Thus in each step, this function deals with one incoming image in order to update the estimated directions, and the next incoming image can be stored over the previous one. The first estimated vectors (corresponding to the largest eigenvalues) in incremental PCA correspond to the vectors that carry the most efficient information. As a result, the processing of incremental PCA-LDA can be restricted to only a specified number of first eigenvectors. On the other side, the decision of efficient vectors in PCA can be done only after calculating all the vectors, so the program will spend a certain time calculating unwanted vectors. Also, LDA works usually in a batch mode where the extraction of discriminative components of the input eigenvectors can be done only when these eigenvectors are present simultaneously at the input. It is very clear that from the time efficiency concern, incremental PCA-LDA will be more efficient and requires less execution time than batch PCA-LDA algorithm. It should also be noted that this algorithm has the advantage of updating the inverse of the within class scatter matrix without calculating its inverse.

### 3. Experimental Results and Discussions

#### A. Face recognition Evaluated by Nearest Neighbor Algorithm:

The nearest neighbor algorithm was used to evaluate the face recognition technique. The following L1 similarity measure (inner product formula) was adopted:

$$L1 = \sum_i |w_{test}(i) - w_{train}(i)| \quad (6)$$

It should be noted that the incremental PCA-LDA algorithm will give small size basis, with respect to the number of training input images. Other similarity measures could have been used and similar comparative results will be obtained.

Each Face Database was split into two sets. The training set that contains images used to calculate the discriminative vectors and come up with the appropriate basis. And the test set that contains images to be tested by the face recognition algorithm in order to evaluate the performance of the proposed method. The whole set of training images (rows in the image data matrix) is projected into the basis found in order to calculate the coordinates of each image with respect to the basis  $v_{train}$ . Each new testing image  $v_{test}$  is compared to whole set of training images  $v_{train}$  in order to come up with nearest one that corresponds to the minimum L1 in equation (6). The generalization performance (or % accuracy) is equal to the number of correctly classified testing images divided by the total number of testing images (multiplied by 100).

#### B. Face Recognition Performance:

Three popular face databases were used to demonstrate the effectiveness of the proposed PCA-LDA algorithm.

The ORL [23] contains a set of faces taken between April 1992 and April 1994 at the Olivetti Research Laboratory in Cambridge. It contains 40 distinct persons with 10 images per person. The images are taken at different time instances, with varying lighting conditions, facial expressions and facial details (glasses/no-glasses). All persons are in the up-right, frontal position, with tolerance for some side movement.

The UMIST [24] taken from the University of Manchester Institute of Science and Technology. It is a multi-view database, consisting of 575 images of 20 people, each covering a wide range of poses from profile to frontal views.

The Yale [25] taken from the Yale Center for Computational Vision and Control. It consists of images from 15 different people, using 11 images from each person, for a total of 165 images. The images contain variations with following total expressions or configurations: center-light, with glasses, happy, left-light, without glasses, normal, right-light, sad, sleepy, surprised, and wink. And the BIOID database [33]. The dataset consists of 1521 gray level images with a resolution of 384x286 pixel. Each one shows the frontal view of a face of one out of 23 different test persons.

Each image in the ORL database is scaled into  $(92 \times 112)$ , in the UMIST Database is scaled into  $(112 \times 92)$ , the Yale Database is cropped and scaled into  $(126 \times 152)$  and the BIOID is cropped and scaled to  $(128 \times 95)$

Figures 1,2, 3, and 4 show a sample of 6 images from all the 4 databases.



Fig. 1. Some sample images of 6 persons in the ORL Database



Fig. 2. Some sample images of 6 persons in the UMIST Database



Fig. 3. Some sample images of 6 persons in the YALE Database

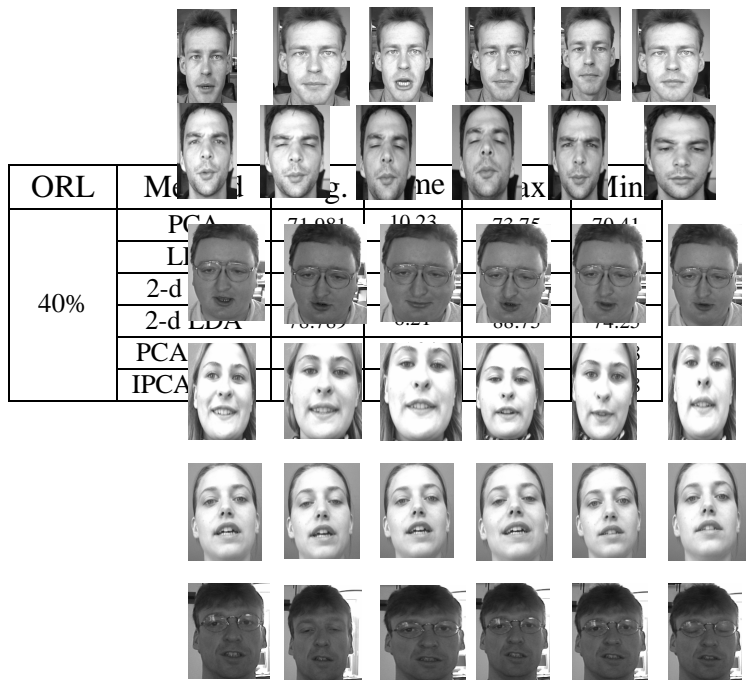


Fig. 4. Some sample images of 6 persons in the BioidDatabase

To start the face recognition experiments, each one of the three databases is randomly partitioned into a training set and a test set with no overlap between the two. 10 different partitions were made. A comparison between the average performances, Matlab time in seconds on our machine Pentium(R) D CPU 3.4 Ghz, the minimum and maximum generalization performances of these algorithms using the four databases is shown in Table 1 for 40%, 60% training and 10-fold cross validation. Figure5 shows examples from all the databases of both successful (the first 4 faces) and failed recognized images.



Fig. 5: Examples of both successful and failed recognized images.

Table1 shows for all the databases, the average (over 10 runs), the minimum, the maximum generalization performance, and the time (in sec) for 40%, 60%, and 10-fold cross validation of the training database.

2-d PCA and 2-d LDA can be considered as 2-d filters which operate directly on the 2-d image.

Table1: Comparisons between time and generalization performances for the 4 databases

60%	PCA	72.25	11.77	77.51	70
	LDA	86.808	11.36	88.12	83.73
	2-d PCA	89.9	8.88	92.65	71.45
	2-d LDA	91.72	7.98	95.62	76.87
	PCA-LDA	92.187	14.92	95.5	90
	IPCA-LDA	92.062	5.57	95.5	90
10-fold	PCA	82.823	13.77	86.98	80

CV	LDA	86	13.67	88.75	70
	2-d PCA	89.67	10.92	92.35	82.23
	2-d LDA	92.45	9.11	95.65	85.65
	PCA-LDA	95	18.80	95.54	91.25
	IPCA-LDA	95.825	7.92	96.5	93.75

UMIST	Method	Avg.	Time	Max	Min
40%	PCA	53.088	12.34	56.25	50.83
	LDA	53.622	12.44	57.5	50
	2-d PCA	61.25	8.65	68.87	52.25
	2-d LDA	63.77	6.21	69.22	51.23
	PCA-LDA	63.655	16.78	69.5	60.33
	IPCA-LDA	64.155	5.57	69.5	60.41
60%	PCA	74.935	13.04	77.5	71.87
	LDA	56.185	13.01	63.12	52.5
	2-d PCA	76.94	8.33	78.87	72.54
	2-d LDA	64.31	6.57	66.56	56.70
	PCA-LDA	64.31	17.89	66.87	62.5
	IPCA-LDA	64.81	6.01	67.5	62.5
10-fold CV	PCA	75.25	14.89	80	71.25
	LDA	73.5	14.73	77.5	70
	2-d PCA	80.67	11.56	82.23	73.34
	2-d LDA	82.57	10.87	87.25	71.23
	PCA-LDA	83.5	19.11	87.5	80
	IPCA-LDA	83.5	9.11	87.5	80

YALE	Method	Avg.	Time	Max	Min
40%	PCA	64.281	6.23	79.52	45.71
	LDA	60.614	6.27	69.52	45.23
	2-d PCA	66.76	4.73	80.52	47.65
	2-d LDA	68.87	4.21	82.78	53.37
	PCA-LDA	70.595	8.34	81.52	55.23
	IPCALDA	71.35	4.11	80.52	56.21
60%	PCA	65.934	7.01	79.33	54
	LDA	60.932	7.07	73.33	50
	2-d PCA	70.76	4.98	82.76	62.33
	2-d LDA	74.21	4.67	84.25	55.21
	PCA-LDA	74.236	8.89	85.71	61.33
	IPCALDA	74.236	4.23	85.71	61.33
10-fold CV	PCA	67.778	8.11	78.89	35.56
	LDA	65.891	8.09	77.78	30
	2-d PCA	68.67	5.98	82.23	35.56
	2-d LDA	69.23	5.01	80.23	30
	PCA-LDA	70.67	9.23	85.78	30
	IPCALDA	72.576	4.98	87.78	30

BIOID	Method	Avg.	Time	Max	Min
40%	PCA	60.671	18.67	66.59	54.27
	LDA	63.178	18.54	67.89	60.11
	2-d PCA	71.576	12.33	78.11	62.37
	2-d LDA	73.89	9.21	79.78	61.65
	PCA-LDA	74.123	26.80	79.25	68.55
	IPCA-LDA	75.01	8.57	79.5	69.64
60%	PCA	62.34	19.04	66.11	59.12
	LDA	64.879	19.01	73.12	60.76
	2-d PCA	67.11	13.56	77.28	62.33
	2-d LDA	70.11	10.11	78.98	67.12
	PCA-LDA	71.12	27.96	76.13	67.34
	IPCA-LDA	72.45	9.23	77.67	68.5
10-fold CV	PCA	74.78	20.76	81.23	70.87
	LDA	76.11	20.64	82.88	72.31
	2-d PCA	80.67	14.21	83.76	70.45
	2-d LDA	82.57	11.66	88.66	80.78
	PCA-LDA	85.5	29.22	89.88	82.7
	IPCA-LDA	86.67	11.01	90.12	82.7

It should be noted that the incremental PCA-LDA has slightly higher performance than the batch PCA-LDA. This is due to the fact that the first estimated vectors (corresponding to the largest eigenvalues) in incremental PCA-LDA correspond to the vectors that carry the "most" efficient discriminant vectors. The incremental PCA-LDA concentrates first from the whole data on getting the first eigenvector and then projects to it the data in order to get the LDA vectors. So there is a correlation between the first eigenvector (independent of the other eigenvectors) and the LDA data. This is true for the second, the third, till the kth eigenvector. On the other hand the batch PCA-LDA gets first all the eigenvectors and then projects the data.

For our experiments, the number of PCA eigenvectors used for both algorithms are the number of different classes (c) and eventually the number of the LDA features are c-1 (which is the maximum number of possible features). Our experiments show that as you increase the number of features, the recognition performance increases as well. For example for the Yale database there are 15 different persons (c=15), for the UMIST database there are 20 classes (c=20).

The performance of the incremental PCA-LDA was also assessed using 2 types of error: The false acceptance rate (FAR) and false rejection rate (FRR). For all the databases 4 different persons are considered as imposters and the training is done using 80 % of the other persons. It should be noted that these 2 measures are ratios (no unit of measure is given). The following results were obtained:

It should be noted that Table1 and Table2 compares incremental PCA-LDA to 4 related algorithms: PCA, LDA, 2-d PCA, 2-d LDA, and batch PCA\_LDA. This comparison is done in Table1 using the recognition performance (Average, minimum, and maximum) for different training sizes and the time in seconds of each algorithm. Table 2 assesses the performance of these algorithms using the FAR and the FRR measures.

Table2: FAR and FRR for the 4 databases.

<b>ORL</b>	<b>FAR</b>	<b>FRR</b>
PCA	0.103	0.0388
LDA	0.0811	0.0166
2-d PCA	0.065	0.0145
2-d LDA	0.045	0.0134
Batch PCA-LDA	0.029	0.0130
I PCA-LDA	0.027	0.0122

<b>UMIST</b>	<b>FAR</b>	<b>FRR</b>
PCA	0.381	0.122
LDA	0.211	0.201
2-d PCA	0.178	0.145
2-d LDA	0.158	0.107
Batch PCA-LDA	0.156	0.106
I PCA-LDA	0.123	0.102

<b>YALE</b>	<b>FAR</b>	<b>FRR</b>	<b>BIOID</b>	<b>FAR</b>	<b>FRR</b>
PCA	0.561	0.478	PCA	0.336	0.178
LDA	0.478	0.321	LDA	0.234	0.189
2-d PCA	0.356	0.287	2-d PCA	0.167	0.11
2-d LDA	0.301	0.245	2-d LDA	0.132	0.107
Batch PCA-LDA	0.311	0.234	Batch PCA-LDA	0.133	0.108
I PCA-LDA	0.247	0.189	I PCA-LDA	0.124	0.105

As stated before, LDA has the supervised property over PCA. It uses the class labels in order to get the optimum directions which separates the data. As the tables show the performances of LDA is not always better than PCA. This is due mainly to the size of the training set. In the non representative (small) training set PCA outperforms LDA. In that case, the PCA vectors are better than the LDA vectors. To overcome this problem is to use the two-stage feature extraction method PCA followed by LDA. The tables show that Batch PCA-LDA and incremental PCA\_LDA outperforms the PCA and LDA algorithms in %generalization (better generalization performances) and in the FAR and the FRR (less number of false acceptances and less number of false rejections). It should be noted that other mixed techniques exist in the literature. For example in [1] incremental PCA – ICA was used to transform the principle components to independent directions irrespective of the class label (unsupervised property vs. the supervised property of the LDA). Another example the PCA-support vectors uses kernel PCA and solving a quadratic optimization problem (batch mode vs. the incremental mode of this paper).

## 4. CONCLUSIONS

In this paper a recursive algorithm of calculating the discriminant features of the PCA-LDA procedure is introduced. The method concentrates on a challenging issue of computing discriminating vectors from an incrementally arriving high-dimensional data stream without computing the corresponding covariance matrix and without knowing the data in advance. Because real-time face identification is necessary in

most practical applications, this proposed method can process face images (including training and identifying) in high speed and obtain good results. Its effectiveness and good performance has been proven by experiments. The proposed incremental PCA-LDA algorithm is very efficient in memory usage (only one input image is needed at every step). And it is very efficient in the calculation of the first basis vectors (unwanted vectors do not need to be calculated). In addition to these advantages, this algorithm gives an acceptable face recognition success rate in comparison with very famous face recognition algorithms such as the PCA and LDA. Even though this algorithm gave similar results to the batch PCA-LDA, it has the advantage of its simple updates of all the parameters when introducing new image in the training set. Batch PCA-LDA need to use all the training images to recalculate the new basis.

## References

- [1] H Zhao, PC Yuen, "Incremental Linear Discriminant Analysis for Face Recognition", *Systems, Man, and Cybernetics, Part B, IEEE Transactions on*, Vol. 38, No. 1. (2008), pp. 210-221.
- [2] Shaoning Pang, Seiichi Ozawa, Nikola Kasabov, "Chunk Incremental LDA Computing on Data Streams", *Lecture Notes in Computer Science (Advances in Neural Networks – ISNN 2005)*, Volume 3497/2005, pp. 51-56
- [3] J. Ye, H. Xiong Q. Li, H. Park, R. Janardan, and V. Kumar." IDR/QR: An Incremental Dimension Reduction Algorithm via QR Decomposition", In Proc. ACM SIGKDD Int. Conf. on Knowledge Discovery and Data Mining, pages 364–373, 2004.
- [4] M. Uray, D. Sko&#269;aj, P. Roth, H. Bischof and A. Leonardis, "Incremental LDA learning by combining reconstructive and discriminative approaches", *Proceedings of British Machine Vision Conference (BMVC ) 2007*, pp. 272-281
- [5] Tae-Kyun Kim; Shu-Fai Wong; Stenger, B.; Kittler, J.; Cipolla, R., "Incremental Linear Discriminant Analysis Using Sufficient Spanning Set Approximations" *Computer Vision and Pattern Recognition, 2007. IEEE Conference on*, Volume , Issue , 17-22 June 2007 pp. 1-8
- [6] Haitao Zhao; Pong Chi Yuen; Kwok, J.T.; Jingyu Yang," Incremental PCA based face Recognition", *ICARCV 2004 Dec. 2004* Page(s): 687 - 691 Vol. 1
- [7] Ghassabeh, Y.A.; Ghavami, A.; Moghaddam "A New Incremental Face Recognition System" *Intelligent Data Acquisition and Advanced Computing Systems: Technology and Applications, 2007. IDAACS 2007. 6-8 Sept. 2007* Page(s):335 – 340
- [8] Fengxi Song, David Zhang, Qinglong Chen1, and Jingyu Yang," A Novel Supervised Dimensionality Reduction Algorithm for Online Image Recognition" , *Lecture Notes in Computer Science ; PSIVT 2006, LNCS 4319*, pp. 198 – 207, 2006. Springer-Verlag
- [9] Fengxi Song , Hang Liu, David Zhang, Jingyu Yang "A highly scalable incremental facial feature extraction method", Elsevier. *Neurocomputing* 71 (2008) 1883– 1888
- [10] Dagher, I.; Nachar, R. "Face recognition using IPCA-ICA algorithm", *Pattern Analysis and Machine Intelligence, IEEE Transactions on* Volume 28, Issue 6, June 2006 Page(s):996 – 1000
- [11] B. Raducanu, J. Vitria "Learning to learn: From smart machines to intelligent machines", *Pattern Recognition Letters* 29 (2008) 1024–1032
- [12] A Haitao Zhao Pong Chi Yuen Kwok, J.T. "novel incremental principal component analysis and its application for face recognition Systems", *Man, and Cybernetics, Part B, IEEE Transactions on*. Aug. 2006, Volume: 36, Issue: 4 On page(s): 873-886
- [13] J. Karhunen and J. Joutsensalo," Representation and separation of signals using non linear PCA type learning", *Neural Networks*, 7(1),1994.
- [14] K. Fukunaga, "Introduction to statistical pattern recognition", Second ed., Academic Press, 1990
- [15] J. J. Atick and A. N. Redlich, "What does the retina know about natural scenes?", *Neural Comput.*, vol. 4, pp. 196-210, 1992.
- [16] D. L. Swets and J. Weng, "Using discriminant eigenfeatures for image retrieval", *IEEE Trans. Pattern Anal. Mach. Intell.*, vol. 18, no. 8, pp. 831–836. August 1996
- [17] H. Murase and S.K. Nayar, "Visual Learning and Recognition of 3-D Objects from

- Appearance," *Int'l J. Computer Vision*, vol. 14, no. 1, pp. 5-24, Jan. 1995.
- [18] Y. Cui and J. Weng, "Appearance-Base Hand Sign Recognition from Intensity Image Sequences," *Computer Vision and Image Understanding*, vol. 78, pp. 157-176, 2000.
- [19] S. Chen and J. Weng, "State-Based SHOSLIF for Indoor Visual Navigation," *IEEE Trans. Neural Networks*, vol. 11, no. 6, pp. 1300-1314, 2000.
- [20] J. Weng and I. Stockman, eds., *Proc. NSF/DARPA Workshop Development and Learning*, Apr. 2000.
- [21] A. M. Martinez and A. C. Kak, "PCA versus LDA", *IEEE Trans. Pattern Anal. Mach. Intell.*, vol. 23, no. 2, pp. 228–233, Feb 2001
- [22] M. Turk and A. Pentland, "Eigenfaces for Recognition," *J. Cognitive Neuroscience*, vol. 3, no. 1, pp. 71-86, 1991.
- [23] ORL face database, website: <http://www.cam-orl.co.uk/facedatabase.html>, AT&T Laboratories Cambridge.
- [24] UMIST face database, website: <http://images.ee.umist.ac.uk/danny/database.html>, Daniel Graham.
- [25] Yale face database, website: <http://www1.cs.columbia.edu/~belhumeur/pub/images/yalefaces/>, Columbia University.
- [26] Bioid face database, website: [www.bioid.com/downloads/facedb/](http://www.bioid.com/downloads/facedb/)
- [27] Yunhong Wang, Tieniu Tan and Yong Zhu, "Face Verification Based on Singular Value Decomposition and Radial Basis Function Neural Network+", "Institute of Automation, Chinese Academy of Sciences, Beijing, P. R. China, 100080.
- [28] Hakan Cevikalp, Marian Neamtu, Mitch Wilkes, and Atalay Barkana, "Discriminative Common Vectors for Face Recognition," *IEEE Trans. Pattern Analysis and Machine Intelligence*, vol. 27, pp.6-9, 2005.
- [29] H. Yu and J. Yang, "A direct LDA algorithm for high-dimensional data—With application to face Recognition" *Pattern Recognition*, vol. 34, pp. 2067–2070, 2001.
- [30] P. N. Belhumeur, J. P. Hespanha, and D. J. Kriegman, "Eigenfaces vs Fisherfaces: recognition using class specific linear projection", *IEEE Transactions on Pattern Analysis and Machine Intelligence*, vol. 19, no. 7, pp. 711–720, 1997.
- [31] Yang J, Zhang D, Frangi A.F., and Yang J.Y. " two dimensional PCA: a new approach to appearance-based face representation and recognition" IEEE PAMI, vol 26, no 1 pp:131-137, Jan 2004.
- [32] Ye J., Janardan R., and Li Q., "two dimensional linear discriminant analysis", NIPS 2004.
- [33] Xiong H., Swamy M.N.S, and Ahmad M.O." two dimensional FLD for face recognition" *Pattern Recognition*, vol 38, pp1121-1124, 2005.

# CALL FOR PAPERS

**Journal:** International Journal of Biometrics and Bioinformatics (IJBB)

**Volume:** 4 **Issue:** 2

**ISSN:** 1985-2347

**URL:** <http://www.cscjournals.org/csc/description.php?JCode=IJBB>:

## About IJBB

The International Journal of Biometric and Bioinformatics (IJBB) brings together both of these aspects of biology and creates a platform for exploration and progress of these, relatively new disciplines by facilitating the exchange of information in the fields of computational molecular biology and post-genome bioinformatics and the role of statistics and mathematics in the biological sciences. Bioinformatics and Biometrics are expected to have a substantial impact on the scientific, engineering and economic development of the world. Together they are a comprehensive application of mathematics, statistics, science and computer science with an aim to understand living systems.

We invite specialists, researchers and scientists from the fields of biology, computer science, mathematics, statistics, physics and such related sciences to share their understanding and contributions towards scientific applications that set scientific or policy objectives, motivate method development and demonstrate the operation of new methods in the fields of Biometrics and Bioinformatics.

To build its International reputation, we are disseminating the publication information through Google Books, Google Scholar, Directory of Open Access Journals (DOAJ), Open J Gate, ScientificCommons, Docstoc and many more. Our International Editors are working on establishing ISI listing and a good impact factor for IJBB.

## IJBB LIST OF TOPICS

The realm of International Journal of Biometrics and Bioinformatics (IJBB) extends, but not limited, to the following:

- Bio-grid
- Bioinformatic databases
- Biomedical image processing (registration)
- Biomedical modelling and computer simulation
- Computational intelligence
- Computational structural biology
- Bio-ontology and data mining
- Biomedical image processing (fusion)
- Biomedical image processing (segmentation)
- Computational genomics
- Computational proteomics
- Data visualisation

- DNA assembly, clustering, and mapping
- Fuzzy logic
- Gene identification and annotation
- Hidden Markov models
- Molecular evolution and phylogeny
- Molecular sequence analysis
- E-health
- Gene expression and microarrays
- Genetic algorithms
- High performance computing
- Molecular modelling and simulation
- Neural networks

## **CFP SCHEDULE**

**Volume:** 4

**Issue:** 3

**Paper Submission:** May 2010

**Author Notification:** June 30 2010

**Issue Publication:** July 2010

## **CALL FOR EDITORS/REVIEWERS**

CSC Journals is in process of appointing Editorial Board Members for ***International Journal of Biometrics and Bioinformatics***. CSC Journals would like to invite interested candidates to join **IJBB** network of professionals/researchers for the positions of Editor-in-Chief, Associate Editor-in-Chief, Editorial Board Members and Reviewers.

The invitation encourages interested professionals to contribute into CSC research network by joining as a part of editorial board members and reviewers for scientific peer-reviewed journals. All journals use an online, electronic submission process. The Editor is responsible for the timely and substantive output of the journal, including the solicitation of manuscripts, supervision of the peer review process and the final selection of articles for publication. Responsibilities also include implementing the journal's editorial policies, maintaining high professional standards for published content, ensuring the integrity of the journal, guiding manuscripts through the review process, overseeing revisions, and planning special issues along with the editorial team.

A complete list of journals can be found at <http://www.cscjournals.org/csc/byjournal.php>. Interested candidates may apply for the following positions through <http://www.cscjournals.org/csc/login.php>.

*Please remember that it is through the effort of volunteers such as yourself that CSC Journals continues to grow and flourish. Your help with reviewing the issues written by prospective authors would be very much appreciated.*

Feel free to contact us at [coordinator@cscjournals.org](mailto:coordinator@cscjournals.org) if you have any queries.

## Contact Information

### **Computer Science Journals Sdn BhD**

M-3-19, Plaza Damas Sri Hartamas  
50480, Kuala Lumpur MALAYSIA

Phone: +603 6207 1607

+603 2782 6991

Fax: +603 6207 1697

### **BRANCH OFFICE 1**

Suite 5.04 Level 5, 365 Little Collins Street,  
MELBOURNE 3000, Victoria, AUSTRALIA

Fax: +613 8677 1132

### **BRANCH OFFICE 2**

Office no. 8, Saad Arcad, DHA Main Boulevard  
Lahore, PAKISTAN

### **EMAIL SUPPORT**

Head CSC Press: [coordinator@cscjournals.org](mailto:coordinator@cscjournals.org)

CSC Press: [cscpress@cscjournals.org](mailto:cscpress@cscjournals.org)

Info: [info@cscjournals.org](mailto:info@cscjournals.org)

**COMPUTER SCIENCE JOURNALS SDN BHD**  
**M-3-19, PLAZA DAMAS**  
**SRI HARTAMAS**  
**50480, KUALA LUMPUR**  
**MALAYSIA**